MASTERARBEIT | MASTER'S THESIS

Titel | Title

Characterisation of the molecular cross-linking behaviour of cereal arabinoxylans and proteins by oxidative coupling enzymes

verfasst von | submitted by

Patrik Roch BSc

angestrebter akademischer Grad | in partial fulfilment of the requirements for the degree of

Master of Science (MSc)

Wien | Vienna, 2025

Studienkennzahl lt. Studienblatt	Degree programme code as it appears on the student record sheet:	UA 066 659
Studienrichtung lt. Studienblatt	Degree programme as it appears on the student record sheet:	Masterstudium Lebensmittelchemie
Betreut von	Supervisor:	Univ.-Prof. Mag. Dr. Margit Cichna-Markl

Preface

This master´s thesis was a cooperation between the University of Vienna and the Austrian Agency for Health and Food Safety (AGES). The work was conducted from March 2024 to August 2024 at the Department for Feed Analysis and Quality Testing, Institute for Animal Nutrition and Feed at AGES under the supervision of Mag. Katharina Höfler and Dr. Stefano D`Amico, and Univ.-Prof. Mag. Dr. Margit Cichna-Markl from the Department of Analytical Chemistry, Faculty of Chemistry at University of Vienna. The thesis was part of the project “PROTAX” and was funded by the Austrian Science Fund (FWF) under the project number 5891-N and the German Research Foundation (DFG) under the project number 493413680.

Abstract

Gluten, an important component of many baked goods, is essential for the desired baking properties. However, the consumption of gluten poses a major challenge for people with celiac disease (CD) or non-celiac gluten sensitivity, as currently the only effective therapy is a strict gluten-free diet. This work is part of a current research project which investigated the enzymatic cross-linking of proteins and arabinoxylans (AXs) to form gluten-like networks. The focus of this thesis was the characterisation of five different enzymes, laccase (Lac), tyrosinase (TYR), horseradish peroxidase (HRP), glucose oxidase (GOX) and pyranose oxidase (POX). First, the optima of pH and temperature, and subsequently main kinetic values were determined. Then, these enzymes were evaluated for cross-linking under optimal conditions. The analysis of the products was performed using advanced analytical techniques, such as high performance liquid chromatography with a UV detector (HPLC-UV) and liquid chromatography coupled with a mass spectrometer (LC-MS/MS). Focusing on the substrates ferulic acid (FA) and tyrosine (Y), cereal-specific peptide models were then applied to bridge the gap between simple monomers and complex proteins. The results demonstrated the successful cross-linking of FA and Y monomers, as well as grain-specific peptides and FA-glycoside (FAG). The study revealed homogeneous as well as heterogeneous coupling reactions between FAG and the peptides, leading to the formation of various products with different molecular weights and polarities. In particular, peptides with terminal Y residues exhibited a higher cross-linking efficiency than those with Y within the chain. Furthermore, the analysis demonstrated that certain enzymes yielded a more diverse range of products than others, for instance Lac and HRP generated highly similar products, whereas TYR produced partially distinct products. These findings provide a foundation for further investigations into gluten-free dough structures, through a comparative characterisation of the effects of coupling tools.

Table of contents

Abstract ..... **- 4 -**

List of abbreviations ..... **- 7 -**

1 Introduction ..... **- 8 -**

2 Theoretical background ..... **- 10 -**

2.1 Arabinoxylans ..... - 10 -

2.2 Cereal proteins ..... - 11 -

2.3 Oxidoreductases ..... - 12 -

2.3.1 Characterisation ..... - 12 -

2.3.2 Methods for evaluation of enzyme characteristics ..... - 13 -

2.3.3 Laccase ..... - 15 -

2.3.4 Peroxidase ..... - 17 -

2.3.5 Tyrosinase ..... - 18 -

2.3.6 Glucose oxidase ..... - 19 -

2.3.7 Pyranose oxidase ..... - 20 -

2.4 Cross-linking of ferulic acid and tyrosine/tyrosine-containing peptides ..... - 22 -

2.4.1 Cross-linking between ferulic acid and arabinoxylans ..... - 22 -

2.4.2 Cross-linking between tyrosine, tyrosine-containing peptides and cereal proteins ..... - 24 -

2.4.3 Cross-linking between FA or AXs with Y, Y-containing peptides or proteins ..... - 26 -

2.5 Methods for evaluation of cross-linking behaviour ..... - 29 -

2.5.1 High performance liquid chromatography (HPLC) ..... - 30 -

2.5.2 Mass spectrometry ..... - 31 -

3 Aims ..... **- 34 -**

4 Materials and methods ..... **- 35 -**

4.1 Chemicals and solutions ..... - 35 -

4.2 Instruments ..... - 38 -

4.3 Methods ..... - 40 -
4.3.1 Enzyme characterisation ..... - 40 -
4.3.2 Enzyme substrate specificity for ferulic acid and tyrosine ..... - 43 -
4.3.3 Cross-linking with monomers ..... - 43 -
4.3.4 Cross-linking with oligomers ..... - 46 -
4.4 Statistical analysis ..... - 48 -
5 Results and discussion ..... - 49 -
5.1 Enzymatic characterisation ..... - 49 -
5.1.1 Determination of molar extinction coefficients ..... - 49 -
5.1.2 Protein concentration ..... - 53 -
5.1.3 pH optimum of each enzyme ..... - 55 -
5.1.4 Temperature optimum of each enzyme ..... - 59 -
5.1.5 Kinetic parameters ..... - 62 -
5.2 Substrate specificity towards ferulic acid and tyrosine ..... - 66 -
5.3 Cross-linking behaviour of monomers (FA, Y) ..... - 72 -
5.3.1 Influence of solvents and tensides on enzyme activity ..... - 72 -
5.3.2 UV-Vis measurements ..... - 74 -
5.3.3 HPLC-UV analysis ..... - 77 -
5.4 Cross-linking behaviour of oligomers ..... - 81 -
6 Conclusion and Outlook ..... - 93 -
List of figures ..... - 95 -
List of tables ..... - 98 -
References ..... - 100 -
Appendix ..... - 107 -
I. Zusammenfassung ..... - 107 -
II. Other data ..... - 108 -

List of abbreviations

ABTS	2,2'-Azino-bis(3-ethylbenzothiazoline-6-sulphonic acid)
ABTS$^{\bullet+}$	ABTS radical cation
AGES	Austrian Agency for Health and Food Safety
AMAC	Ammonium acetate buffer (pH 4.5)
AMBIC	Ammonium bicarbonate buffer (pH 6.5)
ANOVA	Analysis of variance
AXs	Arabinoxylans
BSA	Bovine serum albumin
CD	Celiac disease
DAD	Diode array detector
DMF	Dimethylformamide
ESI	Electrospray ionisation
FA	Ferulic acid
FAD	Flavin adenine dinucleotide
GOX	Glucose oxidase
GYG	Glycine-Tyrosine-Glycine tripeptide
HPLC-UV	High performance liquid chromatography coupled with a UV detector
HRP	Horseradish peroxidase
Htyr	Hydroxytyrosol
Lac	Laccase
LC-MS/MS	Liquid chromatography coupled with mass spectrometry
MBTH	3-Methyl-2-benzothiazolinone hydrazone
MS	Mass spectrometry / mass spectrometer
P1	Peptide VNLYQNA
P2	Peptide LIIPQHY
P3	Peptide KAEREGC
P4	Peptide EYFDEKNEQFQCTGT
P5	Peptide KQGDVVALPAGIVHWCY
P6	Peptide YQLPSYRTNPCGVSAA
POX	Pyranose oxidase
Q-MBTH	Quinone MBTH complex
Q-ToF	Quadrupole Time-of-Flight
RP	Reversed Phase
SEA	Specific enzyme activity
TYR	Tyrosinase
UPLC	Ultra performance liquid chromatography
VEA	Volumetric enzyme activity
WE-AXs	Water-extractable arabinoxylans
WU-AXs	Water-unextractable arabinoxylans
Y	Tyrosine

1 Introduction

Gluten is a typical component of bread, baked goods and various cereal products. It ensures optimal baking properties, through high gas holding capacity, adequate water absorption, dough strength, extensibility and elasticity [1]. The primary issue with gluten is that over 1 % of the global population suffers from celiac disease (CD) or non-celiac gluten sensitivity, with these numbers continuing to increase. Furthermore, the number of gluten-free (GF) products is growing rapidly and the market is expected to almost double by 2030 [2]. However, the disadvantages of these GF bakery products are that they lack cohesive and elastic properties, which results in a reduction in volume, an increase in crumbling texture and a loss of flavour. Therefore, several additives, including hydrocolloids, emulsifiers and oxidising agents are applied to achieve better baking properties [1, 3]. Nevertheless, the quality is still not comparable to *e.g.* wheat bread. To improve GF systems there are projects like PROTAX, which aim to create alternative biopolymer networks within GF systems.

The PROTAX project is concerned with the investigation of enzymatically induced networks of proteins and arabinoxylans (AXs), a group of dietary fibres, in GF systems with the aim of improving the quality of GF products. This can be achieved by coupling tyrosine (Y) and ferulic acid (FA) with process enzymes to form a gluten-like network, while avoiding the use of label required additives. Within this project, this thesis focused on the characterisation of cross-linking enzymes and cross-linking of model peptides derived from the GF cereals rice, oat and maize with FA.

Enzymes should be present in dough systems in certain pH and temperature ranges and therefore the initial step was to characterise oxidoreductases suitable for cross-linking reactions. The resulting data, which was provided spectrophotometrically, allowed the determination of the enzyme kinetics. The use of different substrates allowed comparison of the enzyme behaviour to provide data on the cross-linking ability of the enzymes. In order to establish the identity of the produced cross-linking products, analytical techniques, specifically high performance liquid chromatography with ultraviolet detection (HPLC-UV) and liquid chromatography coupled with mass spectrometry (LC-MS/MS), were employed. Prior to utilizing the model substances, it was important to elucidate the precise reaction mechanism of the reaction sites within these molecules. The amino acid Y and the FA bound in the AXs were particularly suitable for this purpose [4-7]. However, as the amino acid sequence in cereal proteins is considerably more complex, it was essential to select cereal-specific peptide sequences as a means of establishing an intermediate phase between the smaller monomers and the larger, more complex peptides. The utilisation of cereal-specific models thus facilitated the acquisition of several key insights, including the identification of amino acid sequences that function optimally as reaction sites,

and the investigation of the impact of the ratio of proteins and AXs. This information is crucial for advancing from the level of model molecules to the analysis of actual grain samples.

2 Theoretical background

2.1 Arabinoxylans

Arabinoxylans (AXs) are an important part of the non-starch polysaccharides of cereals that are mainly composed of the pentose sugars arabinose and xylose (see Figure 1). These polysaccharides are the predominant dietary fibre in cereals like wheat, rye, oat, rice, maize and barley, even in various grasses such as bamboo shoots, pangola grass and rye grass [8]. Although AXs make up mostly only a small amount of the whole grain, they play a crucial role in plant cell walls. The water-absorbing ability of these substances has been demonstrated to reduce hardness, enhance elasticity, and support nutrient transport through a hydrated network around cellulose. The thin walls surrounding the cells in the starchy endosperm are mainly composed of about 60 – 70 % AXs, with the exception of rice, which contains about 40 % AXs [9].

Structurally, AXs have a linear backbone consisting of β-(1→4)-D-xylopyranosyl units, with α-L-arabinofuranosyl groups attached at the O-2 or O-3 positions (Figure 1). Some of these arabinose units are further linked to ferulic acid (FA) through ester bonds at the O-5 or O-6 position [10, 11].

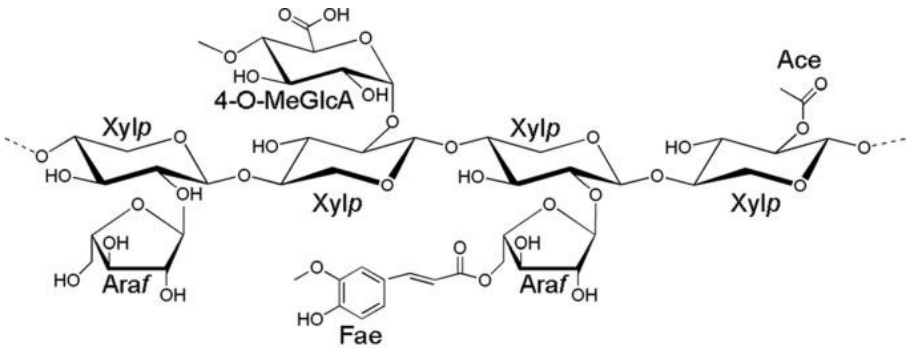

Figure 1: Chemical structure of arabinoxylan. Reused from Correia *et al.,* with permission from Journal of Biological Chemistry [11].

Despite the general structure in Figure 1, AXs can be divided into two different classes. First, the water-extractable AXs (WE-AXs) which consist of about 25 – 30 % of AXs in flour and are loosely attached to the surface of the cell wall. Second, the water-unextractable AXs (WU-AXs), which represents the remaining AXs content. Unlike WE-AXs, WU-AXs are held within the cell wall through covalent and non-covalent interactions with AXs and proteins, lignin or cellulose [12].

AXs can form highly viscous solutions after extraction, which can form gels through covalent cross-linking. This reaction occurs by dimerisation of FA on the side chains, either chemically, such as ferric chloride or ammonium persulphate, or enzymatically, such as the free radical generating agents laccase or the peroxidase/H_2O_2 system. Such covalent cross-links, including diferulic acid (di-FA) and triferulic acid (tri-FA), play a key role in solubility, viscosity and gelling behaviour, and can generate an aqueous three-dimensional network [10]. These properties are related to the chemical structure and molecular interactions of AXs and offer attractive properties such as neutral taste and odour, high water retention capacity and stability over a wide pH range. Consequently, their application as baking additives in the food industry is extensive [8, 13].

2.2 Cereal proteins

Proteins are one of the essential macromolecules found in the human diet, along with carbohydrates and fats. In the human diet, protein sources can be divided into two types – animal and plant proteins. Typical animal protein sources include meat, eggs and dairy products, while nuts, legumes and cereals are typical non-animal protein sources. Cereals generally contain 10 – 15 % protein, which can be increased by refining [14].

These cereal proteins can be divided into four the so-called Osborne fractions according to their solubility: water-soluble albumins, salt-soluble globulins, alcohol-soluble prolamins and insoluble glutelins. Each cereal has a characteristic composition, but in general prolamins are the main proteins, as in maize (50 – 55 % prolamins). Exceptions are oats, where globulins are the main proteins (75 – 80 %), and rice, which has exceptionally high levels of glutelins (80 – 95 %). These fractions are often named after the specific cereals, such as avenins for oats, zeanins for maize and oryzenins for rice [15, 16]. Albumins and globulins are mainly derived from cytoplasmic residues involved in the grain formation, where enzymes can also be present. The other two fractions, prolamins and glutelins, are storage proteins. The resulting differences in the structure and composition of these proteins are thought to be responsible for the triggering of CD [16].

Tyrosine (Y), one of the major amino acids, is the main target of enzyme-catalysed reactions in peptides and proteins. After single-electron oxidation and successive deprotonation, Y is converted into a phenolic radical species that can react at three different positions in the aromatic ring. It can bind either to the phenolic oxygen of another tyrosine radical or to one of two *ortho*-positions on the aromatic ring (Figure 2). These tyrosyl radicals primarily form the dityrosine (di-Y) and in a lesser amount dityrosine bonds, which allow inter- and intramolecular cross-linking of peptides or proteins [7, 16].

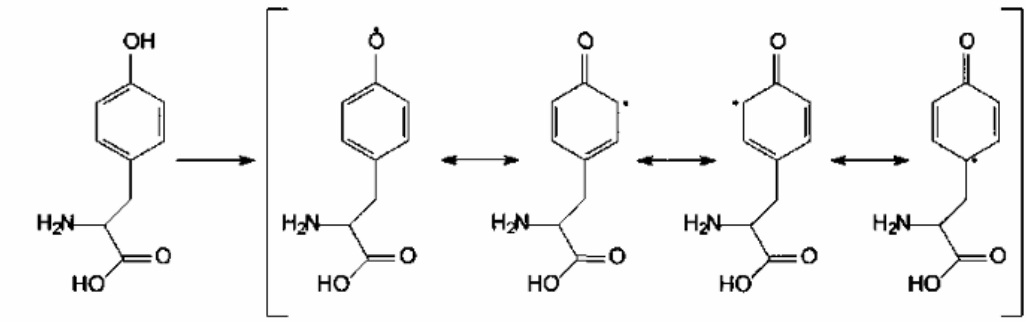

Figure 2: Tyrosine and the corresponding mesomeres of its radical after oxidation. Reused with the permission from Oudgenoeg [58].

2.3 Oxidoreductases

2.3.1 Characterisation

Enzymes are globular proteins that contain a catalytic activity to initiate, support or especially accelerate various chemical reactions. They are divided into six main groups according to the type of reaction they carry out: oxidoreductases, transferases, hydrolases, lyases, isomerases and ligases [16]. The focus of this work was on oxidoreductases, which catalyse the reduction/oxidation reactions in which an electron is transferred from one molecule to another. These enzymes often need to act as electron donors or electron acceptors. In addition, molecular oxygen (O_2) is often used as an electron acceptor, which is reduced to water (H_2O) or hydrogen peroxide (H_2O_2) during the redox reactions. The applied enzymes are laccase (Lac), horseradish peroxidase (HRP), tyrosinase (TYR), glucose oxidase (GOX) and pyranose oxidase (POX).

Enzyme kinetics are mainly characterised by the simple mathematical approach of Michaelis and Menten and follow Equation 1.

$$E + S \underset{k_{-1}}{\overset{k_1}{\longleftrightarrow}} ES \xrightarrow{k_2} E + P$$

Equation 1: Enzymatic reaction followed by the Michaelis-Menten theory with E = enzyme, S = substrate, ES = enzyme substrate complex, P = product, and $k_{1, -1, 2}$ = corresponding reaction rate.

$$v_0 = \frac{v_{max} * [S]}{K_m + [S]}$$

Equation 2: Michaelis-Menten equation, with v_0 = initial velocity, v_{max} = maximal velocity, [S] = substrate concentration, and K_m = Michaelis-Menten constant.

In the first step the pH and temperature optima of each enzyme has to be ascertained in order to subsequently determine the kinetic parameters. The enzyme (E) combines with the substrate (S) to form the enzyme-substrate complex (ES) as shown in Equation 1. In the second step the ES breaks down to produce the product (P) with a first order catalytic constant (k_2) (Equation 1). The main

assumptions are that the substrate binds quickly to the enzyme and the resulting product is then released, allowing the enzyme to repeat the process. From this equation the two main kinetic parameters can be obtained – the maximum enzyme velocity v_{max} and the Michaelis constant K_M (Equation 2). V_{max} describes the maximum enzyme activity under the applied conditions and K_M is the sensitivity of the catalysis or, in other terms, the substrate concentration at half of v_{max} [17, 18]. However, as the curve (Figure 3) only approaches v_{max} asymptotically, a linearisation method is necessary. This is achieved by a simple mathematical conversion, whereby v_{max} can be calculated more precisely. One of such methods is the Hanes-Woolf plot (Figure 3). Since only one mathematical transformation takes place ($\frac{[S]}{v}$), the distance between the measuring points remains the same and the size of the error does not change with the size of the measured data [19, 20].

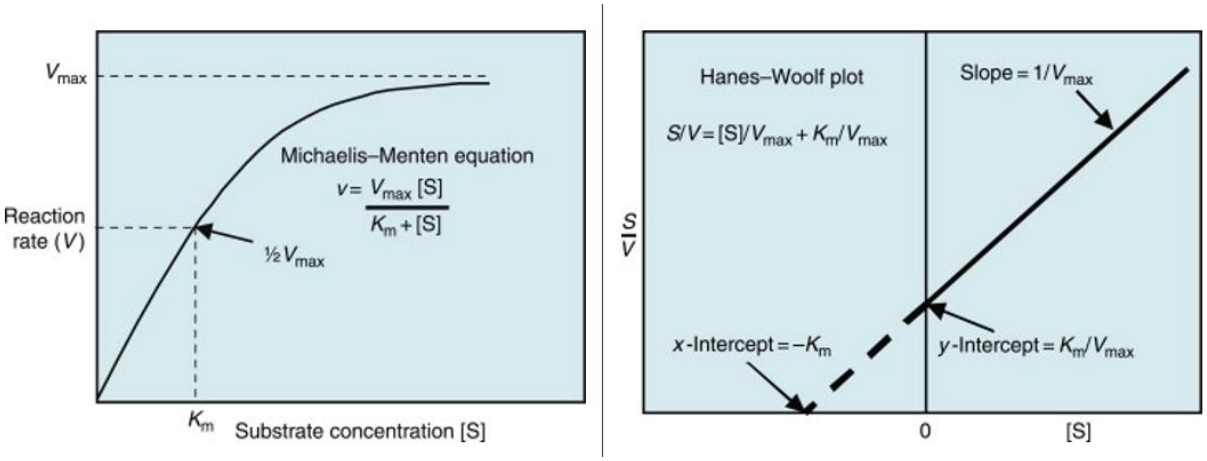

Figure 3: Michaelis-Menten (left) and Hanes-Woolf (right) equations and plots reused from Prince *et.al.,* with permission from Comprehensive Biotechnology (Second Edition) [20].

2.3.2 Methods for evaluation of enzyme characteristics

2.3.2.1 ABTS assay

ABTS (2,2'-Azino-bis(3-ethylbenzthiazoline-6-sulphonic acid)) is a water-soluble mediator which undergoes single-electron oxidation to form the stable blue coloured radical cation $ABTS^{+\bullet}$ (Figure 4). The oxidation is usually performed by using an oxidising enzyme (*e.g.* laccase, peroxidase) and is measured spectrophotometrically over time at 420 nm (absorption maximum of ABTS). The measurement over time is important because the formed $ABTS^{+\bullet}$ can also react to the less stable dication $ABTS^{++}$, which appears red-coloured (Figure 4) [21].

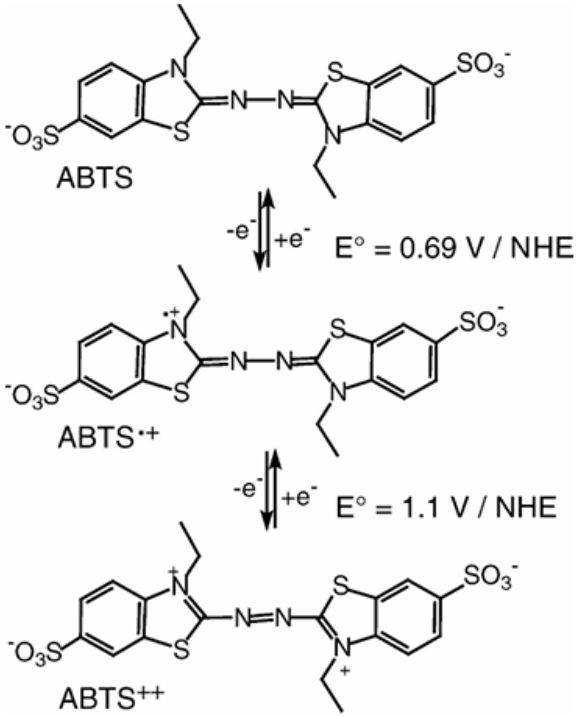

Figure 4: The two-step oxidation of ABTS. Reused from Branchi *et al.,* with permission from Organic & Biomolecular Chemistry [21].

The ABTS assay is one of the most widely used assays for enzyme characterisation due to its very high sensitivity compared to other methods. ABTS is also used as an indicator for ozone, hydrogen peroxide or in antioxidant tests. The enzyme activity is expressed in units, where one unit is defined as the conversion of 1 µmol of ABTS per minute [22].

2.3.2.2 ABTS-peroxidase co-assay

The ABTS-peroxidase co-assay is an adapted ABTS assay for the determination of glucose oxidase (GOX) and pyranose oxidase (POX) activity using an additional enzyme, peroxidase. The reaction is divided into two steps – first, GOX or POX convert glucose (substrate) to glucono-1,5-lactone and hydrogen peroxide. The produced H_2O_2 is then stoichiometrically converted by the peroxidase to oxidise the chromogen ABTS, producing the same products as in the ABTS assay above. The chemical reactions of these two steps are given in Equation 3 [23].

$$Glucose + O_2 + H_2O \xrightarrow{GOX} Glucono - 1{,}5 - lactone + H_2O_2$$

$$H_2O_2 + ABTS\ (reduced) \xrightarrow{peroxidase} ABTS\ (oxidised)(\lambda = 420\ nm) + H_2O$$

Equation 3: The two reaction steps of the ABTS peroxidase co-assay.

In this assay, one unit of GOX or POX is defined as the amount of enzyme required to oxidise 2 µmol of ABTS per minute due to the stochiometric reaction described in Equation 3. The spectrophotometric evaluation is the same as in the ABTS assay [24].

2.3.2.3 Htyr-MBTH assay

MBTH (3-Methyl-2-benzothiazolinone hydrazone) is used as a coupling reagent due to its strong nucleophilic profile which is caused by the amino group. In the first step, an o-diphenol, in this case hydroxytyrosol (Htyr), is enzymatically oxidised to the corresponding o-quinone, which is then coupled with MBTH to form a MBTH-quinone adduct (Equation 4). This is measured spectrophotometrically with time at around 500 nm [25].

$$Hydroxytyrosol \xrightarrow{Lac} Quinone$$

$$Quinone + MBTH \rightarrow MBTH - quinone\ complex\ (\lambda = 500\ nm)$$

Equation 4: Chemical reaction of the formation of hydroxytyrosol to its quinone, followed by MBTH-quinone complex formation.

This coupling method is highly sensitive, reliable and accurate for enzyme characterisation. MBTH plays a crucial role due to its ability to react with unstable quinones, which are intermediates formed during enzyme activity, to form a stable chromophore. This chromophore absorbs light at a higher wavelength (around 500 nm), thereby reducing interference from other compounds and enhancing assay sensitivity and specificity. An important step is the addition of dimethylformamide (DMF) to improve the solubility of the formed quinone complex [26].

2.3.3 Laccase

Laccase (Lac), also known as benzenediol oxygen oxidoreductase (EC 1.10.3.2), belongs to a group of oxidoreductases that act on diphenols and related substances as electron donors and use oxygen as an electron acceptor. It catalyses the reduction of O_2 to H_2O, typically accompanied by the oxidation of a phenolic compound (Equation 5). In summary, Lac oxidises many polyphenols, aromatic diamines, differently substituted phenols and many other compounds but is less effective when oxidising tyrosine compared to tyrosinases [27].

$$4\ substrate\ (reduced) + O_2 + 4\ H^+ + 4\ e^- \xrightarrow{Lac} 4\ substrate\ (oxidised) + 2\ H_2O$$

Equation 5: Chemical reaction of the oxidation by Lac.

Lac also belongs to a group of oxidoreductases that contain copper in their catalytic centre. The overall structure of Lac from *Trametes versicolor*, which was applied in this work, was described by Piontek *et. al.* [28]. The polypeptide consists of four copper ions and five different N-glycosylation sites with seven

N-acetyl glucosamine moieties. The Lac reaction mechanism is governed by four copper atoms, categorised into three Cu site types (Figure 5). The type 1 Cu site (T1) serves as the primary electron acceptor, while the reducing substrate is subsequently oxidised [7, 29, 30]. This site has an absorption peak at 600 nm giving a blue colouration [31]. The electron is then transferred through a Cys-His pathway to the active trinuclear system consisting of coppers from type 2 site (T2) and type 3 site (T3) located between domains 1 and 3. The copper in T2 activates the molecular oxygen and shows no significant absorption between 200 – 800 nm. The T3, consisting of two coppers coupled binuclear, is responsible for the oxygen uptake and exhibits an absorption peak at 330 nm. This process results into a four electron oxidation leading to the reduction of dioxygen [30].

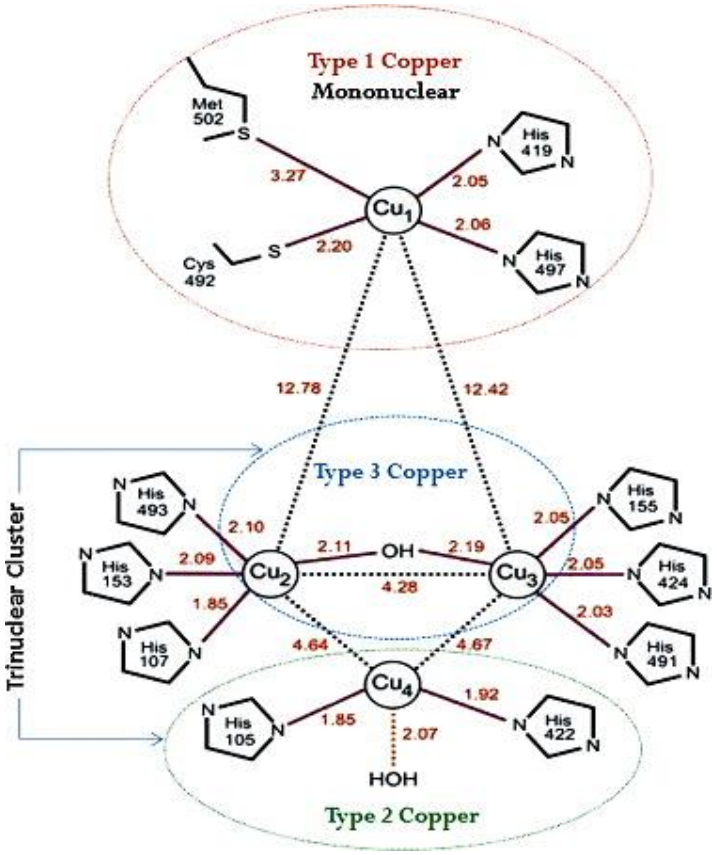

Figure 5: Schematic representation of the three copper site types and their coordination, including the distances between the ligands. Reused from Dwivedi, with permission from Journal of Molecular Catalysis [29].

The result of this reaction is a radical substrate that can initiate further reactions which undergo non-enzymatic reactions that can cause cross-linking [32]. These Lac catalysed reactions are categorised as environmentally friendly because water is the only by-product, as already shown in Equation 5 [33]. Nevertheless, an alkaline environment and the presence of some cations, such as Ag^{+} and Fe^{3+}, or anions, such as Cl^{-} or NO_3^{-}, can significantly decrease the enzyme activity [34].

The copper-containing enzyme can be typically found in eukaryotes as plants and fungi. The main role in plants is the participation in lignin polymer formation which is accompanied by the radical formation [35]. The fungal Lac includes much more roles compared to the plant-based such as stress defence, morphogenesis and the interactions between pathogens and their hosts [36]. So far, Lac has been purified from more than 100 different species, almost all of which have been characterised. The majority of these enzymes has been isolated from the wood-decaying white basidiomycetes, a division in the fungal kingdom. The typical molecular weight of these fungal laccases varied between 60 – 70 kDa [27]. In fungal species were also several isoenzymes detected. One example of such fungal species is the Lac from *Trametes versicolor*, which produces multiple Lac isoenzymes [37].

2.3.4 Peroxidase

Peroxidases (EC 1.11.1.7) are classified as oxidoreductases which differ from Lac in that they can catalyse a wider range of organic and inorganic compounds using hydrogen peroxide (H_2O_2) or organic hydroperoxides (R–OOH) as electron acceptors. While peroxidases can act on a diverse spectrum of substrates, they exhibit a higher degree of substrate specificity compared to Lac towards certain classes of compounds, such as monophenols and monoamines. This implies that peroxidases can convert these specific substrates more efficiently and potentially with a greater preference than Lac, even though their overall substrate range is broader. Although peroxidases include a wide range of subcategories, their reaction mechanism remains the same and can be simplified in Equation 6 [34, 36, 38].

$$donor + H_2O_2 \xrightarrow{peroxidase} oxidsed\ donor + 2\ H_2O$$

Equation 6: Reaction definition of peroxidases.

Peroxidases are mostly haem proteins containing a ferric protoporphyrin IX as their active site. Their molecular weight varies from 30 – 150 kDa [39]. One such example is horseradish peroxidase (HRP), which was also used in this work. Horseradish (*Armoracia rusticana*) is a hardy plant grown mainly in temperate regions of the world. Apart from its culinary value, it is also a huge source of peroxidase, which is already used on a large commercial scale [40]. One such example is its use in enzyme-linked immunosorbent assay (ELISA), where peroxidase is one of the most suitable enzymes for the preparation of enzyme-conjugated antibodies. In general, peroxidases are found in microorganisms, plants and animals, where they are involved, for instance, in the defence mechanism of damaged or infected tissues or in lignification [39].

The catalytic cycle of HRP is shown in Figure 6 using ferulate as a substrate example. In the first step (k_1), H_2O_2 reacts with Fe (III) of the enzyme to form the oxidised Fe (IV) intermediate (compound I).

This is followed by two single-electron reduction steps. First, the reduced substrate undergoes a one-electron reduction (k_2) to form the oxoferryl oxide of Fe (IV) (compound II). Finally, compound II is reduced back to the resting state of the enzyme by a further one-electron reduction. In summary, one complete catalytic cycle produces two free radicals and hydrogen peroxide is reduced to water [40].

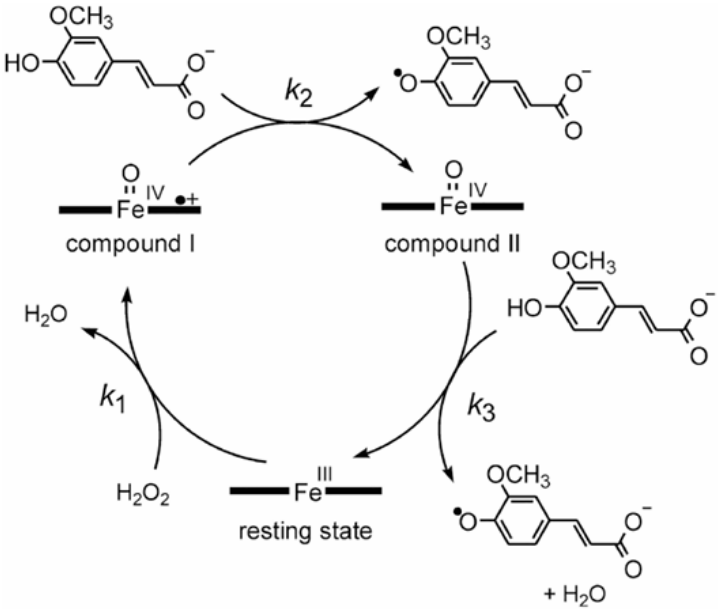

Figure 6: Catalytic cycle of HRP with ferulate as a reducing substrate. Reused from Veitch, with permission from Journal of Phytochemistry [40].

2.3.5 Tyrosinase

Tyrosinase (TYR) (EC 1.14.18.1) also belongs to the class of oxidoreductases, but unlike the previous two enzymes, it is acting on paired donors, incorporating or reducing molecular oxygen, with one donor compound and the incorporation of a single oxygen atom [41]. This means, it catalyses the o-hydroxylation of monophenols to o-diphenols (monophenolase activity), assisted by the presence of oxygen. In addition, under the same conditions, the o-diphenol is oxidised to o-quinones (diphenolase activity) (Figure 7). These o-quinones produced by the bifunctional activity of TYR are very reactive and can furthermore react non-enzymatically with *e.g.* proteins. Measuring quinones is challenging due to this high reactivity and instability, leading to rapid oxidation, which therefore complicates the accurate detection and quantification in assays [26].

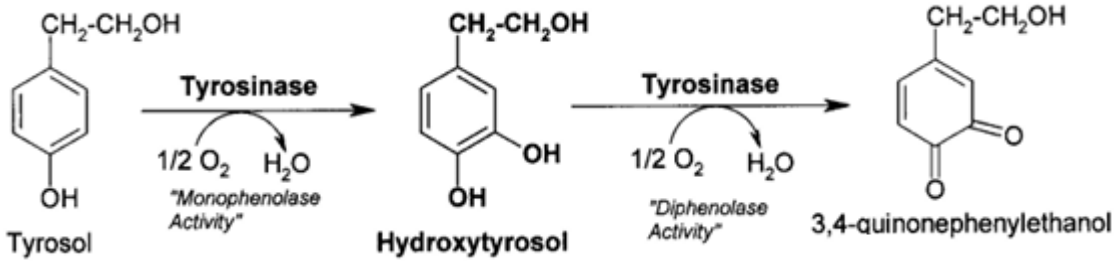

Figure 7: Formation of the o-quinone from the monophenol tyrosol in the presence of TYR and O_2. Reused from Espín *et. al.*, with permission from Journal of Agricultural and Food Chemistry [26].

Tyrosinase, like Lac, is a copper-containing oxidoreductase. It contains two type-III Cu atoms in their active site, which transfer electrons from the oxidised substrate to oxygen. The molecular O_2 is used as a terminal electron acceptor [42]. Compared to laccase, TYR has a lower specificity for phenolic compounds, *e.g*. TYR does not convert ferulic acid (FA). In addition, Lac requires four times less oxygen to oxidise monophenolic compounds and two times less O_2 to oxidise diphenolic compounds than TYR does, as shown in Equation 5 and Figure 7 [5].

This enzyme is widespread in nature, where it performs a variety of functions from the storage, transport and uptake of metal ions to the electron transfer and enzymatic catalysis. It can be found in various plants, fruits, bacteria, fungi and animals. It is also known by another name, polyphenol oxidase, and has a wide substrate range for various phenolic compounds (tyrosine, DOPA, catechol e.g.) [25]. It is thought to be responsible for converting the amino acid tyrosine into one of the melanin pigments directly responsible for the browning of food [43]. In addition, TYR is already widely used commercially, for example in the medical production of L-3,4-dihydroxyphenylalanine (L-DOPA), which is used to treat Parkinson´s disease [44].

2.3.6 Glucose oxidase

Glucose oxidase (GOX) or also known as β-D-glucose:oxygen or 1-oxidoreductase (EC 1.1.3.4) is also an oxidoreductase, but it acts on the CH–OH group of donors with oxygen as the acceptor. It catalyses the oxidation of β-D-glucose to δ-D-gluconolactone and the simultaneous reduction of molecular O_2 to hydrogen peroxide (Figure 8). Other sugars such as galactose, mannose and xylose can also act as substrates, but they show a much lower reaction rate [45].

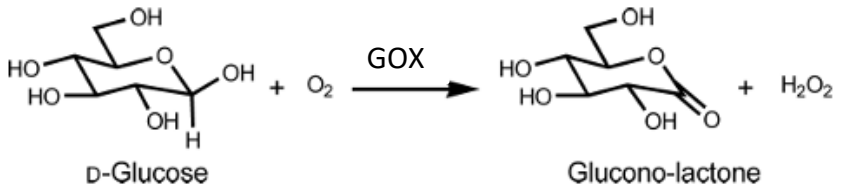

Figure 8: General reaction of β-D-glucose with glucose oxidase (GOX) to form δ-D-gluconolactone and hydrogen peroxide. Reused from Wongnate and Chaiyen, with permission from FEBS Journal [47].

The hydrogen peroxide produced can furthermore react with various compounds. The main reaction sites in proteins are the free thiol groups of cysteine [5]. Tyrosine and phenolic compounds such as FA, can also be oxidised by the presence of peroxidase in the system. As a result, GOX indirectly converts various proteins and phenolic compounds, but the condition that peroxidase is present must be fulfilled. Furthermore, these conditions can promote the cross-linking between the substrates and have a positive impact on the gelling properties [6].

GOX is a glycoprotein with a molecular weight of approximately 150 kDa. The carbohydrate content is ~16 %, with predominantly mannose. The enzyme contains two moles of bound flavin adenine dinucleotide (FAD) per mole protein as a prosthetic group [45]. This co-factor, FAD, is an important part of the two-step mechanism where it oxidises the glucose to gluconolactone and an enzyme-$FADH_2$ intermediate, followed by electron transfer to oxygen to produce hydrogen peroxide (*cf*. Figure 8) [46].

GOX has been identified in a number of different organisms, including fruits, fungi, bacteria, insects and mammals. GOX is already being used as a bread improver, which has been shown to increase the strength and elasticity of dough with surface dryness. Despite its use in the food industry, it is also widely applied in biosensors due to its high specificity, stability and turnover [46].

2.3.7 Pyranose oxidase

Pyranose oxidase (POX), also known as pyranose:oxygen or 2-oxidoreductase (EC 1.1.3.10), is a similar enzyme compared to GOX. It is also a FAD-dependent oxidoreductase that produces hydrogen peroxide, which can be further used for various reactions. The main difference between these two enzymes is that POX produces a different product. Whereas GOX oxidises at the C1 position of glucose (see Figure 8), POX oxidises at the C2 position of glucose, producing 2-ketoglucose (Figure 9) [47]. Another difference between these enzymes is that POX has a broader substrate specificity. POX shows a much higher reaction rate of reaction with other sugars such as galactose, xylose and sorbose, compared to GOX [46].

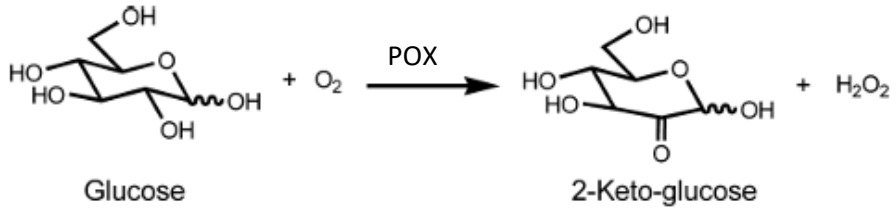

Figure 9: General reaction of β-D-glucose with pyranose oxidase (POX) to form 2-keto-glucose and hydrogen peroxide. Reused from Wongnate and Chaiyen, with permission from FEBS Journal [47].

The catalytic mechanism of POX can be divided into two half-reactions. The first one is the reductive half-reaction in which two electrons are transferred as a hydride ion from the sugar to the oxidised co-factor FAD, resulting in the formation of $FADH_2$ and a 2-ketopyranose. The histidine residue (as H548 in Figure 10) acts as the catalytic base for this reaction. The other one is the oxidative half-reaction, where two electrons are transferred from the reduced $FADH_2$ to oxygen to form the initial state of the flavin and hydrogen peroxide [47]. Aldopyranoses are the preferred electron donors, while oxygen, various quinones and metal ions are the commonly applied electron acceptors [48]. The entire catalytic cycle is summarised in Figure 10.

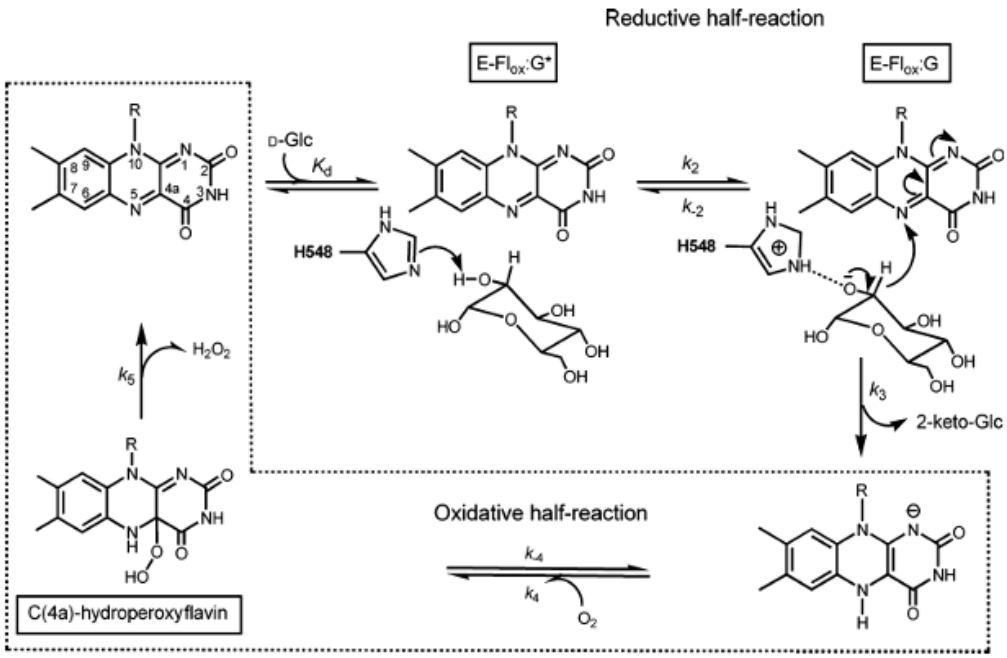

Figure 10: The catalytic cycle of pyranose oxidase with glucose as a substrate. Reused from Wongnate and Chaiyen, with permission from FEBS Journal [47].

The occurrence of POX is as well similar to that of GOX. POX is commonly characterised from the wood-decomposing fungi, where it is secreted extracellularly [49]. The physiological role of POX is also depending on the production of H_2O_2, which is used as a substrate for lignin-degrading enzymes. In some organisms, it is also involved in the secondary metabolism, where it helps fungi to protect themselves from bacterial attack [50].

2.4 Cross-linking of ferulic acid and tyrosine/tyrosine-containing peptides

2.4.1 Cross-linking between ferulic acid and arabinoxylans

The homogeneous cross-linking behaviour between FAs has been studied in various literature. The most commonly applied enzymes for these reactions are Lac and HRP. Cross-linking with GOX and POX is less common, and TYR does not oxidise FA. The enzyme-catalysed oxidation of FA leads to the formation of several intermediate radicals (Figure 11). The radicals are initially formed at the hydroxyl group and then rapidly move to different positions on the aromatic ring. In addition, strong oxidative conditions can lead to the cleavage of the methoxy group, increasing the potential number of possible polymers [51].

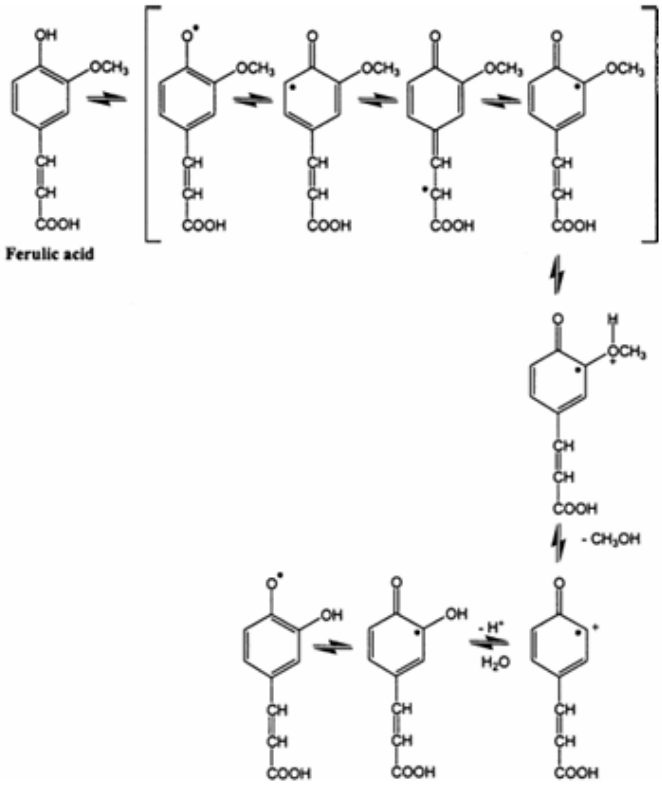

Figure 11: Ferulic acid and the corresponding mesomeres of its radical after oxidation. Reused from Mattinen *et al.*, with permission from FEBS Journal [51].

Liquid chromatography coupled with mass spectrometry (LC-MS) is one of the most widely applied analytical techniques for the determination of ferulated cross-linking products. The chromatographic separation is principally achieved through the use of a reversed-phase (RP) C18 column, with a mobile phase comprising methanol, acetonitrile, or fluoroacetic acid, thereby ensuring the effective separation of all major monomers. Furthermore, a diode array detector (DAD) is frequently employed after LC separation, as FA can be quantified at wavelengths of 280 and 320 nm. To gain further structural information and enhance the analysis, the eluent from the LC-UV system is often subjected to MS. Usually, this analysis is performed under both negative and positive ionisation conditions, using different mass analysers such as Quadrupole-Time of Flight (Q-ToF) or Matrix assisted laser desorption ionisation-Time of flight (MALDI-ToF) [4, 13, 51]. In the context of examining baked goods, rheological analyses are typically conducted subsequent to cross-linking reactions, where the gel structure formed is examined. A study by Berlanga-Reyes *et.al.* revealed that the incubation time plays a crucial role in the development of stable and hard gels consisting of ferulated AXs, as for instance, the reaction time of 0.5 h did not generate any gels [10].

In a further study, the enzymatic cross-linking reactions with Lac were investigated on wheat water-extractable arabinoxylans (WEAXs) using RP-HPLC-UV, and the resulting gelation was assessed through rheological measurements. The homogeneous incubation process revealed a decrease in the FA content with approximately 70 % of the initial FA content being oxidised after 40 min. Simultaneously, an increase in the di-FA and tri-FA content was observed. After 120 min the di- and trimeric content remained constant, indicating physical interactions occurring between adjacent AXs chains and the formation of oligomeric structures higher than trimers. As the reactions were also conducted in the presence of the protein ovalbumin, the findings imply that WEAXs gels have the potential to be employed for the protein entrapment [52].

The review by Bento-Silva *et. al.* described the cross-linking of FAs in maize cell walls [13]. The cross-links of cell wall polysaccharides were formed through photochemical reactions or by enzymatic reactions catalysed by, for instance, Lac or peroxidase on FAs. Dimeric isomers of FA represented about 2.5 % of maize bran, with 8-5'-linkages (35 – 45 % of total dimers) being the most abundant, followed by 5-5' (19 – 25 %) and 8-8' linkages (17 – 21 %). The cyclic form of 8-5-diferulate was found to be the only one formed under biological conditions using HRP with H_2O_2. Higher oligomers were also found, with the 8-O-4/5-5 linkage being the most predominant trimer (86 %). Tetramers were also found, but in this case, it is uncertain whether the tetramers are formed by coupling of a fourth FA to a trimer or by coupling of two dimers. In total, nine dimeric isomers, eight trimeric isomers and two tetrameric isomers of FA have been identified in maize bran [13, 53, 54].

2.4.2 Cross-linking between tyrosine, tyrosine-containing peptides and cereal proteins

The homogeneous cross-linking behaviour between tyrosine and Y-containing peptides was studied in various literature. The most commonly applied enzymes for these cross-linking reactions were Lac and TYR, with HRP, GOX and POX used less frequently. The cross-linking behaviour was typically determined using a HPLC-UV or a LC-MS method. In this instance too, a UV detector was employed at the wavelengths of 280 and 320 nm [42, 55-57]. Furthermore, rheological tests were also carried out in conjunction with the studies relating to the properties of bread [42, 57]. Another frequently applied method for the determination of cross-linking between proteins is the sodium dodecyl-sulphate polyacrylamide gel electrophoresis (SDS-PAGE). This method involves the separation of protein molecules into multiple peptide bands based on their differential mobility. In comparison to the LC-MS method, the SDS-PAGE technique allows the determination of significantly higher molecular weights [7, 57].

According to Mattinen *et. al.*, Lac was found to oxidise Y and Y-containing peptides, glycine-tyrosine (GY) and glycine-leucine-tyrosine (GLY), with simultaneous polymerisation of the compounds [51]. Y and GY polymers of up to eight units and GLY polymers of up to five units were identified by MALDI-ToF MS. The main covalent linkage between these compounds was found to be an ether bond. Di-Y bonds were less frequently identified. The potential radicals generated in these Lac-catalysed reactions are shown in Figure 2 [51].

Selinheimo *et. al.* also cross-linked the tripeptide GLY with Lac, but additionally with the enzyme TYR [42]. Both enzymes oxidised the Y-containing peptide, but the product patterns were significantly different. TYR-catalysed reactions produced less divergent product patterns compared to Lac. In addition, the colour of the solution changed to red after the reaction with TYR, whereas the reaction solution with Lac remained colourless. The enzymatic reaction mechanism of these two enzymes is also different. While TYR produces quinones that may undergo further non-enzymatic reactions, the Lac-catalysed oxidation is based on the generation of free radicals. In addition, TYR appeared to be much more effective at cross-linking gliadin proteins than Lac, where cross-linking was only observed at higher enzyme levels and longer incubation times [42].

A study by Steffensen *et. al.* analysed the oligomerisation of seven various peptides with sequences between three and eleven amino acids by Lac [55]. The results demonstrated that the Y-containing peptides exhibited the capacity for cross-linking, with peptides bearing a terminal Y demonstrating the optimal cross-linking efficiency. MS/MS analysis revealed that the cross-links were primarily located within the Y residues, with the potential for the formation of di-Y bonds. Furthermore, the MS spectra revealed the presence of various oligomeric structures, with a degree of oligomerisation reaching up

to a pentamer. In summary, the occurrence of Ys and cysteines was found to be essential for peptide cross-linking [55].

Jia *et. al.* described the coupling mechanism of the Lac-catalysed polymerisation of Y to Y-oligomers by MALDI-ToF-MS [56]. Y was oxidised by Lac, namely the phenolic hydroxyl group, forming a phenoxy radical. In one case, this radical was transferred to the benzene ring, which after polymerisation formed the Product 1 in Figure 12. Another case is the radical polymerisation between the radical intermediates forming di-Y either through a benzene linkage (Product 2) or through a benzene oxygen linkage (Product 3). In addition, despite the C-C bonds and C-O bonds, trimeric Ys could be formed by Michael addition reaction between the benzene ring radical and the primary amino groups of Y (Product 4, Figure 13) [56].

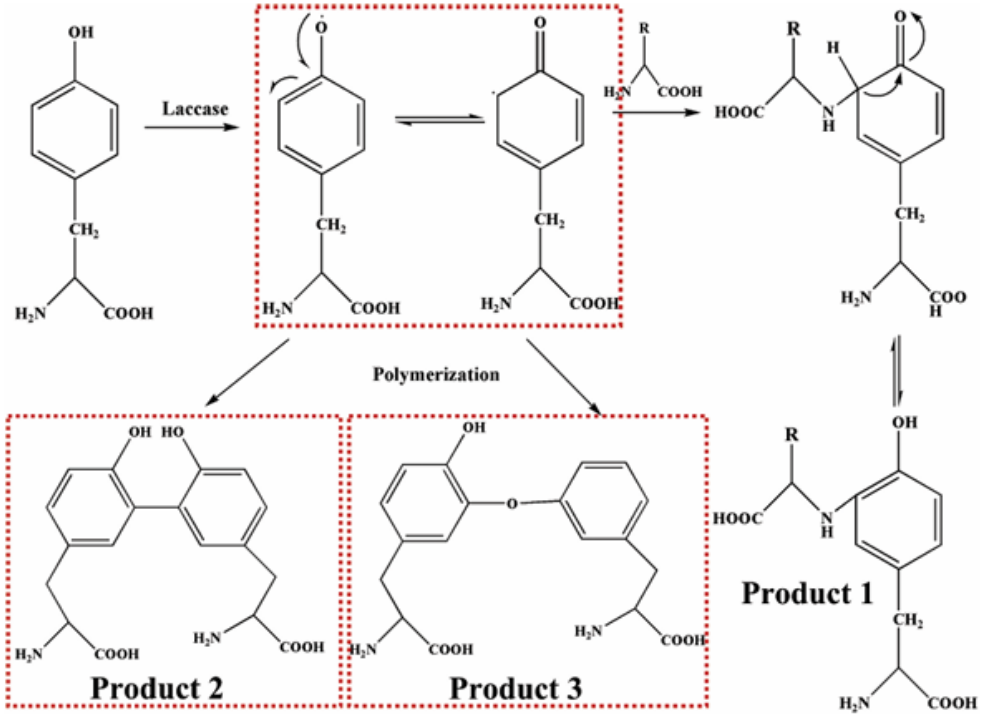

Figure 12: The potential cross-linking products of tyrosine by Lac. Reused from Jia *et al.*, with permission from Journal of Natural Fibers. R = $(OH)C_6H_5CH_2$– [56].

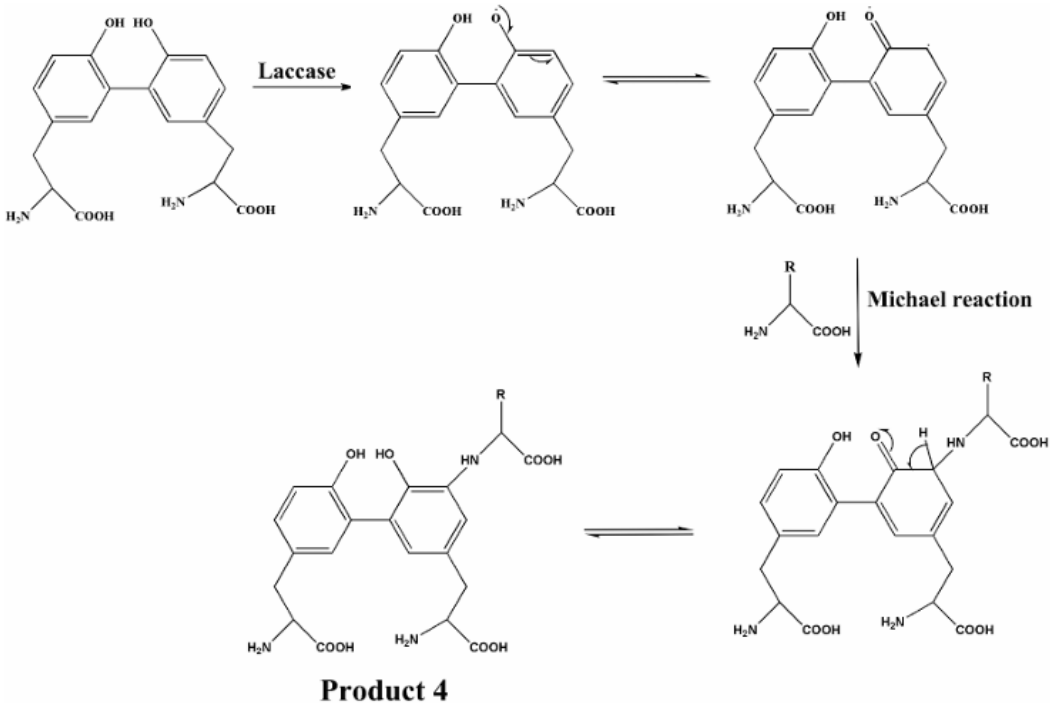

Figure 13: Proposed formation of tri-Y through a Michael addition reaction. Reused from Jia *et al*., with permission from Journal of Natural Fibers [56].

2.4.3 Cross-linking between FA or AXs with Y, Y-containing peptides or proteins

Heterogeneous cross-linking between FA and Y has also been investigated in various literature [4, 7, 51, 55, 58, 59]. In most of the cases, Lac and TYR were the most commonly used enzymes, while HRP, GOX and POX were rarely used. In the paper by Mattinen et. al., not only the homogeneous polymerisation between Y and Y-containing peptides was analysed, but also the influence after the addition of FA [51]. In the case of the monomer Y, the presence of FA did not significantly affect the chemical composition of the Y polymers in a 1:1 ratio. Only traces of heteropolymers could be identified. This process was assumed to be more complex, as both substrates were oxidised simultaneously, and several non-enzymatic reactions may take place at the same time. However, the cross-linking of peptides (GY, GLY) with FA resulted in much more polymeric products, including several heteropolymers. In this study various analytical techniques were applied such as MALDI-ToF-MS, HPLC-fluorescence, SDS-PAGE, electron paramagnetic resonance (EPR) or Fourier transform infrared spectroscopy (FTIR) microscopy. EPR was applied for the analysis of radical formation (see Figure 2), while FTIR microscopy determined the chemical bonds between peptide monomers [51].

Oudgenoeg et. al., analysed the cross-linking behaviour between FA and the tripeptide GYG in a 2:1 ratio with HRP and H_2O_2 by HPLC-MS [59]. In summary, HRP-catalysed cross-linking between FA and GYG resulted in a complex range of different isomeric products (Figure 14 – 15) with varying degrees of polymerisation. An important step in the oligomerisation to higher FA oligomers appeared to be the

generation of decarboxylated FA dimers, as the higher heterogeneous products are always 1- or 2-fold decarboxylated. In addition, the type of oligomerisation appeared to be highly dependent on the substrate concentrations and the kinetic control of the reaction [59].

The review by Wu *et. al*., described the cross-linking between feruloylated polysaccharides and proteins [7]. The enzymes used were Lac, HRP and transglutaminase, but only Lac- and HRP-catalysed reactions allowed the conjugation between proteins and polysaccharides due to their broad substrate specificity. Feruloylated polysaccharides, such as AXs, sugar beet pectin and corn fibre gum could cross-link with proteins, with the FA moiety apparently involved in the cross-linking reaction. However, it was concluded that there is still a lack of studies on the cross-linking between higher oligomers such as feruloylated oligosaccharides and peptides/proteins. Despite the successful implementation of heterogeneous cross-linking, further research is required on the effects of side reactions and homogeneous cross-linking to ensure a comprehensive understanding. The majority of studies have focused on the enzymatic cross-linking of proteins with feruloylated polysaccharides, while feruloylated oligosaccharides have received less attention and there is a gap in the literature between the step from monomers to oligomers and subsequently to polymers. Oligosaccharides, due to their lower molecular weight and higher solubility compared to polymers, may achieve higher cross-linking efficiency and enhance protein properties more effectively [7]. Despite the application of diverse peptides in numerous studies, no studies have utilised cereal peptide sequences that would effectively simulate model systems.

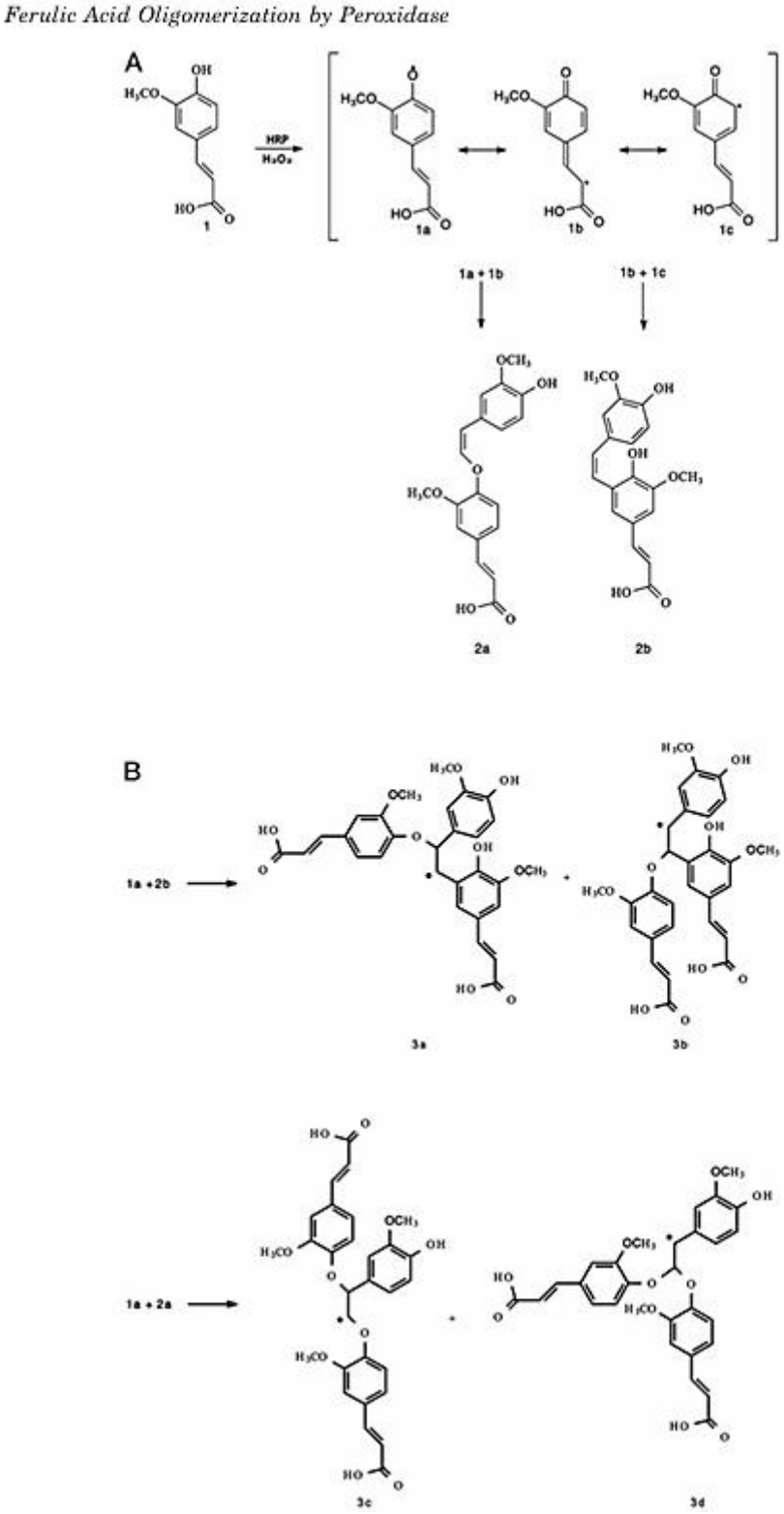

Figure 14: Oxidation of FA by HRP (A) leading to various FA trimers (B). Reused from Oudgenoeg *et al*., with permission from Journal of Biological Chemistry [59].

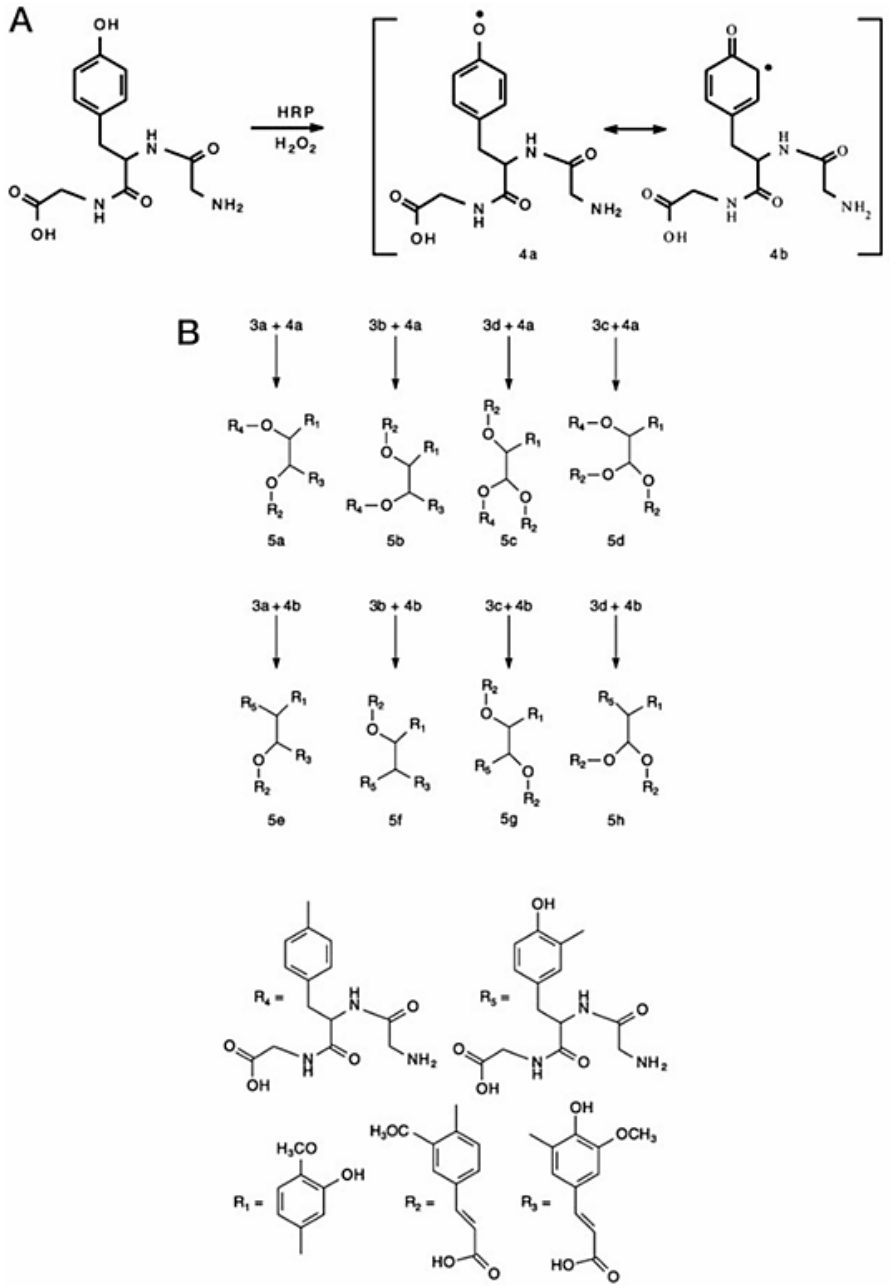

Figure 15: Oxidation of the tripeptide GYG by HRP (A) and the eight possible heterogenous products resulting from two isomeric GYG radicals (A) and four isomeric FA trimer radicals (shown in Figure 14B) (B). Reused from Oudgenoeg *et al*., with permission from Journal of Biological Chemistry [59].

2.5 Methods for evaluation of cross-linking behaviour

As already seen from the mentioned studies, the most applied analytical techniques for the determination of cross-linking between the substrates is HPLC coupled with either a MS that combines different mass analysers, or with a UV-Vis spectrophotometer, which applies the two main

wavelengths of 280 and 320 nm. Both these methods were also applied in this work and will be described in more detail below. MALDI and SDS-PAGE were not used in this thesis but will be applied in the further project. These will enable the separation and identification of greater molecular masses. The detection of complex arabinoxylan/protein networks poses significant challenges due to their heterogeneous structures and various binding interactions. Consequently, a model-based step-by-step approach is preferable, as it allows for a systematic and targeted analysis of individual reactions and binding mechanisms, facilitating a more precise understanding of these intricate networks.

2.5.1 High performance liquid chromatography (HPLC)

Chromatography is an analytical method in which substances are separated using two phases (mobile and stationary). One of the most applied techniques is high performance liquid chromatography (HPLC). In this case, the mobile phase is a liquid that transports the compounds across a fixed stationary phase, which is either a solid or a liquid that is immiscible with the mobile phase. HPLC provides qualitative and quantitative information in a single analytical step and allows high-resolution separations in a wide range of compound classes in a short time. As the name suggests, the analyte must be dissolved in a liquid solvent. In general, a HPLC system consists of a solvent reservoir, a pump, an injection valve, a column, a detector and a data processing unit. The general instrumentation is shown in Figure 16 [60, 61].

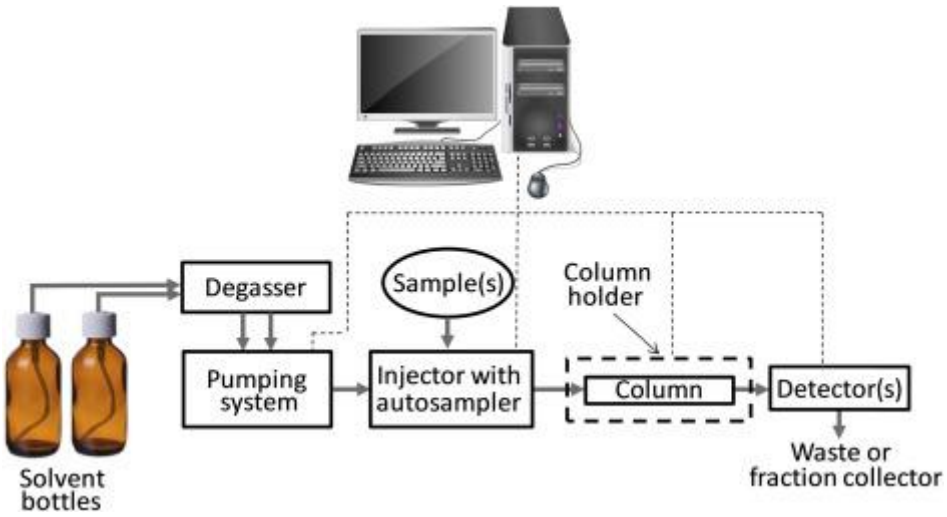

Figure 16: General instrumentation of a high-performance liquid chromatography (HPLC). Reused from Moldoveanu and David, with permission from Selection of the HPLC Method in Chemical Analysis [61].

The chromatographic separation process can be based on different methods such as normal phase, reversed phase (RP) or ion pair chromatography. The RP method, which was used in this work, is based on hydrophobic interactions in aqueous buffers, with increasing organic solvent concentrations employed for elution, typically acetonitrile (ACN) with trifluoroacetic acid (TFA). TFA facilitates

separation through ion-pairing with analytes and enhances peak shape, while also being transparent to UV detection, a crucial method for analysing proteins. As a stationary phase are mostly chemically modified carrier materials applied, such as octadecylsilane (C-18), which allow effective retention and separation of a wide range of nonpolar and moderately polar analytes and offer stability at high pH. The separation process can be optimised by varying various parameters such as the mobile phase composition (pH, gradient, flow rate, solvent strength), selecting an proper stationary phase (particle size, column dimension, pore size), and controlling operational conditions (temperature, sample preparation, injection volume) [60, 62].

The detection method is frequently based on UV/Vis detection, although it is important to note that its sensitivity and linear range can act as limitations in certain applications. Such detectors register substances that absorb UV radiation or visible light at defined wavelengths. For example, FA absorbs at 325 nm and Y at 280 nm [7]. The measurement is conducted at either a fixed wavelength or a variable set of wavelengths, with a diode array detector (DAD) being the most prevalent instrument employed for this purpose [60].

2.5.2 Mass spectrometry

Mass spectrometry (MS) is an analytical method for separating and measuring ions of different masses in a gaseous phase. The sample to be analysed is introduced into the mass spectrometer, where it is vaporised and ionised. In the context of mass spectrometry, the process of ionisation can be executed directly within the gas phase, employing techniques such as electron impact ionisation (EI) or chemical ionisation (CI). However, when a mass spectrometer is linked to a liquid chromatographic system, it is essential to first evaporate the solvent before proceeding with ionisation. The most common techniques employed in this instance are electrospray ionisation (ESI), atmospheric pressure chemical ionisation (APCI), and atmospheric pressure photoionisation (APPI). The mass-to-charge ratio (m/z) of the corresponding ion is determined in the mass analyser, and the intensity of the ion beam can be employed for quantitative analysis. The most common mass analysers are a quadrupole (Q), ion traps, Time-of-Flight (ToF) or hybrid MS, such as Q-ToF or Q-Trap. Furthermore, MS enables the structural clarification of diverse organic compounds and the identification of the element composition and isotope ratios. A mass spectrometer consists of four principal components: an inlet system for the sample, an ion source, a mass analyser and a recording unit. Figure 17 illustrates the construction of the MS system employed in this work [60, 63].

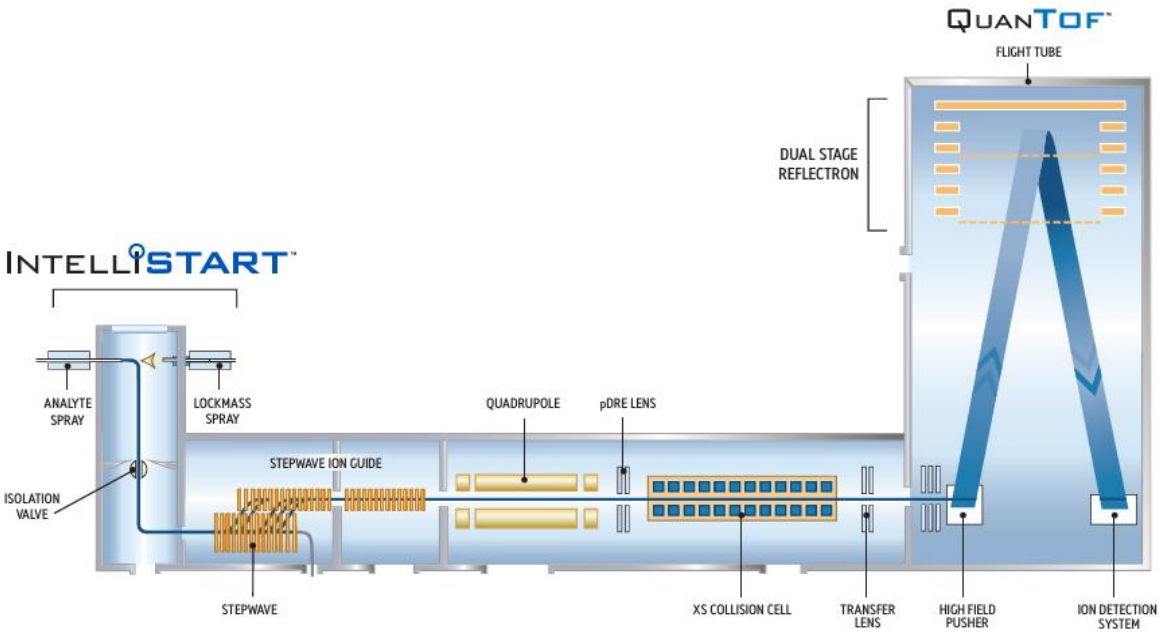

Figure 17: Construction of the Xevo G2-XS QTof mass spectrometer by Waters applied in this work. Reused with the permission from Waters Technology Corporation [63].

In this thesis ESI was applied as an ion source, as the MS was linked to a LC system. The function of the ion source is to facilitate the generation of ions from the analysed molecules. This soft ionisation method is conducted under atmospheric conditions, thus preventing the fragmentation of the analyte by ionisation. This makes it particularly suitable for the analysis of large, non-volatile compounds such as proteins. The interface of the ESI apparatus contains a steel capillary, which is connected to the end of a LC column. A hot inert gas, typically nitrogen, is employed to atomise the liquid sample in a high-voltage field of approximately 3 – 6 kV, thereby creating a Taylor cone with charged droplets. With an increasing solvent evaporation, the droplet size decreases until a critical point is reached (Rayleigh limit), at which a Coulomb explosion occurs, tearing the droplet apart. At the end of this simultaneously repeating cycle, free charged gaseous ions are formed and focussed into the mass spectrometer through an electrical lens system [60, 64].

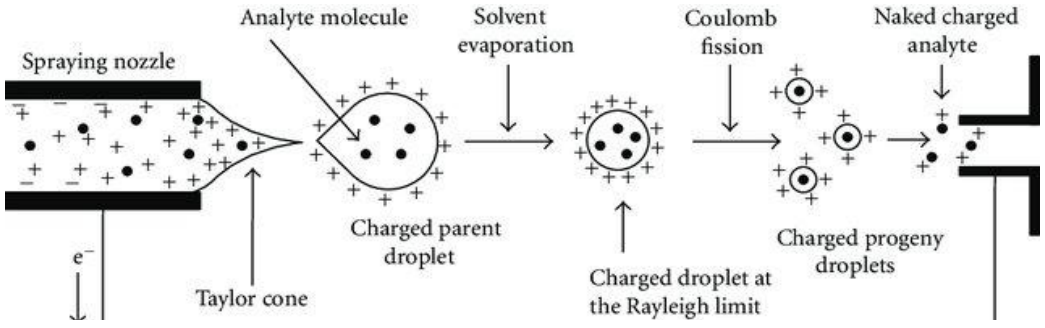

Figure 18: Schematic illustration of an ESI ion source generating ions. Reused from Banerjee and Mazumdar, with permission from International Journal of Analytical Chemistry [64].

In a mass analyser the masses m and the charges z of the ions are analysed, resulting in the mass-to-charge ratio (m/z). In this thesis, a Q-ToF MS was employed (Figure 17). The ions generated by ESI are initially focused into a ray and transferred through the quadrupole. The quadrupole consists of four parallel bars that generate an electric field. Through variation of this field, ions of a specific m/z ratio are permitted to pass through, while other ions are deflected. In addition, to achieve optimal mass resolution, the ion ray must undergo focusing through a series of lenses, including the pDRE lens and transfer lens, as illustrated in Figure 17. Afterwards, the focused ions are able to enter the ToF analyser, where they are analysed in pulses. ToF measures the time taken for the ion to travel a high vacuum chamber, which is referred to as the flight tube in Figure 17. In the flight tube, the ions are accelerated by a high-field pusher, which is applied simultaneously in order to achieve a continuous ion flow divided into small segments of pulses. Lighter ions reach the detector in a shorter time than heavier ions, which allows the determination of their exact m/z values. Consequently, the Q-ToF can offer high resolution, sensitivity and quick scanning, in addition to the structural identification of the compound in a wide mass range. This makes it an ideal instrument for the precise determination of complex samples [63, 65]. In MS, a positive and negative ionisation mode are utilised to detect different types of molecules based on their chemical properties. In the positive ionisation mode, molecules are ionised by gaining a proton or by associating with positively charged ions, such as sodium. This mode is ideal for detecting basic compounds, including molecules with an amino group, such as peptides and proteins. Conversely, the negative ionisation mode is characterised by the ionisation of molecules through the loss of a proton or by association with negatively charged ions, such as chloride. This mode is particularly suited for detecting acidic compounds, such as phenolic compounds [60].

3 Aims

This work investigated the potential of several oxidoreductases, namely Lac, HRP, TYR, GOX and POX, in cross-linking reactions relevant to food systems. The focus of this research stemmed from the growing interest in the use of enzymes to modify food components, with the aim of enhancing their functional properties. A key challenge was the efficient and controlled conversion of target substrates, such as ferulic acid (FA) and tyrosine (Y), and the subsequent application of these modified compounds in cross-linking reactions. The objective of this research was to address several key questions: Firstly, how do these enzymes compare in terms of their catalytic activity and substrate specificity, particularly within a system that ensures compatibility between substrates and measurement techniques? Specifically, what is the efficiency of substrate conversion by the enzymes? Secondly, the study examined how these oxidoreductases differed in their cross-linking behaviour. Do they show a preference for the formation of diverse cross-linking products? Finally, the influence of peptide length and amino acid sequence on the cross-linking ability/efficiency was investigated.

In order to address the previously mentioned questions, a multi-stage approach was employed. Initially, the enzymes were characterised using UV-Vis spectroscopy and enzyme assays with ABTS and Htyr-MBTH to determine their optimal pH, temperature, and kinetic parameters. This facilitated a comparative analysis of enzyme activity and substrate preference. Subsequently, the conversion of FA and Y by individual enzymes and enzyme combinations was assessed. Following this, cross-linking reactions were conducted with monomers, and cereal-specific peptides linked to FA-glycosides, with reaction products identified by LC-MS/MS and RP-HPLC-UV.

4 Materials and methods

4.1 Chemicals and solutions

All used chemicals are listed in Table 1 and the correspondingly prepared solutions are listed in Table 2.

Table 1: Applied chemicals and the corresponding manufacturer and CAS or Lot number.

Chemical	Manufacturer	CAS no./ Lot
2,2'-Azino-bis(3-ethylbenzothiazoline-6-sulfonic acid) diammonium salt, 98 % (ABTS)	Thermo Fisher	30931-67-0
3-Methyl-2-benzothiazolinone hydrazone hydrochloride monohydrate (MBTH)	Sigma-Aldrich	38894-11-0
Acetonitrile ≥ 99.9 %, for HPLC LC-MS grade – suitable for UPLC/UHPLC instruments, HiPerSolv CHROMANORM	VWR	75-05-8
Ammonium acetate ≥ 99 % for LC-MS, HiPerSolv CHROMANORM®	VWR	631-61-8
Ammonium bicarbonate	Honeywell	J2030
Ammonium formate ≥99 % for LC-MS, HiPerSolv CHROMANORM®	VWR	540-69-2
Citric acid monohydrate for analysis, EMSURE® ACS, ISO, Reag. Ph Eur	Merck	5949-29-1
Disodium hydrogen phosphate dihydrate, ≥ 99.5 %, p.a.	Carl Roth	10028-24-7
Disodium hydrogen phosphate, ≥ 99%, p.a., ACS, water free	Carl Roth	500160369
Ferulic acid acyl-beta-D-glucoside, 95 %	AstaTech	7196-71-6
Formic acid, ≥ 99 % for LC-MS, HiPerSolv CHROMANORM®	VWR	64-18-6
Glucose, 99.5 %	Sigma-Aldrich	1002302332
Glucose-oxidase from *Aspergillus niger*, type X-S, lyophilized powder	Sigma-Aldrich	G7141 / 9001-37-0
Hydrogen peroxide 30 %, (Perhydrol®) for analysis, EMSURE®, ISO	Merck	K52245709 013
Hydroxytyrosol, > 97.5 %	Fisher Scientific	10597-60-1
Laccase from *Trametes versicolor*,	Sigma-Aldrich	38429 / 80498-15-3
L-Tyrosine, Ultra; ≥ 99.0 %	Fluka	1288522
N, N-Dimethylformamide for spectroscopy, Uvasol®, ≥ 99.9 %	Merck	68-12-2

Peroxidase from horseradish, type II	Sigma-Aldrich	P8250 / 9003-99-0
Potassium dihydrogen phosphate for analysis, EMSURE®, ISO	Merck	7778-77-0
RapiGest™ SF;	Waters	231981
Sodium acetate trihydrate, EMSURE®, ACS, ISO, Reag. Ph. Eur.	Merck	6131-90-4
Sodium periodate, ACS reagent, ≥ 99.8 %	Sigma-Aldrich	7790-28-5
Tyrosinase from mushroom	MedChem	288356 / 9002-10-2
Tyrosinase from mushroom	Sigma-Aldrich	T3824 / 9002-10-2
Ultrapure water (UHQ), type 1 (conductibility: 0.055 µS/cm, devoid of ionic impurities, microorganisms, organic substances and particles larger than 0.2 µm)	VWR Puranity TU water purification system	NA
Val-Tyr-Val (VYV) peptide, crystalline, V8376, 100 mg	Sigma-Aldrich	102730088
Peptide 1; VNLYQNA, 96.7 %	GenScript	U940NFJPG0-1/PE0796
Peptide 2; LIIPQHY, 95.3 %	GenScript	U940NFJPG0-3/PE0797
Peptide 3; KAEREGC, 98.2 %	GenScript	U940NFJPG0-5/PE0798
Peptide 4; EYFDEKNEQFQCTGT, 98.3 %	GenScript	U940NFJPG0-7/PE0799
Peptide 5; KQGDVVALPAGIVHWCY, 95.2 %	GenScript	U940NFJPG0-9/PE0800
Peptide 6; YQLPSYRTNPCGVSAA, 96.3 %	GenScript	U940NFJPG0-11/PE0801

Table 2: Prepared solutions divided according to the two main experimental parts.

Experiment	Solution name	Preparation
Enzyme characterisation/ Enzyme feasibility with FA & Y	ABTS stock solution (0.5 M)	29.4 mg ABTS dissolved in 5 mL McIlvaine buffer of each pH.
	Acetate buffer (pH 5; 0.1 M)	3 g Na-acetate-trihydrate + 2.9 mL Acetic acid filled to 1 L with water and pH was at 5.0 adjusted.
	Bradford working solution	NA
	BSA stock solution (1 mg/mL)	100 mg BSA dissolved with 100 mL ultra-pure water.
	FA stock solution (10 mM)	48 mg dissolved in 25 mL acetate buffer.
	Glucose stock solution (12.5 mM)	0.991 g D-glucose dissolved in 50 mL McIlvaine buffer pH 5.5.
	GOX stock solution (383 U/mL)	63 mg GOX dissolved in 25 mL acetate buffer.
	H_2O_2 stock solution (1 M)	78.2 µL hydrogen peroxide (30 %) + 921.8 µL water.
	HRP stock solution (1368 U/mL)	21.2 mg HRP (235.8 U / mg solid) dissolved in 30.12 mL acetate buffer.

	Htyr stock solution (10 mM)	38.5 mg Htyr dissolved with 25 mL McIlvaine buffer of the corresponding pH.
	Lac stock solution (1.01 U/mL)	50.4 mg Lac dissolved 25 mL of the corresponding buffer.
	MBTH stock solution pH 4-5.5 (10 mM)	23.4 mg MBTH dissolved with 10 mL McIlvaine buffer of the corresponding pH.
	MBTH stock solution pH 6-6.5 (10 mM)	23.4 mg MBTH dissolved with 1 – 2 mL DMF (100 %) and filled up to 10 mL with McIlvaine buffer of the corresponding pH.
	McIlvaine buffer pH 4, 4.5, 5, 5.5, 6, 6.5 (0.3 M)	According to McIlvaine, 1921 [66]
	NaIO4 stock solution (10 mM)	21.4 mg sodium periodate dissolved in 10 mL McIlvaine buffer with the corresponding pH.
	Pyranose-oxidase from *Phanerocheate chrysosporium rekombinant* prepared in E.coli	NA
	Roti®Quant working solution	1 mL Roti®Quant + 5.5 mL ultra-pure water
	TYR stock solution (6540 U/mL)	3.82 mg TYR from Sigma-Aldrich (6540 U/mg solid) dissolved in 4 mL McIlvaine buffer pH 6.5.
	Y stock solution (0.5 mM)	45.4 mg L-tyrosine dissolved in 500 mL water.
Cross-linking behaviour of monomers/ oligomers	Ammonium acetate (AMAC) buffer (pH 4.5; 0.1 M)	0.69 g ammonium acetate dissolved in 100 mL water and pH adjusted with acetic acid to 4.5.
	Ammonium bicarbonate (AMBIC) buffer (pH 6.5; 0.1 M)	0.70 g ammonium bicarbonate dissolved in 100 mL water and pH adjusted to 6.5.
	FA stock solution (4 mM)	19.5 mg FA dissolved in 25 mL water.
	FAG stock solution (4 mM)	12.0 mg FA glucoside dissolved in 8 mL water.
	Formic acid MS grade (0.1 %)	101 µL Formic acid filled up to 100 mL with water.
	HPLC eluent	0.01 M potassium dihydrogen phosphate + 300 mL methanol
	HRP stock solution (1388 U/mL)	19.2 mg HRP (236 U/mg solid) dissolved in 27.3 mL McIlvaine buffer pH 6.5.
	Potassium dihydrogen phosphate buffer (KH_2PO_4) (pH 6.5; 10 mM)	0.34 g potassium dihydrogen phosphate dissolved in 50 mL water a pH was adjusted with NaOH (1 M) to pH 6.5.
	Lac stock solution (1.01 U/mL)	40.3 mg Lac dissolved in 20 mL AMAC buffer.

	Leucine enkephalin (LeuEnk) stock solution (1 mg/mL)	NA
	P1 stock solution (2.5 mM)	9.3 mg P1 dissolved with 11.34 µL RapiGest solution and filled with 4.534 mL water and vortexed at 35°C for 1 h.
	P2 stock solution (2.5 mM)	9.7 mg P2 dissolved with 10.99 µL RapiGest solution and filled with 4.394 mL water.
	P3 stock solution (2.5 mM)	9.7 mg P3 dissolved with 12.25 µL RapiGest solution and filled with 4.901 mL water.
	P4 stock solution (2.5 mM)	9.4 mg P4 dissolved with 5.11 µL RapiGest solution and filled with 2.045 mL water and vortexed at 35°C for 1 h.
	P5 stock solution (2.5 mM)	9.4 mg P5 dissolved with 5.07 µL RapiGest solution and filled with 2.026 mL water.
	P6 stock solution (2.5 mM)	9.5 mg P6 dissolved with 5.50 µL RapiGest solution and filled with 2.201 mL water.
	RapiGest solution	3 mg disolved in 2 mL 50 mM AMBIC.
	SPE elution solution	0.1 % Formic acid in 90 % ACN
	SPE washing solution	0.1 % Formic acid in ultra-pure water
	TYR stock solution (1250 U/mL)	4 mg of TYR from MedChem (5 kU) dissolved in 4 mL AMBIC buffer pH 6.5.
	VYV tripeptide solution (5 mM)	22.8 mg VYV dissolved in 12 mL water.
	Y stock solution (1 mM)	27.3 mg L-tyrosine dissolved in 150 mL water.

4.2 Instruments

Table 3: Used equipment with the corresponding name and manufacturer, divided according to the experimental parts.

Experiment	Device name	Manufacturer
Enzyme characterisation/ Enzyme feasibility with FA & tyrosine	Analytical balance, 1 mg, XSR225DU/M, d = 0.01 mg / 0.1 mg	Mettler Toledo
	Analytical balance, 10 mg, XPR504S, 1 mg	Mettler Toledo
	Magnetic stirring table MR 3000	Heidolph
	pH electrode LE438	Mettler Toledo
	pH meter SevenCompact	Mettler Toledo
	Plate reader NanoQuantinfinite M200 PRO	TECAN.
	Plate reader software i-control 1.12	TECAN.
	Spectrophotometer Software Spectra Measurment-V-630	Jasco
	Spectrophotometer V-630	Jasco

	Ultrasonic bath SONOREX RK 510 H	Bandelin
Cross-linking behaviour of monomers/oligomers	Analytical balance (min. 1 mg) CP225D	Sartorius
	Centrifugal Concentrator Membrane Vivaspin® 500; 10,000 MWCO PES	Sartorius
	Centrifuge Multifuge X1R Pro	ThermoFisher
	Thermoshaker ThermoMixer C	eppendorf
	Ultracentrifuge Centrifuge 5415 D	eppendorf
	UV-Spectrophotometer Software UV-Probe	Shimadzu
	UV-Spectrophotometer UV-1800	Shimadzu
	Vacuum Concentrator SpeedVac SPD1030	ThermoFisher
HPLC-UV system:	Autosampler Chromaster 5210	VWR Hitachi
	Column Oven Chromaster 5310	VWR Hitachi
	Diode Array Detector Chromaster 5430	VWR Hitachi
	Organizer Chromaster	VWR Hitachi
	Pump Chromaster 5110	VWR Hitachi
	RP C18 column, 10XE184E2G 100 x 3 mm Eurospher II 100-3 C18A	Knauer
	Software Chromaster System Manager V1.2	VWR Hitachi
LC-MS/MS system:	ESI Zspray™	Waters
	LC column ACQUITY UPLC® CSH™ C18 1.7µm (1.0x150mm)	Waters
	MS Software MassLynx V4.2	Waters
	Q-ToF G2-XS QToF	Waters
	Quaternary Solvent Manager Premier QSM	Waters
	Sample Manager FTN Acquity Premier	Waters
	TUV Detector Premier TUV Det	Waters

4.3 Methods

The stepwise approach is divided into 4 main chapters and is summarised in Figure 19.

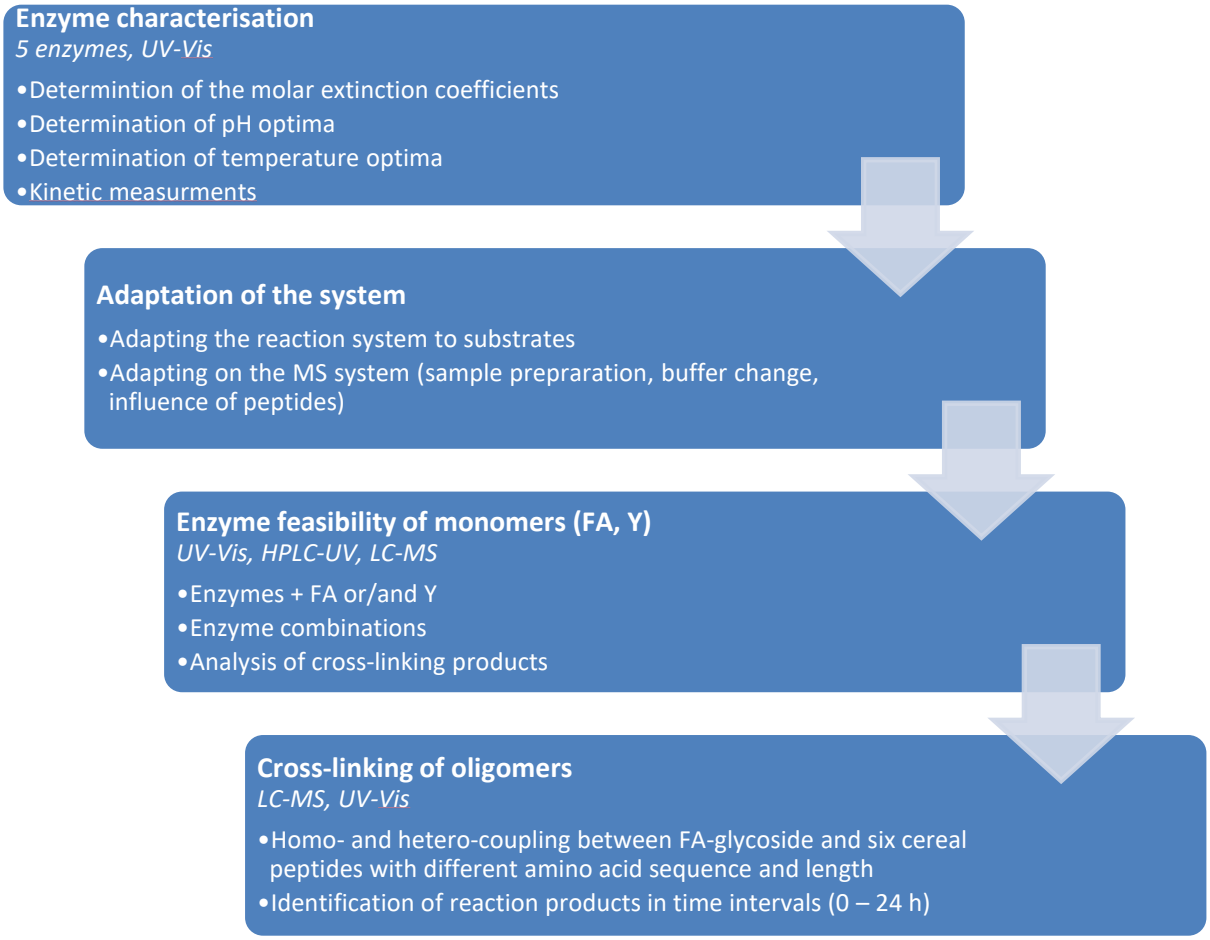

Figure 19: The entire experimental procedure divided into three main categories, with each category involving a series of experiments.

4.3.1 Enzyme characterisation

The measurements were conducted at a temperature of 25 °C and within the pH range of 4 to 6.5 at a speed of 886.9 rpm using the plate reader (plate UV-STAR® Microplate, 96 well, clear by Greiner) and McIlvaine buffer of the corresponding pH value at eight different substrate concentrations (*cf.* Table 10 – 11, Appendix). To determine the enzyme activity, measurement intervals of 20 s up to 180 s, with wavelength of 415 nm for ABTS and 500 nm for Htyr-MBTH were applied.

4.3.1.1 Molar extinction coefficient

The molar extinction coefficient (ε), a pH and concentration dependent substrate parameter, was determined for two different substances ($ABTS^{+\bullet}$ and Htyr-MBTH) during enzyme characterisation. The coefficients for ABTS and Htyr-MBTH through oxidation to the corresponding radicals were calculated at six defined pH values (4, 4.5, 5, 5.5, 6 and 6.5). In the ABTS assay, Lac was used at a concentration of 2 mg / mL, while the Htyr-MBTH assay used a 10 mM $NaIO_4$ solution. The periodate solution was

utilised as an oxidising agent to oxidise Htyr, and as the Htyr-quinone is not stable, the coupling reagent MBTH was applied to generate a Htyr-MBTH complex that could be spectrophotometrically determined. The molar extinction coefficient was calculated using the Lambert-Beer law as shown in Equation 7.

$$A = \varepsilon_{ABTS\ or\ MBTH} * c_{ABTS\ or\ MBTH} * d * f \rightarrow \varepsilon_{ABTS\ or\ MBTH} = \frac{A}{c_{ABTS\ or\ MBTH} * d * f}$$

Equation 7: Lambert-Beer law, with A = absorbance; $\varepsilon_{ABTS\ or\ MBTH}$ = molar extinction coefficient of the corresponding substrate [$M^{-1} \cdot cm^{-1}$]; $c_{ABTS\ or\ MBTH}$ = concentration of each substrate [M]; d = optical path length [cm]; f = dilution factor.

The procedure for the determination of the molar extinction coefficient for Htyr-MBTH, according to Manzano-Nicolas *et al*., involved different steps compared to ABTS [67]. First, various concentrations of Htyr, ranging between 15 – 53 µM, were mixed with a fivefold excess of $NaIO_4$ solution. This mixture was allowed to react for 15 – 25 min to form the quinone. Subsequently, DMF (10 %) was added along with an excess of MBTH to support the solubility of the generated Htyr-MBTH adduct [25]. The reaction was then measured immediately till the maximum absorbance was reached [67].

To obtain the optical path length of the used plate, three samples, previously evaluated on the plate reader, underwent measurements under the same conditions in 1 cm cuvettes (semi-micro, PS by Fisherbrand) on the spectrophotometer in triplicate. The corresponding mean values (Equation 10) were calculated from the measured absorbances, and the layer thickness of the plate was determined by subtracting the values measured in the plate from the values measured in the cuvettes with known layer thickness. Furthermore, the standard deviation (Equation 11) and the relative standard deviation (Equation 12) were calculated.

4.3.1.2 pH optima

The pH optima were determined spectrophotometrically at six different pH values (4 – 6.5 pH) by monitoring the oxidation of the corresponding substrate for each of the five enzymes (Lac, HRP, TYR, GOX and POX). The reactions were started by adding the corresponding enzyme to the mixture and the change in absorbance was measured immediately every 20 s for the duration of 180 s. Substrates were diluted, if necessary, to achieve an increase in absorbance between 0.1 – 0.2 per min. The ABTS-HRP co-assay, which was used for GOX and POX, always contained 16.2 mM glucose and 34 µL of HRP solution. Both assays, ABTS and HTyr-MBTH, when HRP was analysed contained 1 mM H_2O_2 to activate the HRP. The HTyr-MBTH assay always contained 10 % DMF to enhance product solubility and MBTH in a tenfold excess. A wavelength of 415 nm was used for the ABTS assays and 500 nm for the Htyr-MBTH assay. The enzyme activity was calculated according to Equation 8, which was adapted from the Lambert-Beer law from Equation 7.

$$VEA = \frac{\Delta A}{min} * \frac{V_{total} * f}{V_{sample} * \varepsilon * d}$$

Equation 8: Calculation of the volumetric enzyme activity, with VEA = volumetric enzyme activity [U/mL]; $\frac{\Delta A}{min}$ = absorbance difference per minutes; V_{total} = total volume in reaction well (0.340 mL); F = dilution factor; V_{sample} = sample volume in reaction well [mL]; ε = molar extinction coefficient of ABTS or MBTH at the corresponding pH [$M^{-1} \cdot cm^{-1}$]; d = optical path length [cm].

4.3.1.3 Temperature optima

To establish the temperature profiles of the enzymes at their optimal pH, the enzyme activities were determined after tempering the reaction mixtures at five different temperatures (25 °C, 30 °C, 35 °C, 40 °C & 50 °C). For temperatures between 30 – 40 °C, the mixtures were preheated directly in the plate reader, while the 50 °C temperature condition was preheated in a water bath and afterwards analysed through the plate reader. The ABTS assay was used to verify the optimal temperature for Lac and HRP, the ABTS-HRP co-Assay for GOX and POX, and the HTyr-MBTH assay was used for Lac, HRP and mainly for TYR, as this enzyme is inhibited by ABTS.

4.3.1.4 Kinetics

To determine the kinetic parameters, specifically the Michaelis constant K_m and the maximum reaction velocity v_{max}, the enzyme activity of each enzyme was evaluated at six distinct substrate concentrations at the found pH and temperature optimum. The concentrations of ABTS and Htyr were selected in a manner that would result in the generation of a typical Michaelis-Menten plot, as illustrated in Figure 3. Substrate concentrations that were too low resulted in a sharp increase in the observed rate, while those that were too high resulted in a plateau as the active sites of the enzymes became saturated with the substrate. The kinetic values were calculated using the following equations, obtained from Michaelis-Menten kinetics and the Hanes-Woolf plot (Figure 3).

$$\frac{[S]}{v} = \frac{[S]}{v_{max}} + \frac{K_m}{v_{max}}$$

Equation 9: Reorganisation of the Michaelis-Menten equation (Equation 2) to calculate the kinetic values through the Hanes-Woolf plot, with v = volumetric enzyme activity [U/mL]; v_{max} = maximum reaction velocity [U/mL]; [S] = substrate concentration [mM]; K_m = Michaelis constant [mM].

4.3.1.5 Protein concentration

In order to establish the specific enzyme activity, it was necessary to quantify the protein amount, which was done by the Bradford method [68]. This rapid and reproducible analytical method is based on the binding of the dye Coomassie Brilliant Blue G-250 to proteins, which causes a shift in the absorption maximum from 465 to 595 nm [68]. To determine the amount of protein, a bovine serum albumin (BSA) standard solution was prepared with concentrations ranging between 0.001 – 0.5 mg / mL. HRP and GOX were diluted tenfold, TYR was diluted fivefold, POX was diluted 100-fold and Lac was measured undiluted to be in a linear absorbance range (see Table 2, section Experiments: “Enzyme characterisation/ Enzyme feasibility with FA & Y”). In a microtiter plate, 50 µL

of the blank (UHQ water), standard, or diluted enzyme were added and mixed with 200 µL of the Roti®Quant working solution. Each solution was prepared in triplicate. Subsequently, the reaction mixtures were incubated for a period of five minutes in the dark, after which the absorbance was measured at wavelength of 595 nm.

4.3.2 Enzyme substrate specificity for ferulic acid and tyrosine

To determine the substrate specificity for FA and Y, the reaction of each enzyme was observed at pH 4.5 or 6.5 at 30 °C for each monomer by recording a UV-Vis spectrum between 230 – 800 nm in 5 nm steps. The concentrations applied were 2 mM for FA and 0.2 mM for Y. The conversion of FA results in a reduction in absorbance at a wavelength of 280 and especially at 320 nm as during oxidation FA forms quinones that often involve a loss on conjugation in the aromatic system. This reduced conjugation decreases the molecule's ability to absorb light in the UV-Vis, leading to a decrease in absorbance. On the other hand, Y causes an increase in absorbance at the wavelength of 280 nm as Y leads to the formation of dopaquinone, which often involves an increased conjugation or additional chromophoric groups. These changes enhance the molecule's light absorption, resulting in an increase in the absorbance [69]. To observe the individual reactivities, a spectrum was recorded at the start of the reaction (after enzyme addition) up to 5 min in 30 s steps, after 30 min and after 60 min.

Subsequently, the kinetic parameters for FA with Lac and HRP, and for Y with TYR were determined. In addition, three enzyme combinations, namely Lac with TYR, HRP with GOX and HRP with POX, were kinetically analysed. The procedure was identical to chapter 4.3.1.4 Kinetics, with the difference that six various FA and Y concentrations were applied. The molar extinction coefficients for FA and Y were derived from the literature with 13,738 L mol^{-1} cm^{-1} for FA and 5,375 L mol^{-1} cm^{-1} for Y [70, 71].

4.3.3 Cross-linking with monomers

4.3.3.1 Reaction & UV-Vis

In order to examine which enzyme concentrations yield the highest amounts of cross-linking products, preliminary experiments were conducted. Enzyme concentrations of Lac, HRP and TYR were varied (Lac = 0.001 – 0.1 mg / mL; HRP = 0.003 – 0.3 mg / mL; TYR = 0.0005 – 0.05 mg / mL) and reacted individually with the respective monomers. Incubation times ranging from 0 to 60 min were applied (30 °C; 112 g-force), to investigate the formation of different products over time. Subsequent to the completion of the respective reaction times, a UV-Vis scan (200 – 400 nm) was conducted to observe the progress of the reaction. The reactions were terminated by the addition of 10 µL of 10 % formic acid.

Afterwards, the stopped reaction mixtures were processed accordingly. The first step involved ultra-filtration (Pierce™ Protein Concentrators PES, 3K MWCO, 0.5 mL by Thermo-Fisher Scientific) of the solutions (10 min; 10,000 g-force) to separate the enzymes, followed by a purification through solid phase extraction (SPE). For SPE, self-made stage tips were applied. For this purpose, five layers of filter (Empore™ Extraction Disks SDB-XC, 47 mm) were put in a 1 mL pipette tip and the tip was put on a drilled through Eppendorf tube (2 mL and 1.5 mL). Firstly, the filters were pretreated with 250 µL of methanol (3 min; 7,168 g-force) and then with 250 µL of 0.1 % formic acid (3 min; 7,168 g-force). Subsequently, the filter was loaded with 200 µL of the analyte mixture (20 min; 1,508 g-force) and washed with 500 µL of 0.1 % formic acid (12 min; 4,032 g-force). The analyte was then eluted into a new vessel with 300 µL of 0.1 % formic acid in 90 % ACN (8 min; 1,792 g-force). Lastly, the sample mixtures were evaporated in a vacuum centrifuge (~1 h; 45 °C; 800 Pa). Prior to measurement the dried sample was redissolved in 200 µL of 30 % ACN with 0.03% formic acid and diluted 10 times in low protein binding vials for further analysis by LC-MS/MS to determine cross-linking products.

In order to provide a more realistic representation of cross-linking reactions, the FA/Y ratio was varied. Firstly, it was acknowledged that the amount of Y present within the grain is 5 – 10 times higher than bound phenolic acids (BPA). Secondly, the reactivity of Y is approximately 10 times lower than that of FA [51]. For this reason, the reactions were conducted with not only a FA/Y ratio of 1:1 but also 1:5, as the ratio of five was determined to be the median in earlier analysis. A total of six enzymes or enzyme combinations were applied for this purpose. The reactions involving Lac, HRP, Lac/TYR and HRP/GOX were conducted at pH 4.5, while those involving HRP and TYR were performed at pH 6.5. All experiments were prepared in triplicate in a total volume of 3 mL and incubated at 30 °C in a water bath. Each series of experiments contained 33 µM FA, 33 µM or 167 µM Y, and 0.03 U / mL enzyme (1 unit = change in absorbance of 0.01/min at 280 nm, respectively 320 nm, at pH 4.5, respectively 6.5, in an AMAC, respectively AMBIC buffer (0.1 M), at 30 °C in a reaction volume of 0.34 mL containing 33 µM FA, respectively 167 µM Y). Furthermore, 1 mM H_2O_2 was used in the reactions involving HRP and 18 mM glucose was employed for the enzyme combination of HRP/GOX. The buffers used were 50 mM AMAC (pH 4.5) and AMBIC (pH 6.5). The reaction mixtures were analysed after 0, 0.25, 0.5, 1, 2, 4, 6 and 24 h. A rapid scan between 200 – 600 nm was recorded on the photometer within 40 s in each case. Subsequently, 100 µL was aliquoted twice and stopped with 10 µL of 10 % formic acid. These samples were then evaporated in a vacuum centrifuge (~1 h; 45 °C; 800 Pa) and frozen at -20 °C.

4.3.3.2 HPLC-UV

In addition to the UV-Vis measurements, the analysis by RP-HPLC-UV was performed. The dried samples were resuspended in 200 µL of KH_2PO_4 buffer containing 15 % methanol (10 mM; pH 6.5). To detect potential cross-linking products, a run time of 30 min with a flow rate of 0.7 mL / min and a

column temperature of 40 °C was applied. The HPLC gradient of eluent A (20 mM KH_2PO_4, pH 2.0), eluent B (25 % ACN (w/w) in KH_2PO_4 buffer, pH 2.0) and eluent C (50 % ACN (w/w) in water) is shown in Table 4. The specific settings for the RP-HPLC-UV method are listed in Table 5. The evaluation process involved an external calibration for FA and Y, utilising a concentration range from 0.78 to 100 µM. The calibration curves are shown in Appendix, Figure 39.

Table 4: Applied gradient of eluent A (20 mM KH_2PO_4, pH 2.0), eluent B (25 % ACN (w/w) in KH_2PO_4 buffer, pH 2.0) and eluent C (50 % ACN (w/w) in water) for the HPLC measurements.

Time [min]	Solvent A [%]	Solvent B [%]	Solvent C [%]
0	100	0	0
1.0	100	0	0
4.0	100	0	0
5.0	0	100	0
12.0	0	100	0
13.0	0	0	100
16.0	0	0	100
17.0	100	0	0
19.0	100	0	0

Table 5: Settings for the RP-HPLC-UV analysis.

Category	Parameter	Settings
Configuration parameters	Channel 1 detector 5430	NA
	Column oven 5310	NA
	Autosampler 5210 + thermostat	NA
	Pump 5110	NA
	Setting temperature	20 °C ± 5 °C
Column parameters	Column type	RP C18, 10XE184E2G, Eurosphere II
	Column length	100 mm
	Column diameter	3 mm
Detector setup	Spectral bandwidth	4 nm
	Sampling period	400 (2.5 Hz) ms
	Wavelength range	200 to 600 nm
	Monitoring wavelength	280 & 320 nm

4.3.4 Cross-linking with oligomers

In respect of the relatively high salt content of the used McIlvaine buffer employed for LC-MS/MS, it was necessary to modify and adapt the buffer to a MS friendly system. For this reason, an ammonium acetate buffer (AMAC) was used for pH 4.5, while an ammonium bicarbonate buffer (AMBIC) was used for pH 6.5. Initially, a range of buffer concentrations (0.1 – 0.02 M) were analysed to obtain whether they influenced the enzyme activities to any significant degree. Furthermore, as the peptides were not water soluble, a solubility improver had to be applied. Therefore, the influence of DMF and Rapigest, as detergents that enhance solubility in aqueous solutions without compromising MS, was investigated in relation to the activity of the enzyme. In this instance, two concentrations of Rapigest (0.1 % and 0.05 %) and one DMF concentration (10 %) were analysed.

For LC-MS/MS analysis, an ultra-performance liquid chromatography (UPLC) with an ACQUITY UPLC® CSH™ C18, 1.7 µm, 1.0x150 mm column was coupled with a MS consisting of a quadrupole and time-of-flight (Q-ToF) mass analysers. Furthermore, a UV detector was used to detect FA at a wavelength of 320 nm and Y at 280 nm. To identify the cross-linking products, a run time of 43 min with a flow rate of 0.1 mL / min and a column temperature of 60 °C were applied. The LC gradient of eluent A (0.1 % formic acid in H_2O) and eluent B (0.1 % formic acid in 98 % ACN and 2 % H_2O) is shown in Table 6. The measurements were performed using a positive ionisation. The specific settings of the LC-MS/MS are listed in Table 7.

Table 6: Applied LC gradient of eluent A and B. Eluent A = 0.1 % formic acid in H_2O; eluent B = 0.1 % formic acid in 98 % ACN and 2 % H_2O.

Time [min]	Eluent A [%]	Eluent B [%]
0	99	1
1	99	1
5	75	25
25	50	50
28	40	60
30	20	80
34	90	10
34.1	99	1
43	99	1

Table 7: Settings for the measurements with LC-MS/MS.

Category	Parameter	Settings
Acquisition	Source	ES
	Polarity	Positive
	Analyser Mode	Sensitivity
	Dynamic Range	Normal
TOF MS	Low Mass	100 Da
	High Mass	3000 Da
	Scan Time	0.5 s
Collision Energy	Low Collision Energy	6 V
	High Ramp Collision Energy	15 to 45 V
Cone Voltage	Cone Voltage	30 V

Subsequently, reactions were also carried out with larger molecules. In place of Y, the tripeptide VYV (valine-tyrosine-valine) and the pentapeptide Leu-enkephalin (LeuEnk) (tyrosine-glycine-glycine-phenylalanine-leucine) were applied, and in place of FA, the FA glycoside was employed. Afterwards, FA glycoside (FAG) was enzymatically linked with six small peptides. The peptides were selected to be representative of three short, not variety specific cereal sequences (P1 – P3) and three longer cereal-specific sequences (P4 – P6). P1 contained a Y residue within the peptide sequence, P2 had a terminal Y, and P3 had no Y. Conversely, P4 was a unique rice peptide from a glutelin type-B 4, P5 was an oat peptide from a 12S seed storage globulin 1, and P6 was a maize peptide from a zein-beta protein. A total of five enzymes or enzyme combinations were used for the formation of linkages (Lac, HRP, TYR, Lac/TYR and HRP/GOX). The two enzyme combinations, Lac/TYR and HRP/GOX (both at pH 4.5), were hetero-linked in a FA/Y ratio of 1:5, whereby the individual enzymes Lac, HRP (both at pH 4.5) and TYR (pH 6.5), were also homo-linked. The homogeneous reactions were performed in duplicate, while the heterogeneous reactions were performed in triplicate. The concentrations of the substrates were 0.1 mM for FAG, 0.5 mM for the peptides and 0.03 U / mL (1 unit = change in absorbance of 0.01 / min at 280 nm, respectively 320 nm, at pH 4.5, respectively 6.5, in an AMAC, respectively AMBIC buffer (0.1 M), at 30 °C in a reaction volume of 0.34 mL containing 33 µmol FA, respectively 167 µM Y) for the enzymes. Additionally, each peptide solution contained 0.25 % Rapigest, as the peptides were not water soluble. Moreover, 1 mM H_2O_2 was applied in the reactions involving HRP alone, and 18 mM glucose was employed for the enzyme combination of HRP/GOX. The buffers used were 50 mM AMAC (pH 4.5) and AMBIC (pH 6.5). The formation of cross-linking products was analysed at three time points: 0.5 h, 2 h and 24 h. The reactions were incubated at 30 °C in a water bath and stopped at the corresponding time interval with 10 µL of 10 % formic acid. Subsequently, the solutions were

evaporated using the SpeedVac and frozen at -20 °C. For the LC-MS/MS measurement, the dried samples were resuspended in 200 µL of 30 % ACN with 0.03 % formic acid, followed by a tenfold dilution. The evaluation was carried out by selecting the identified peaks from the chromatogram and determining the m/z ratio from the MS spectra, from which the mass of the products or fragments could then be identified.

4.4 Statistical analysis

The mean value was calculated according to equation 10.

$$\bar{X} = \sum \frac{x_i}{n}$$

Equation 10: Determination of the mean value $\bar{X}$, with x_i…determined value; n…number of values.

The standard deviation (SD) was calculated according to Equation 11.

$$SD = \sqrt{\sum_i^n \frac{(x_i - \bar{X})^2}{n-1}}$$

Equation 11: Determination of the standard deviation (SD).

The relative standard deviation (RSD) was calculated according to Equation 12.

$$RSD\ [\%] = \frac{SD}{\bar{X}} * 100$$

Equation 12: Determination of the relative standard deviation (RSD).

The results of the determination of the pH and temperature optima were statistically analysed by one way analysis of variance (ANOVA) using Microsoft Excel version 2412. An alpha value of 0.05 was applied. In conclusion, if the calculated F-value was higher than the F_{crit}-value and the p-value was lower than 0.05, a significant difference was identified between the analysed data points. As a Post-hoc test was the Tukey´s test applied. In order to identify potential outliers, the Dixon test was provided according to Matissek and Fischer [60].

5 Results and discussion

5.1 Enzymatic characterisation

The objective of this study was to compare the activity of different enzymes by utilising a variety of assay systems. The primary substrates of particular interest were Y and FA. However, it was noted that these substrates were not processed by all of the enzymes under investigation. To obtain a more comprehensive understanding of enzymatic activity, the ABTS, respectively ABTS-HRP co-assay, and the Htyr-MBTH assay were applied according to chapter 4.3.1. The ABTS assay is suitable for all enzymes except TYR, while the Htyr-MBTH assay specifically targets three enzymes (Lac, HRP and TYR), providing a comparative approach. The application of these additional assays was undertaken to ascertain whether any correlations or functional relationships could be inferred beyond the direct substrate specificity of Y and FA.

5.1.1 Determination of molar extinction coefficients

Firstly, the layer thickness of the used plate was determined according to chapter 4.3.1.1. For this purpose, the three reaction mixtures listed in Table 8 were analysed in cuvettes with a defined layer thickness of 1 cm.

Table 8: Applied solutions and the corresponding volumina for the determination of the path length.

Lac pH 4.5 [µL]	ABTS solution [µL]	Total volume [µL]	Resulting ABTS concentration in well [mM]
1020	0	1020	0
960	60	1020	0.0063
894	126	1020	0.0132
795	225	1020	0.0236

Initially, using the Lambert-Beer law (Equation 7), the concentration of each sample was determined within 1 cm cuvettes. Subsequently, this data enabled the determination of the plate's layer thickness that is summarised in Table 9.

Table 9: The measured absorbance of three different ABTS concentrations in cuvettes (d = 1 cm) and plate, and the calculated layer thickness of the plate.

ABTS [µM]	**6.3**			**13.2**			**23.6**		
Absorbance in cuvettes (d = 1 cm)	0.286	0.285	0,285	0.503	0.501	0,498	0.834	0.832	0.831
Absorbance in plate	0.203	0.227	0,228	0.387	0.428	0,498	0.706	0.714	0.835
Mean $_{cuvettes}$		0.285			0.501			0.832	
Mean $_{plate}$		0.220			0.438			0.751	
d $_{plate}$ (Abs_{plate}/ $Abs_{cuvettes}$) [cm]		0.769			0.874			0.903	
d $_{mean}$ [cm]					**0.849**				
d $_{SD}$ [cm]					**0.070**				
d $_{RSD}$ [%]					**8.28**				

In order to determine the molar extinction coefficient of both products, it was necessary to determine the absorption maximum according to chapter 4.3.1.1. In the case of $ABTS^{\bullet+}$, the maximum was identified at the start of the reaction, at 415 nm for each pH (Figure 21), which also corresponded to the findings of previous studies [22, 72, 73]. The generated $ABTS^{\bullet+}$ showed a light green colouration, which became darker as the ABTS amount increased (Figure 20 (A)) and when storing the mixtures for a longer time (> 30 min), a darker colouration was observed. This also resulted in a decrease in absorbance and a slight shift of the absorption maximum to a smaller wavelength (approx. 405 nm). This change was probably caused by the formation of the di-cation radical $ABTS^{++}$, which can occur through further oxidation of $ABTS^{+}$ when the oxidising species, in this case the enzyme Lac, is present in higher concentrations [21]. This effect is described in greater detail in Figure 4 and chapter 2.3.2.1 ABTS assay.

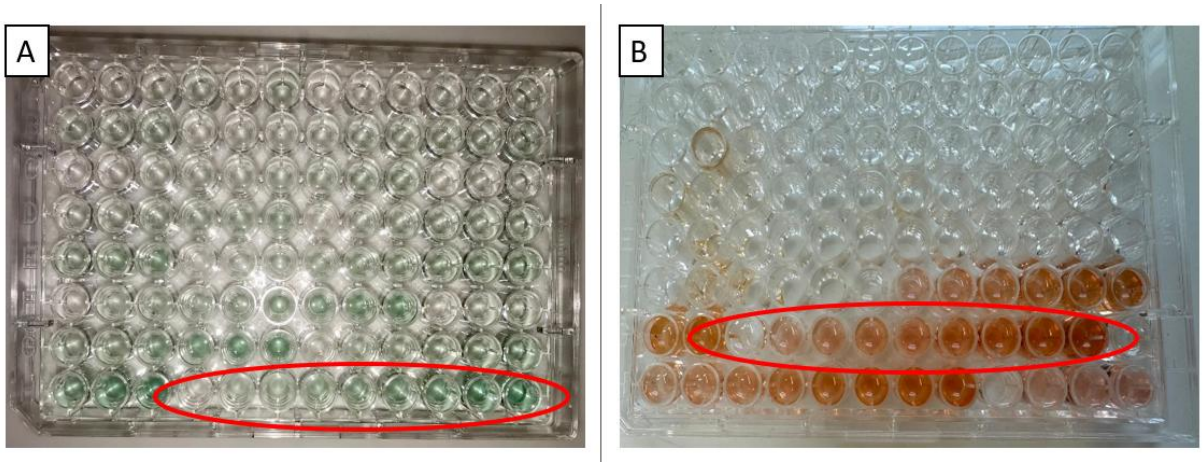

Figure 20: The coloration of the reaction mixtures for ABTS (A) and MBTH (B) is particularly visible in the red circles. The substrate concentration increases from left to right.

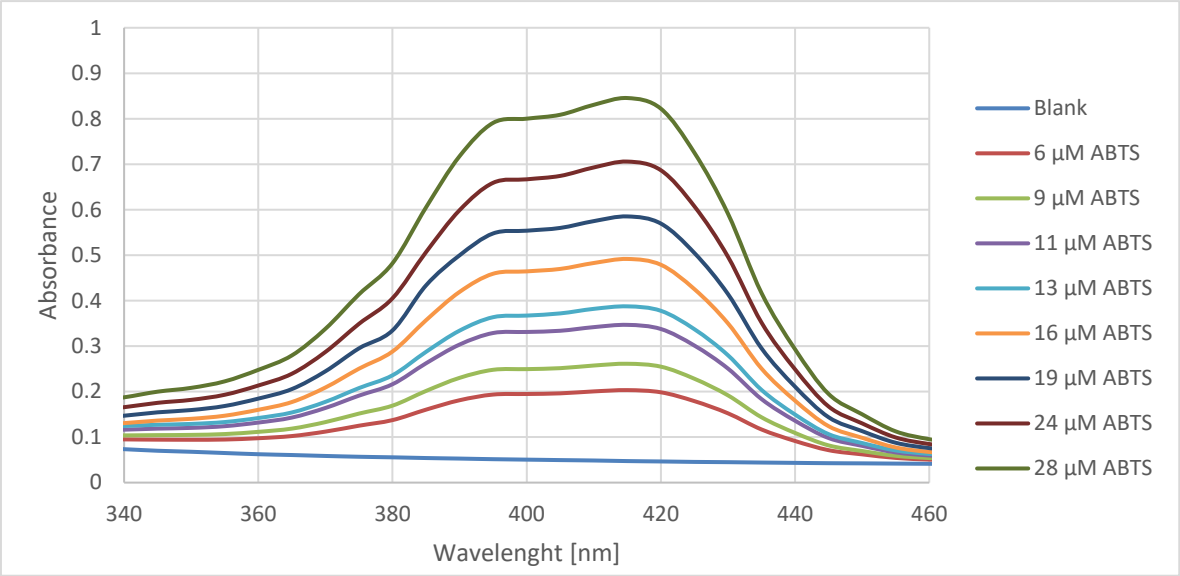

Figure 21: Absorption spectra of different concentrations of ABTS (0 – 28 µM) with laccase in excess in McIlvaine buffer at a pH of 4. The spectra were recorded in triplicate at a temperature of 25 °C. The mean values were then displayed, and an absorption maximum was found at 415 nm after the start of the reaction.

Subsequently, the absorbances measured at 415 nm were plotted against the corresponding ABTS concentrations in the reaction well (see Appendix, Figure 33). The slopes obtained from the measurements represent the corresponding molar extinction coefficient, which must be adjusted based on the path length used in the experiment. According to Equation 7, this adjustment involves dividing the slope by the determined path length of 0.85 cm. A comparison of the molar extinction coefficients experimentally determined with existing literature values are listed in Table 10.

Table 10: Molar extinction coefficients of ABTS at six different pH values compared to the literature. The determined values were provided at 25 °C by using the McIlvaine buffer.

pH	$\varepsilon_{determined}$ [L mol^{-1} cm^{-1}]	$\varepsilon_{literature}$ [L mol^{-1} cm^{-1}]
6.5	33,244	28,500 [74]
6	34,117	21,100 [75] 25,600 [76] 27,000 [74] 36,000 [76]
5.5	31,514	-
5	30,827	31,330 [75] 35,000 [21] 36,000 [77, 78]
4.5	30,971	26,700 [74] 36,000 [79]
4	35,989	33,120 [75] 36,000 [80] 36,800 [81]
Mean value	32,777	-

No observable tendency could be identified in the determined extinction coefficients at the analysed pH range. Moreover, it is difficult to ascertain from the available literature whether there is a pH-dependent trend. It is evident that there are significant variations in the individual literature values in certain cases. For instance, at pH 6 the values are observed to be between 21,100 – 36,000 L mol^{-1} cm^{-1}. A trend was observed only in the thesis by Fürst, whereby the coefficient demonstrated a decrease in a pH range of 3 – 8 with an increasing pH value [75]. However, this hypothesis was not confirmed in the present case, as there was rather a scattering between the selected pH values. To minimise the impact of potential random variations in the determination process, the mean of the experimentally determined values was calculated (32,777 L mol^{-1} cm^{-1}) as seen in Table 10. While the calculation of the mean is an effective method of reducing the influence of random errors by averaging out fluctuations, it is important to note that it does not eliminate systematic errors, which would result in all individual measurements being affected in the same direction. The employment of multiple determinations and the calculation of means was primarily aimed at improving the precision of the molar extinction coefficient by accounting for random variability. This coefficient was subsequently employed in the further calculations.

The same procedure was also applied with the Htyr-MBTH complex. The absorption maximum was identified at 500 nm for each pH (Figure 22), which also corresponds to the findings from various literature [25, 26, 82]. The generated complex was characterised by a light orange-red colouration that became darker as the concentration of Htyr increased (Figure 20 (B)).

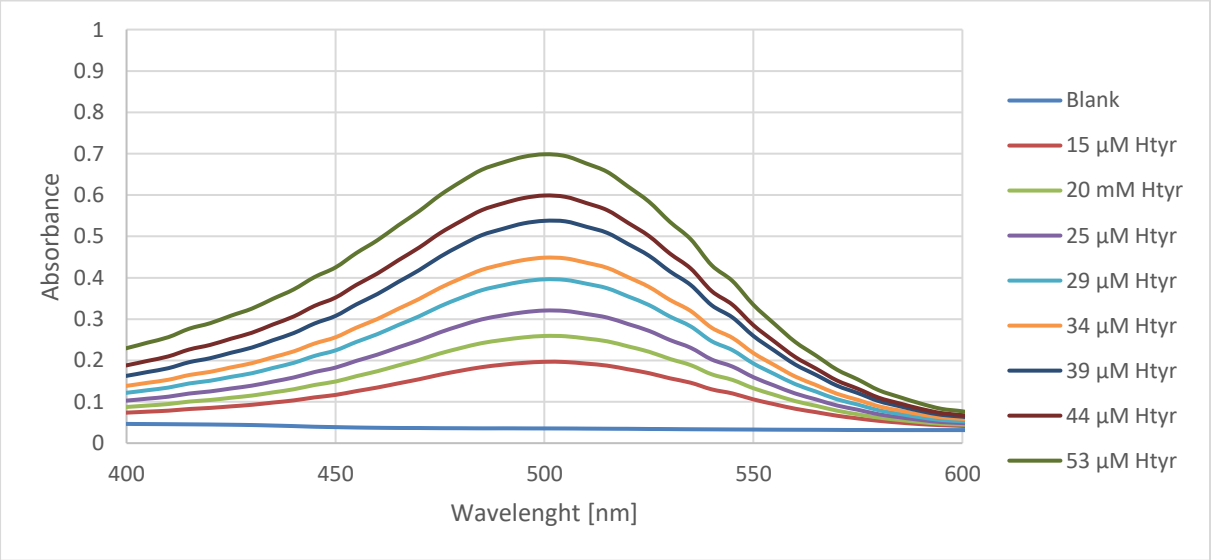

Figure 22: Absorption spectra of different Htyr concentrations (0-53 µM) with $NaIO_4$ and MBTH in excess in McIlvaine buffer at a pH of 4. The spectra were recorded in triplicate at 25 °C, with an absorption maximum found at 500 nm after 15 – 30 min.

The molar extinction coefficients of Htyr were determined in the same way as for $ABTS^{\bullet+}$ described above. The determined absorbances with the plotted Htyr concentrations are shown in the Appendix,

Figure 34. The determined extinction coefficients and the literature values with the corresponding substrate are listed in Table 11.

Table 11: Molar extinction coefficients of Htyr with MBTH as a coupling reagent at six different pH values compared to the literature. The determined values were provided at 25 °C using the McIlvaine buffer.

pH	$\varepsilon_{determined}$ [L mol^{-1} cm^{-1}]	$\varepsilon_{literature}$ [L mol^{-1} cm^{-1}]	Substrate applied in literature
6.5	10,604	22,000 [26] 22,300 [83]	Tyrosol Tyrosine
6	13,105	-	-
5.5	12,062	-	-
5	14,545	17,500 [25] 20,700 [25]	Catechol Dopamine
4.5	16,988	32,500 [82, 84] 38,000 [82]	Phenol, Catechol Tyrosine
4	13,551	-	-
Mean value	13,476	-	-

The determination of the molar extinction coefficient of Htyr with MBTH also showed no pH-dependent trend as shown in Table 11. For this reason, the mean value (Equation 10) of all absorbance values was also calculated and the value of 13,476 L mol^{-1} cm^{-1} was applied for further calculations.

A comparison of the obtained data with the literature values reveals that the measured extinction coefficients are lower than those reported in previous studies. One of the reasons could be the lack of a literature value for Htyr with MBTH. The most relevant substrate is tyrosol (pH 6.5), as this is oxidised to Htyr by TYR, which subsequently produces the reactive quinone [26]. Previous studies applied various phenolic compounds, such as tyrosine, catechol or dopamine [25, 82-84]. Furthermore, the Htyr-MBTH assay is not used as often as the ABTS assay, which results in a limitation of available literature data. Additionally, the stoichiometry of the reaction may also contribute to differences in the values observed between the present work and the literature. It was asserted that two moles of Htyr react to form one mole of Htyr-MBTH adduct. This means that the determined extinction coefficient would require a correction by the stoichiometric factor of two, which would result in a relatively close correlation with the literature values. Nevertheless, this hypothesis has not been confirmed in the existing literature and thus was not applied in this work [85].

5.1.2 Protein concentration

The protein concentration of the enzymes was determined *via* Bradford Assay according to chapter 4.3.1.5. The calibration curve with BSA as a standard is given in Figure 23, with the corresponding

absorbance values listed in Appendix in Table 22 – 23 and the resulting protein concentrations listed in Table 12.

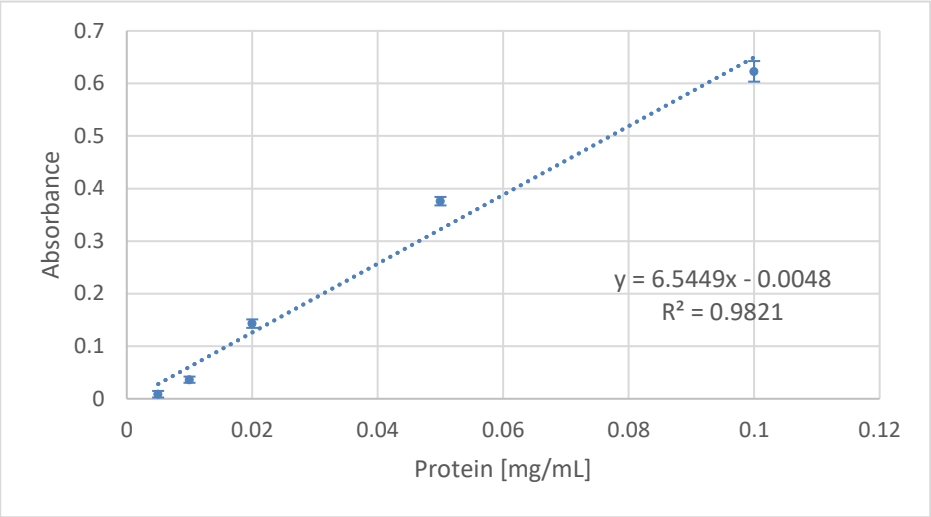

Figure 23: Calibration curve for the determination of the protein concentration determined in triplicate with the corresponding linear regression equation and coefficient of determination on the right.

Table 12: The protein concentrations for Lac, HRP, TYR, GOX and POX calculated in triplicate, along with the respective values of blank-corrected absorbance and dilution factor used for their determination.

Enzyme	**Lac**	**HRP**	**TYR**	**GOX**	**POX**
Dilution factor	1	10	5	10	100
Mean absorbance	0.701	0.935	0.924	1.39	1.48
SD	0.062	0.007	0.004	0.04	0.02
Blank corrected absorbance	0.025	0.212	0.202	0.743	0.840
Mean protein concentration [mg/mL]	0.005	0.33	0.16	1.14	12.9

The protein concentrations of the enzymes utilised in this study differ drastically, with Lac demonstrating the lowest concentration of 0.005 mg / mL and POX exhibiting the highest at 12.9 mg / mL. These differences highlight the requirement for normalisation when conducting comparisons between enzymatic activities. The determination of specific activity, which accounts for enzyme activity relative to protein concentration, is essential for the accurate assessment of catalytic efficiency. The absence of such a normalisation process can potentially lead to misleading conclusions, as higher enzyme concentrations may artificially inflate activity readings. Therefore, including protein concentration is essential for ensuring a more precise evaluation of enzymatic performance across different assays.

5.1.3 pH optimum of each enzyme

This chapter deals with the pH optima of five enzymes (Lac, HRP, TYR, GOX, and POX) by assessing their substrate oxidation at varying pH levels using three different enzyme assays (ABTS assay, ABTS-HRP co-assay and Htyr-MBTH assay) according to chapter 4.3.1.2. The objective was to investigate how pH influences the corresponding enzymatic activity and whether distinct trends can be observed among these enzymes. It was hypothesised that each enzyme possesses a distinct pH range in which it demonstrates its maximal catalytic efficiency. The objective was to determine the narrowest possible pH range that would maximise the enzyme activity while remaining suitable for utilisation in dough-related applications. Ideally, the selected pH range should provide optimal cross-linking with the fewest possible pH adjustments per enzyme. Two various pH values were considered to facilitate efficient enzymatic performance while ensuring practical applicability in food processing.

The absorbances were measured each 20 s for a total of 180 s and a calibration curve for each experiment was created. In some cases, the curve did not start to rise at the start of the reaction. This phase is also called the lag phase, which refers to a time interval that must pass before the enzymes starts the reaction [86]. In other cases, the curve became flatter over time, indicating saturation of the reaction. In order to minimise the systematic error, the values in these ranges were excluded. In addition, only data where the coefficient of determination (R^2) was > 0.99 were included in the calculation. This led to the determination of ΔA / min, which was used in Equation 8 to calculate the enzyme activity. Lac with ABTS at pH 4 is used as an example calculation and the corresponding enzyme activity is calculated in Equation 13.

$$VEA = \frac{\Delta A}{min} * \frac{V_{total} * f}{V_{sample} * \varepsilon * d} = 0.1258 * \frac{0.34\ mL * 40}{0.03\ mL * 32.78\ \frac{mL}{mol * cm} * 0.849\ cm} = 2.78 \frac{U}{mL}$$

Equation 13: Calculation of the enzyme activity according to Equation 8 using Lac at pH 4 as an example. 1 U is defined as the change in absorbance of 0.1 / min at 415 nm for ABTS, respectively 500 nm for Htyr-MBTH, at the corresponding pH between 4 – 6.5 in an McIlvaine buffer (0.3 M), at 25 °C in a reaction volume of 0.34 mL containing 1 mM ABTS, respectively 1 mM Htyr.

Finally, the specific enzyme activity was calculated in Equation 14 using the determined protein concentration from Table 12. The results of the determination of the pH optimum of Lac, HRP, TYR, GOX and POX with the corresponding substrate are shown in Figure 24.

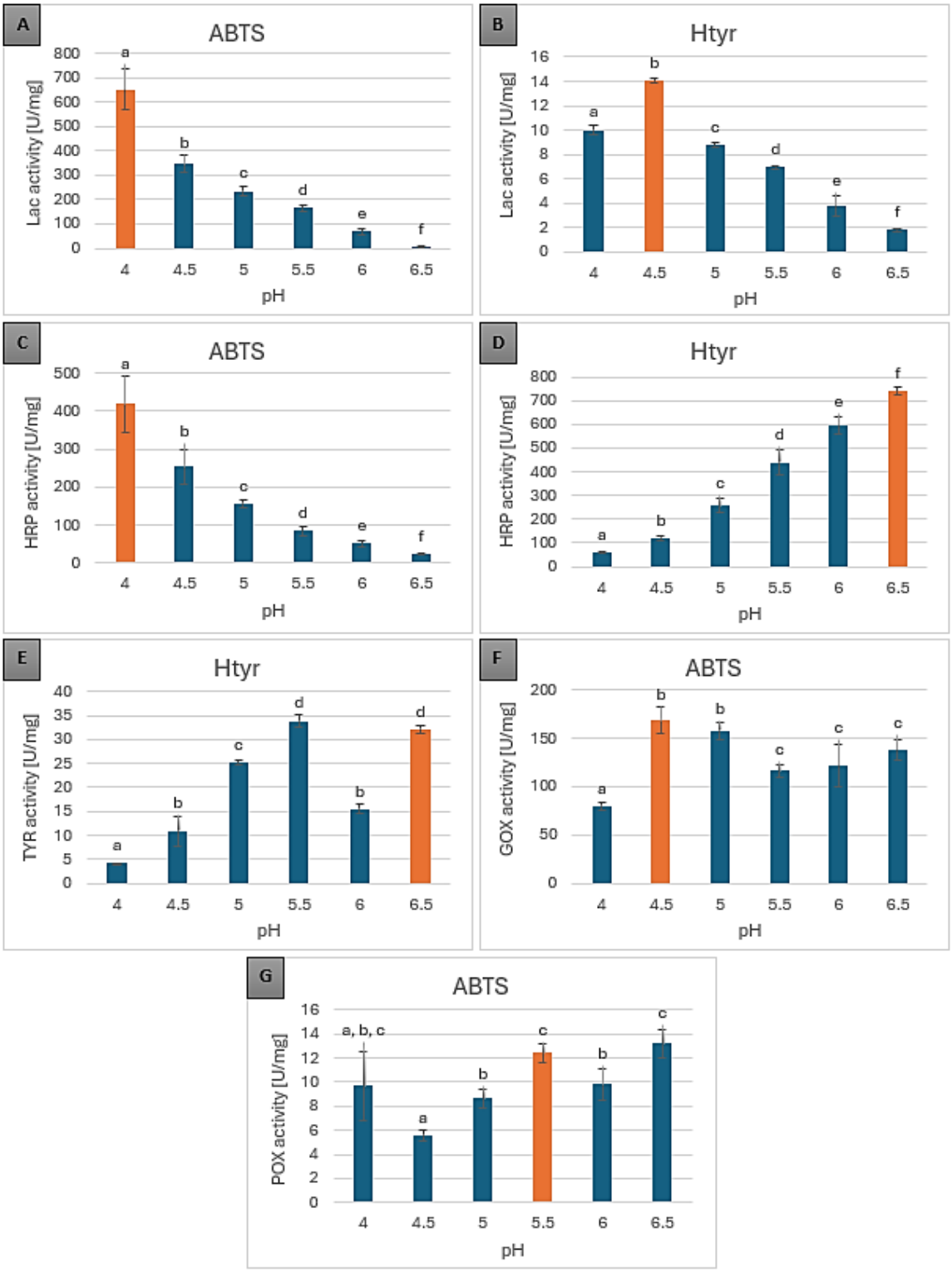

Figure 24: Results of the determination of pH optima for Lac using ABTS assay (A) and Htyr-MBTH assay (B), HRP using ABTS assay (C) and Htyr-MBTH assay (D), TYR using Htyr-MBTH assay (E), GOX (F) and POX (G) using ABTS-HRP co-assay. 1 U is defined as the change in absorbance of 0.1 / min at 415 nm for ABTS, respectively 500 nm for Htyr-MBTH, at the corresponding pH between 4 – 6.5 in a McIlvaine buffer (0.3 M), at 25 °C in a reaction volume of 0.34 mL containing 1 mM ABTS, respectively 1 mM Htyr. The various letters above the bars indicate the significant differences between the corresponding pH values calculated by one-way ANOVA ($p < 0.05$). The pH values highlighted in orange were applied in further determinations.

$$SEA = \frac{VEA}{Protein\ concentration} = \frac{2.78\frac{U}{mL}}{0.0045\frac{mg}{mL}} = 617\frac{U}{mg}$$

Equation 14: Calculation of the specific enzyme activity (SEA) using Lac with ABTS at pH 4 as an example. 1 U is defined as the change in absorbance of 0.1 / min at 415 nm for ABTS, respectively 500 nm for Htyr-MBTH, at the corresponding pH between 4 – 6.5 in a McIlvaine buffer (0.3 M), at 25 °C in a reaction volume of 0.34 mL containing 1 mM ABTS, respectively 1 mM Htyr.

For Lac, a clear trend was identified, as it can be seen in the bar charts illustrated in Figure 24 (A – B). The maximum value for ABTS is at pH 4 (Figure 24 (A)), while for Htyr the maximum was reached at pH 4.5 (Figure 24 (B)). In both cases, there was a reduction in Lac activity with an increasing pH value. However, at pH 4.5, Htyr exhibits an exception, where the enzyme activity achieved its maximum. In literature, similar values were reported. In a review by Baldrian, the pH optima of 49 studies involving the interaction of Lac and ABTS were compared [27]. The optimum pH values were between 2.0 and 5.0, with a median of 3.0. Given that the lowest pH value applied in this work was 4.0, it is reasonable to conclude that the findings are consistent with the data presented. In addition, this review investigated other substrates, such as 2,6-dimethoxyphenol, which may potentially correlate with Htyr, in terms of their reactivity with the enzyme under similar conditions or through shared enzymatic mechanisms. In comparison with ABTS, the pH range was observed to be higher, ranging from 3.0 to 8.0, with a median value of 4.0, which was also higher. This may explain the slight difference in the pH optimum for the substrates analysed, as literature also indicates that various substrates may provide different pH optima, despite the usage of the same enzyme.

The evaluation of the pH maximum for HRP in Figure 24 (C – D) revealed unexpected results. Based on the data sheet for HRP, an optimum at pH 6.0 – 6.5 was expected for Htyr. This was verified by the Htyr-MBTH assay (Figure 24 (D)), which showed a decrease in HRP activity alongside with a lowering pH. The ABTS assay resulted in unexpected outcomes, with the opposite effect being observed. With ABTS as the substrate, the pH optimum was found to be 4.0, and a decrease in enzyme activity was observed with an increasing pH (Figure 24 (C)). Subsequently, part of the experiments was repeated to verify the results, but the outcomes remained consistent. This phenomenon was not found in the literature. One study investigating HRP with ABTS identified a pH optimum at 8 [87], while another identified it at 7.4 [88]. In a separate study, HRP was analysed with Htyr but without MBTH, and a pH optimum of 5.5 was identified [67]. In order to take both results into consideration, both pH values are considered in subsequent experiments with HRP.

As ABTS has been shown to inhibit the TYR activity, the determination was analysed only with the Htyr-MBTH assay. The pH optimum for TYR is illustrated in Figure 24 (E), where a positive correlation between pH value and TYR activity was seen. It is also noteworthy that at pH 6, the activity has

decreased to a level similar to that of pH 4.5. However, the pH optimum for TYR was identified at pH 5.5 and 6.5, with no significant difference between these values. Consequently, pH 6.5 was selected for subsequent measurements, as this value was in accordance with the literature data. In a similar approach, Espín *et al*. applied the MBTH assay with tyrosol as the substrate, where TYR isolated from mushrooms also resulted in the identification of a pH optimum at 6.5 [26]. Similar results were also determined in other studies using tyrosinases from different biological sources [67, 83, 89, 90].

The result of the determination of the pH optimum of GOX by using the ABTS-HRP co-assay is illustrated in Figure 24 (F). It is not possible to observe an obvious trend for GOX, compared to what was seen with the previous enzymes. The maximum was found at pH 4.5 – 5. At lower and higher pH values, the enzyme activity was observed to decrease, with a plateau at the pH range of 5.5 – 6.5. The pH optimum between 4.5 and 5 was also confirmed by the literature data. Similarly, under comparable conditions, the optimum pH for GOX isolated from *Aspergillus niger* was observed to be between 5 and 5.5 [91-93]. Additionally, a specific activity of 135 U / mg at pH 5.5 was determined by Anjum Zia, which correlated well with the results observed in Figure 24 [91]. In this work, the maximum enzyme activity was observed at pH 4.5, with a value of 168 U / mg, which was used for further measurements.

The results of the determination of the pH optimum of POX by using the ABTS-HRP co-assay is shown in Figure 24 (G). As with GOX, no clear trend could be identified. A maximum was found at pH 6.5, 5.5 and 4. As with TYR, while the maximum activity was observed at pH 6.5, pH 5.5 was selected for further experiments because it demonstrated its maximum before averaging the molar extinction coefficient, and there was no significant difference between these two pH values. Nevertheless, the results are in relatively good agreement with the literature data. The publication that used POX of the same biological source reported an pH optimum between 6.0 – 9.0 [94]. In a further publication by Li *et al.,* POX from various biological sources was compared. The optimum pH was found to be between 4.5 – 8.0, depending on the corresponding organism. In addition, the specific activities were given, with values ranging between 1 – 27 U / mg [95]. These values were in relatively good agreement with the activities shown in Figure 24 (G).

In summary, four various pH values were selected for the subsequent measurements (illustrated as orange bars in Figure 24). Specifically, the pH 4 was selected for Lac and HRP with ABTS assay, the pH 4.5 for Lac with Htyr-MBTH and for GOX with ABTS, the pH 5.5 for POX with ABTS, and the pH 6.5 for HRP and TYR with Htyr-MBTH assay. The selection of these pH values was made with two key considerations in mind: firstly, to ensure optimal enzyme activity, and secondly, to consider the further application of these values in dough systems, where pH typically ranges in this area, depending on the ingredients and the fermentation process.

5.1.4 Temperature optimum of each enzyme

The temperature optima are based on the principle of achieving an equilibrium between the enzyme activity at higher temperatures and the risk of protein denaturation. While literature offers valuable reference points, it may not fully capture the stability and activity of the specific enzymes used in this study. Since all enzymes were refrigerated before performing further experiments, it was essential to evaluate any potential functional changes caused by storage. This approach facilitated a more accurate evaluation of both activity and stability under the relevant experimental conditions. The evaluation of the individual enzyme activities at various temperatures (25, 30, 35, 40 and 50 °C) was conducted in a manner identical to that applied for the different pH values, as described in chapter 5.1.3. The results of the determination of the temperature optimum of Lac, HRP, TYR, GOX and POX with the corresponding substrate are shown in Figure 25.

The results of the determination of temperature optimum of Lac at pH 4 by using the ABTS assay is shown in Figure 25 (A). No significant differences were observed within the temperature range of 25 – 50 °C, with enzyme activity varying in a range of approximately 680 ± 50 U / mg. In addition, the review from Baldrian also compared the temperature optima for fungal Lac. A total of 39 experiments identified a temperature range of 25 – 80 °C, with a median value of 55 °C [27]. This relatively wide temperature range was also observed in the present work, where no significant differences were identified between 25 – 50 °C.

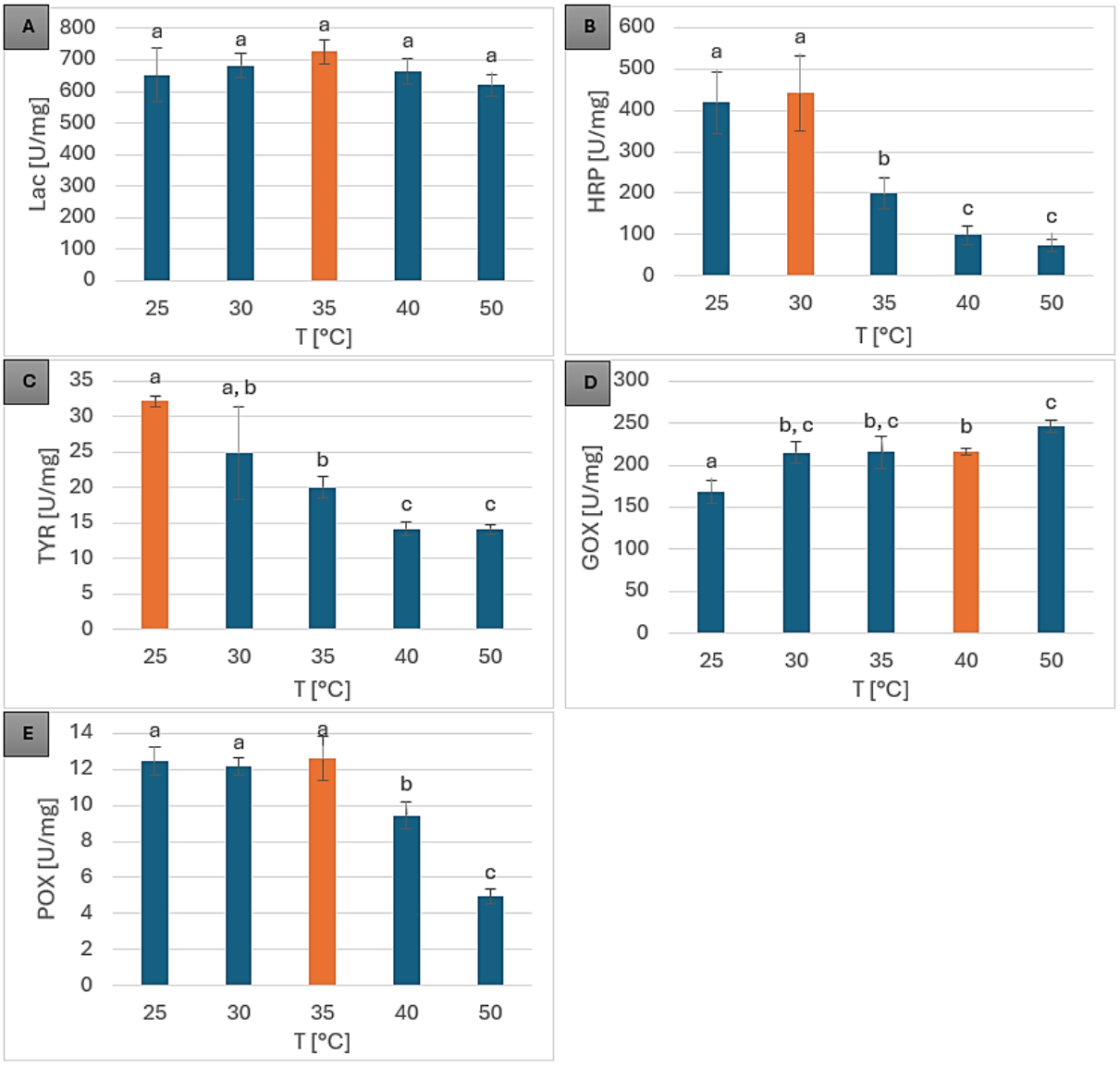

Figure 25: Results of the determination of temperature optima for Lac (A) and HRP using ABTS assay (B), TYR using Htyr-MBTH assay (C), and GOX (D) and POX (E) using ABTS-HRP co-assay. 1 U is defined as the change in absorbance of 0.1 / min at 415 nm for ABTS, respectively 500 nm for Htyr-MBTH, at the corresponding pH in a McIlvaine buffer (0.3 M), at 25 °C in a reaction volume of 0.34 mL containing 1 mM ABTS, respectively 1 mM Htyr. The various letters above the bars indicate the significant differences between the corresponding temperatures calculated by one-way ANOVA ($p < 0.05$). The temperatures highlighted in orange were applied in further determinations.

The determined temperature optimum of HRP at pH 4 using the ABTS assay is shown in Figure 25 (B). In this case, the temperature dependence of HRP is immediately visible. At temperatures between 25 – 30 °C, the enzyme activity remained relatively constant at approx. 400 U / mg. However, at higher temperatures, there was a notable reduction in enzyme activity down to less than 100 U / mg achieved at 50 °C. Most of the enzymes undergo denaturation at higher temperatures, which has a significant impact on their enzymatic activity. It is reasonable to hypothesize that this phenomenon was also observed in Figure 25 (B). The measured temperature optimum between 25 – 30 °C was also confirmed by the existing literature, which typically reports a temperature of 25 °C [67, 88]. One study has even

identified a temperature optimum for HRP at 45 °C [87]. For further kinetic measurements, the temperature of 30 °C was selected as the enzyme displayed a slightly higher enzyme activity at this temperature than that observed at 25 °C.

The result of the experiment, the objective of which was to determine the temperature optimum of TYR at pH 6.5, is shown in Figure 25 (C). As observed with HRP, a decrease in enzyme activity could also be observed with an increasing temperature with TYR. In this case, an almost linear reduction in enzyme activity was observed, from 32 U / mg at 25 °C to 14 U / mg at 40 °C. However, the results at the temperature of 30 °C exhibited a relatively high SD, suggesting the possibility of an error during the measurement process. The almost linear reduction in enzyme activity may be attributed to the denaturation of the enzyme, which begins at 25 °C and decreases with an increase in temperature. These results were also confirmed by the literature data, which showed a temperature optimum at 25 °C [5, 26, 90]. In this regard, the temperature of 25 °C was applied for the further kinetic measurements.

The dependence of GOX activity at pH 4.5 on temperature, from which the optimum can be determined, is illustrated in Figure 25 (D). The results indicate that GOX reached its maximum activity at 50 °C, which was higher than the temperatures at which previous enzymes were most active. As the temperature decreased, the enzyme activity also decreased. At temperatures between 30 to 50 °C, the enzyme activity was very similar, however, a notable decrease was observed at 25 °C. This suggests that while the enzyme activity increased at 25 °C, it subsequently attained a plateau phase. Furthermore, the literature values provided not a clear answer regarding the optimal temperature. GOX of the same biological source was reported to operate at 35 °C in one study and at 40 °C in another [91, 92]. In a different study, in which GOX was isolated from *Penicillium pinophilum*, the optimum temperature was found at 30 °C [96]. It is therefore likely that a plateau in enzyme activity was present, and to avoid potential errors arising from a loss of activity, the maximum tested temperature was set at 40 °C in the plate reader.

The results of the temperature-dependent POX activity at pH 5.5 are shown in Figure 25 (E). As with the previous enzymes, it is likely that the effect of denaturation was observed with POX. The activity remained stable between 25 – 35 °C, but at temperatures above 40 °C, a decrease in POX activity could be observed. The maximum was determined to occur between 25 – 35 °C, which was also confirmed by the publication of Leitner *et al*., in which POX from *Trametes multicolor* showed its optimum at 30 °C [24]. However, in a study from Li *et al.,* in which POX was compared from different organisms, a maximum was identified in four cases at 50 °C and in one case at 44 °C [95]. The recombinant POX

from *Phanerochaete chrysosporium*, which was also applied in this work, was investigated in another study with the ABTS assay at 30 °C. The results showed a slightly higher enzyme activity of 16.5 U / mg compared to the previously determined value of 12.1 U / mg [94]. In summary, four different temperatures were selected for subsequent kinetic measurements. Specifically, 25 °C was designated for TYR, 30 °C for HRP, 35 °C for Lac and POX, and 40 °C for GOX.

5.1.5 Kinetic parameters

A comparison of enzymes using both the ABTS and Htyr-MBTH assays facilitates a more comprehensive understanding of their catalytic efficiency and substrate specificity. In this context, K_M is defined as the substrate concentration at which the enzyme reaches half of its maximum velocity, thereby indicating its affinity for the substrate. Conversely, v_{max} is defined as the maximum reaction rate under saturating substrate conditions. Lower K_M values are indicative of higher substrate affinity, while higher v_{max} values signify greater catalytic capacity. It is further expected that different enzymes will exhibit varying K_M and v_{max} values depending on the assay, reflecting differences in substrate preference and reaction mechanisms.

Enzyme activity was determined following the procedure in Chapter 5.1.3. Mean values from triplicate measurements at different substrate concentrations were used to create a Michaelis-Menten plot, followed by a Hanes-Woolf plot according to chapter 4.3.1.4. From this, the kinetic parameters K_m and v_{max} were derived, with K_m determined from the x-axis intersection and v_{max} from the y-axis intersection. The corresponding Michaelis-Menten and Hanes-Woolf plots for each enzyme are shown in the Appendix, Figure 35. The determined Michaelis constant K_m and the maximum reaction velocity v_{max} of Lac with both substrates are listed in Table 13 with the corresponding literature values. The determined K_M values show a relatively precise accordance with the literature data. In the case of ABTS, the value of 0.039 mM is of significant importance, as it represents the median value of 36 various publications [27]. However, more significant differences can be observed in the determination of v_{max}. These may be caused by several factors, including the origin of Lac, the reaction conditions (pH, temperature, buffer) or the substrate and enzyme concentrations applied.

A comparison of the results for the two substrates from Table 13 reveals that the K_M value for Htyr is more than twice that of ABTS. This suggests that Lac demonstrates a greater affinity for ABTS, which also results in a more rapid oxidation process. This is confirmed by the v_{max} value, which is significantly higher for ABTS than for Htyr. The lower affinity for Htyr may have been the result of weaker interactions or steric effects. For ABTS one unit is defined as the change in absorbance of 0.01 per minute at 415 nm at pH 4.0 in a McIlvaine buffer (0.3 M) at 35 °C in a reaction volume of 0.34 mL containing 0.059 mM ABTS. For Htyr it was defined as the change in absorbance of 0.01 per minute at

500 nm at pH 4.5 in a McIlvaine buffer (0.3 M) at 35°C in a reaction volume of 0.34 mL containing 0.011 mM Htyr.

Table 13: The determined kinetic values, K_M and v_{max}, for Lac with both substrates in triplicate and the corresponding literature values. For ABTS, 1 U is defined as the change in absorbance of 0.01 per minute at 415 nm at pH 4.0 in a McIlvaine buffer (0.3 M) at 35 °C in a reaction volume of 0.34 mL containing 0.059 mM ABTS. For Htyr, 1 U is defined as the change in absorbance of 0.01 per minute at 500 nm at pH 4.5 in a McIlvaine buffer (0.3 M) at 35°C in a reaction volume of 0.34 mL containing 0.011 mM Htyr.

Substrate	Determined K_M [mM]	Literature K_M [mM]	Determined v_{max}	Literature v_{max}
ABTS	0.036	0.037 [97] 0.039 [27] 0.039 [98]	2.64 U/mL 587 U/mg	12.7 U/mL [98] [a] 310 U/mg [97] [b]
Htyr	0.073	0.18 [67]	0.055 U/mL 12.2 U/mg	25.2 U/mL [67] [c]

[a] 1 U was defined as the amount of enzyme that required oxidising 1 µM ABTS per min at a wavelength of 420 nm at pH 5.3 in a McIlvaine buffer (0.1 M) at 30 °C.

[b] 1 U was defined as the increase in absorbance at a wavelength of 436 nm at pH 4.0 in a sodium acetate buffer (0.01 M) at 25 °C oxidising 0.05 mM ABTS.

[c] 1 U was defined as the increase in absorbance at a wavelength of 400 nm at pH 4.0 in a sodium acetate buffer (0.05 M) at 25 °C oxidising 0.55 mM Htyr.

The determined kinetic parameters of HRP with both substrates are listed in Table 14 with the corresponding literature values. In the case of HRP, the determined values could be confirmed by the existing literature data. The same reasons as mentioned in the previous chapter also apply in this context. A comparison of the determined values reveals a lower K_m value for ABTS, which indicates a greater affinity of HRP for ABTS than for Htyr. However, the maximum reaction velocity of Htyr was more than ten times that of ABTS, which makes it a much faster option for implementation. For ABTS one unit is defined as the change in absorbance of 0.01 per minute at 415 nm at pH 4.0 in a McIlvaine buffer (0.3 M) at 30°C in a reaction volume of 0.34 mL containing 0.067 mmol ABTS. For Htyr it is the change in absorbance of 0.01 per minute at 500 nm at pH 6.5 in a McIlvaine buffer (0.3 M) at 30°C in a reaction volume of 0.34 mL containing 0.033 mmol Htyr.

Table 14: The determined kinetic values, K_M and v_{max}, for HRP with both substrates and the corresponding literature values.

Substrate	Determined K_M [mM]	Literature K_M [mM]	Determined v_{max}	Literature v_{max}
ABTS	0.0078	0.0047 [87] 0.012 [99] 0.032 [88]	77.5 U/mL 234 U/mg	1.38 U/mL [88] 211 U/mL [99] 618 U/mL [87]
Htyr	0.30	2.48 [67] 4.82 [100]	1000 U/mL 3014 U/mg	0.025 U/mL [67] 1229 U/mg [101]

The determined K_m and v_{max} value of TYR with Htyr are listed in Table 15 with the corresponding literature values. It is evident that the impact of varying reaction conditions on the kinetic values from literature can be clearly observed. Furthermore, tyrosol was used as a substrate for comparison, as it is oxidised by the monophenolic activity of TYR to Htyr. The K_M value is relatively similar for these substrates, whereas the v_{max} value is much higher for tyrosol. As the TYR activity was determined only with the Htyr-MBTH assay, the determined kinetic parameters are compared with the values determined for Lac and HRP with Htyr from Table 13. TYR showed the lowest K_m value of the three enzymes, indicating the highest affinity for Htyr. Therefore, TYR is capable of efficiently converting Htyr even at low enzyme concentrations. With regard to the v_{max} value, TYR shows a lower value than HRP, but a value that is comparable to that of Lac. For TYR one unit is defined as the change in absorbance of 0.01/min at 500 nm at pH 6.5 in a McIlvaine buffer (0.3 M) at 25°C in a reaction volume of 0.34 mL containing 0.013 mmol Htyr.

Table 15: The determined kinetic values, K_M and v_{max}, for TYR with Htyr and the literature data.

Substrate	Determined K_M [mM]	Literature K_M [mM]	Determined v_{max}	Literature v_{max}
Htyr	0.044	0.57 [67] 0.9 [26] 5.12 [100]	1.69 U/mL 10.7 U/mg	0.136 U/mL [67] 31.1 U/mL [26]
Tyrosol [5]	-	0.06 0.8	-	2680 U/mL 4338 U/mL

The determined kinetic parameters of GOX and POX with ABTS are listed in Table 16 with the corresponding literature values. As with the other enzymes, the literature values differed considerably. Consequently, the determined kinetic parameters are compared with the established values for Lac and HRP (Table 13), which were also evaluated with ABTS. POX displays the lowest K_M value out of the four enzymes, indicating that it is the most effective enzyme for the conversion of ABTS. A similar outcome was observed with GOX, where almost the same K_M value was determined. The maximum specific reaction rate for GOX is the second highest, with v_{max} being almost twice as high for Lac. On the other hand, POX shows a notably lower v_{max} value, indicating that the reaction velocity is considerably lower compared to the other three enzymes. For GOX one unit is defined as the change in absorbance of 0.01/min at 415 nm at pH 4.5 in a McIlvaine buffer (0.3 M) at 40°C in a reaction volume of 0.34 mL containing 0.071 mmol ABTS. For POX it was defined as the change in absorbance of 0.01/min at 415 nm at pH 5.5 in a McIlvaine buffer (0.3 M) at 35°C in a reaction volume of 0.34 mL containing 0.089 mmol ABTS.

Table 16: The determined kinetic values, K_M and v_{max}, for GOX and POX with ABTS and the literature data.

Enzyme	Substrate	Determined K_M [mM]	Literature K_M [mM]	Determined v_{max}	Literature v_{max}
GOX	ABTS	0.0021	2.56 [91] 5.7 [102] 20.7 [93]	303 U/mL 265 U/mg	10.8 U/mg [93] 43.5 U/mg [91] 925 U/mg [102]
POX	ABTS	0.0020	0.070 [24] 1.2 [95] 1.4 [103]	66.7 U/mL 5.16 U/mg	39.2 U/mL [95] 767 U/mL [103] 4.8 U/mg [24]

In order to have a reduced set of different reaction conditions in the subsequent procedure, the optimal conditions for each enzyme were adjusted. Specifically, for each enzyme, conditions were selected where the determined pH and temperature optima showed no significant differences. The values that have been selected, along with the kinetic parameters that have been determined under optimal conditions, are summarised in Table 17.

Table 17: A summary of the determined optimal pH and temperature conditions for all five enzymes with ABTS and Htyr as a substrate. In the absence of enzyme addition or the availability of corresponding values, assays are designated with the symbol -.

	ABTS assay			Htyr-MBTH assay		
Enzyme	**pH**	**Temperature [°C]**	**K_M & v_{max}**	**pH**	**Temperature [°C]**	**K_M & v_{max}**
Lac	4	25 – 50	0.036 mM 587 U/mg	4.5	25 – 50	0.073 mM 12.2 U/mg
HRP	4 – 4.5	25 – 30	0.0078 mM 234 U/mg	6.5	25 – 30	0.30 mM 3014 U/mg
TYR	-	-	-	5.5 & 6.5	25 – 30	0.044 mM 10.7 U/mg
GOX	4.5 – 5	30 – 50	0.0021 mM 265 U/mg	-	-	-
POX	5.5 & 6.5	25 – 35	0.0020 mM 5.16 U/mg	-	-	-

For almost all enzymes, a pH of 4.5 or 6.5 was found to be optimal as shown in Table 17. The only exception is the reaction between Lac and ABTS, for which the optimum pH is 4. Therefore, further experiments were performed at either pH 4.5 (Lac and GOX) or 6.5 (TYR and POX). However, for HRP both values were used, as the optimum differs depending on the substrates used (*cf.* chapter 5.1.3).

The determination of the optimal temperatures allowed the limitation up to a single temperature, namely at 30 °C. By comparing the optimum conditions and minimising the parameters, the number of different reaction conditions was reduced from eight (four pH values and four temperatures) to three (two pH values and one temperature).

In summary, the kinetics of five enzymes Lac, HRP, TYR, GOX and POX were determined using ABTS and Htyr-MBTH assays to assess their potential in dough applications, with the hypothesis that comparison of these assays would reveal activity trends and suitable pH/temperature conditions. The results showed generally lower K_M values with ABTS than with Htyr-MBTH, indicating a higher affinity for ABTS for most of the enzymes. HRP exhibited the highest v_{max} with Htyr, indicating its superior catalytic conversion with this substrate compared to the other enzymes and substrates tested. These results suggest a substrate-dependent catalytic efficiency and highlight the importance of substrate selection. The determined optimal pH and temperature ranges provide the basis for future investigations into the effect of these enzymes on dough properties and their stability during baking.

5.2 Substrate specificity towards ferulic acid and tyrosine

Next, the substrate specificity towards FA and Y was examined in a comparative manner. Existing literature supports the hypothesis that, while Lac and HRP are capable of converting FA, TYR is able to convert Y [10, 13, 51]. In addition to this, some studies suggest that Lac can also convert Y, although at a lower rate compared to TYR [42, 51, 56]. The last two enzymes, GOX and POX, have been found to be capable of indirect conversion of FA and Y in the presence of peroxidase, as the generated H_2O_2 activates the enzymatic reaction of HRP [6]. The objective was to achieve maximum conversion for one of the target substrates according to chapter 4.3.2, as this was found to be crucial for subsequent enzymatic reactions.

The measured UV spectra of the conversion of FA and Y with Lac are presented in Figure 26 (A – B). As already documented in the literature, the conversion of FA was characterised by a decrease at 320 nm, while the conversion of Y was characterised by an increase at 280 nm [7]. The conversion of FA resulted in an absorbance reduction at a wavelength of 280 nm, and especially at 320 nm, as during oxidation FA forms quinones that often involve a loss on conjugation in the aromatic system. This reduced conjugation decreases the molecule's ability to absorb light in the UV-Vis, leading to a decrease in the absorbance. Conversely, the presence of Y results in an increase in the absorbance at 280 nm, due to the formation of dopaquinone, which frequently involves an increase in conjugation or the presence of additional chromophoric groups. This leads to an increase in the molecule's ability to absorb light, as previously reported by Reid *et al.* [69].

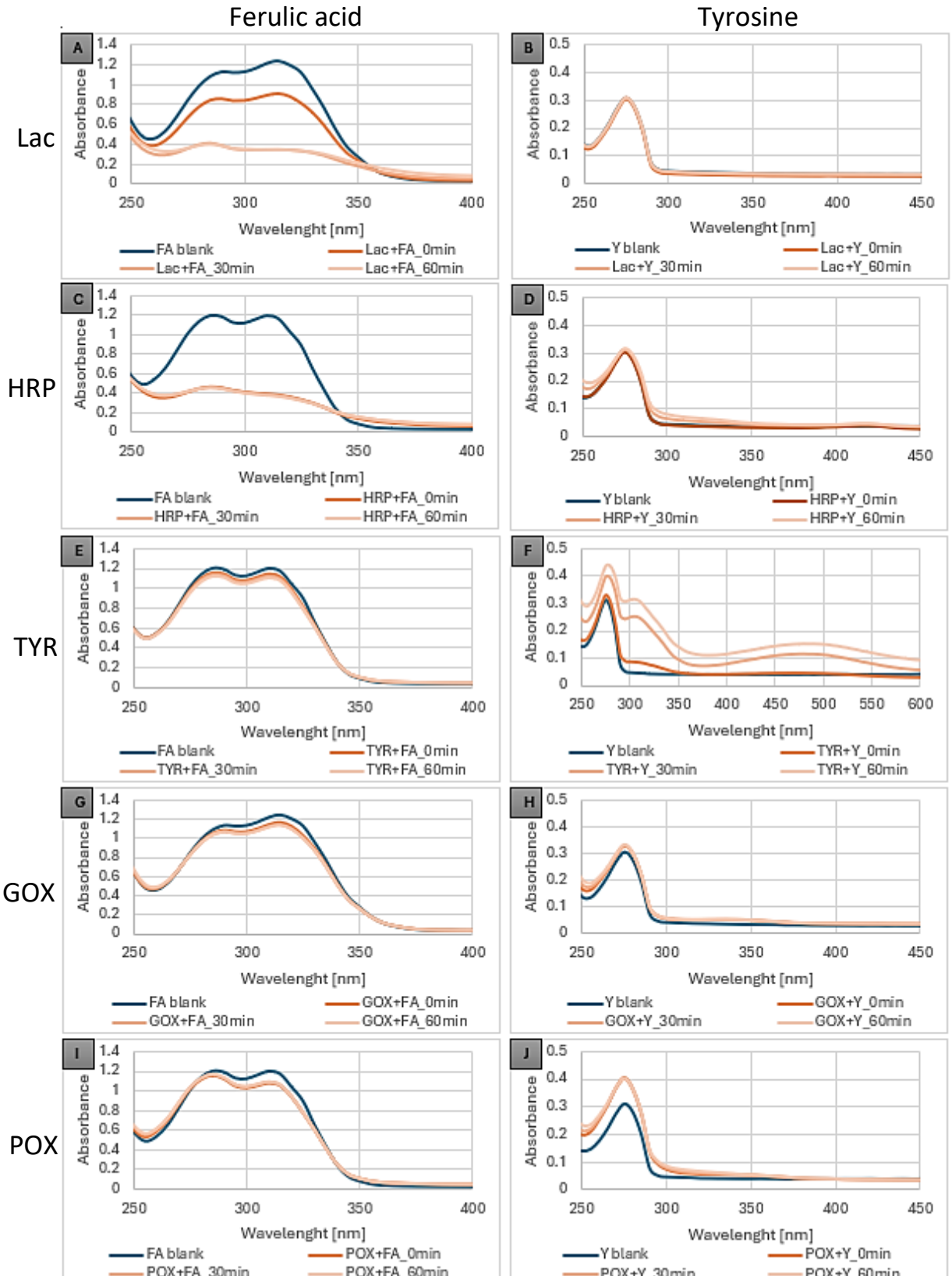

Figure 26: UV spectra of the conversion of FA (2 mM) and Y (0.2 mM) by Lac (A, B), HRP (C, D), TYR (E, F), GOX (G, H) and POX (I, J) at 30 °C. Reactions with Lac, HRP and GOX were performed at pH 4.5, while reactions with TYR and POX were performed at pH 6.5.

Figure 26 (A) shows a decrease in absorbance over time, suggesting that Lac was capable of converting FA. On the other hand, Figure 26 (B) demonstrated no change in absorbance over time, indicating that Y was not converted by Lac. These findings were also partially confirmed by the literature, where FA was oxidised by Lac [7, 13]. In some studies, Lac was also reported to convert Y [42, 51] but this has not been confirmed in this case.

As Lac was only found to convert FA, the kinetic measurements were only determined with this substrate. The determination of the kinetic parameters was analysed as previously described in chapter 5.1.5. The only difference was that a literature value of 13.738 mL mol^{-1} cm^{-1} was applied for the molar extinction coefficient of FA [71]. The created Michaelis-Menten and Hanes-Woolf plots are shown in the Appendix, Figure 37. The determined K_M value was 0.057 mM, and the v_{max} value was 0.966 U / mL, respectively 215 U / mg. A comparison of the results with the kinetic parameters from a study by Perna (K_M = 0.017 mM and v_{max} = 1.14 U / mL) indicates that the determined values are in a close agreement with the literature [104].

The measured UV spectra of the conversion of FA and Y by HRP are presented in Figure 26 (C – D). As demonstrated in Figure 26 (C), the reaction with FA exhibited a decrease in absorbance over time, suggesting that HRP was capable of converting this phenolic acid. In addition, there was a very small change at the wavelength of 420 nm indicating the conversion of Y to its quinone. Similarly to Lac, the literature reported that both substrates should be feasible using HRP but the conversion was observed only with FA [7].

The kinetic measurements were also performed using only FA, where the evaluation was done as previously stated. The created Michaelis-Menten and Hanes plots are illustrated in the Appendix in Figure 37. The determined K_M value was 0.25 mM, and the v_{max} value was 833 U / mL, which equates to 2512 U / mg. Comparing these results with those previously determined for the two substrates, it can be assumed that HRP achieved similarly high kinetic values as those determined with Htyr as a substrate. On the one hand, HRP exhibited a very high reaction velocity with FA, however on the other hand, it showed a much lower substrate affinity compared to ABTS.

The measured UV spectra of the conversion of FA and Y by TYR are shown in Figure 26 (E – F). The reaction with FA (Figure 26 (E)) showed a relatively minor change in absorbance at 320 nm, suggesting that TYR did not oxidise FA, respectively at a very slow rate. However, at the wavelength of 280 nm in Figure 26 (F), a notable change in absorbance was observed. Furthermore, a peak between 450 – 500 nm was observable, which indicated the formation of a quinone product. These findings suggested that TYR did oxidise Y, which was also confirmed by the existing literature [5, 6].

The kinetic measurements were analysed using only Y, as TYR was only capable to convert this substrate. The determined Michaelis-Menten and Hanes plots are illustrated in the Appendix in Figure

37. The determined K_M value was 0.504 mM, and the v_{max} value was 0.231 U / mL, which equates to 1.46 U / mg. A comparison of the kinetic parameters of Htyr with TYR as previously determined (Table 15) indicated, that Y was less efficiently converted than Htyr. On the one hand, the K_M value of Y was more than ten times higher than that of Htyr, which resulted in a lower affinity and a less efficient formation of the enzyme substrate complex, as shown by Equation 1. On the other hand, the v_{max} value for Y was almost ten times lower than that of Htyr, resulting in a much slower conversion rate of the substrate.

The measured UV spectra of the conversion of FA and Y by GOX, respectively POX, are presented in Figure 26 (G – J). Both enzymes resulted only in a small change in absorbance at 320 nm, suggesting that neither were capable of converting FA. The results were similar in Figure 26 (H – J), where no significant changes in absorbance were observed. POX showed a better conversion of Y compared to GOX; however, this was insufficient to achieve a comprehensive conversion. In conclusion, the kinetic measurements were not analysed with any of the applied substrates, as the feasibility of doing so was insufficient for determining the kinetic parameters.

In summary, the results demonstrated that Lac and HRP exhibited efficient conversion of FA, while TYR, GOX, and POX exhibited minimal FA conversion. Conversely, TYR effectively converted Y, with HRP showing only a slight conversion to quinones, and Lac, GOX, and POX demonstrating negligible Y conversion. These observations provided clear evidence to support the hypothesis that the tested enzymes have various substrate specificities. Building upon these findings, the subsequent hypothesis was to apply enzyme combinations, as it was evident that none of the single enzymes could efficiently convert both substrates at once. In this context, the combination of enzymes such as Lac with TYR was hypothesised to result in a synergistic system capable of simultaneous conversion of both FA and Y. Furthermore, exploring combinations such as HRP with either GOX or POX could potentially lead to more efficient conversion of Y, given the efficient conversion of FA by HRP. This approach was hypothesised to enhance the overall conversion efficiency of both substrates and potentially generate novel products.

One of the enzyme combinations analysed was Lac with TYR, since both substrates were efficiently converted by the corresponding enzyme. The reactions were determined at a pH value of 4.5, as the pH 6.5 (optimum of TYR) had a significantly more inhibitory effect on Lac than the pH 4.5 on TYR. The specific Michaelis-Menten and Hanes plots can be found in Appendix, Figure 38.

The determined K_M values for both enzymes were identical for each substrate. The Michaelis constant for FA was 0.107 mM, while that for Y was 0.238 mM. In this enzyme combination, Lac achieved a v_{max}

value with FA of 0.976 U / mL, respectively 217 U / mg, and with TYR of 0.228 U / mL, respectively 1.44 U / mg. A comparison of these values with the kinetic results of the single enzymes revealed a decrease in the affinity of Lac in combination with TYR towards FA compared to the usage of the single enzyme. The maximal reaction velocity remained almost the same. In the case of Y as a substrate, a v_{max} value for Lac was achieved at 0.161 U / mL, respectively 35.9 U / mg, and for TYR at 0.081 U / mL, respectively 0.511 U / mg. A comparison of these values with the results of the conversion of Y with only TYR revealed that the enzyme combination achieved a reaction velocity that was approximately three times slower. Nevertheless, a twofold improvement was observed in the affinity towards the substrate. In conclusion, the kinetic results were not markedly better compared to those of the individual enzymes. However, the combination of the enzymes enabled the conversion of both substrates simultaneously, which was not achieved with any single enzyme.

Another two enzymatic combinations were the combination of HRP with either GOX or POX. Both combinations were performed at 30 °C with the difference that HRP/GOX was performed at pH 4.5, while HRP/POX at pH 6.5. In order to observe whether a significant change between the reactions of GOX alone and those of GOX combined with HRP occurred, the reactions after 30 min were compared with the corresponding substrate. The UV spectra for FA and Y are presented in Figure 27. It was evident that there has been a notable change in absorbance when this particular enzyme combination was applied. With FA as the substrate (Figure 27 (A)), the conversion was as effective as that with HRP alone. However, in the case of Y (Figure 27 (B)), not only was a change at a wavelength of 280 nm observed, but also between 400 – 450 nm, which indicated the formation of a quinone product. This peak could not be identified in either of the two reaction mixtures catalysed by the single enzymes. The increase at 280 nm indicated the efficient conversion of Y, as previously observed with the single enzyme TYR, which efficiently oxidised Y (Figure 26 (F)).

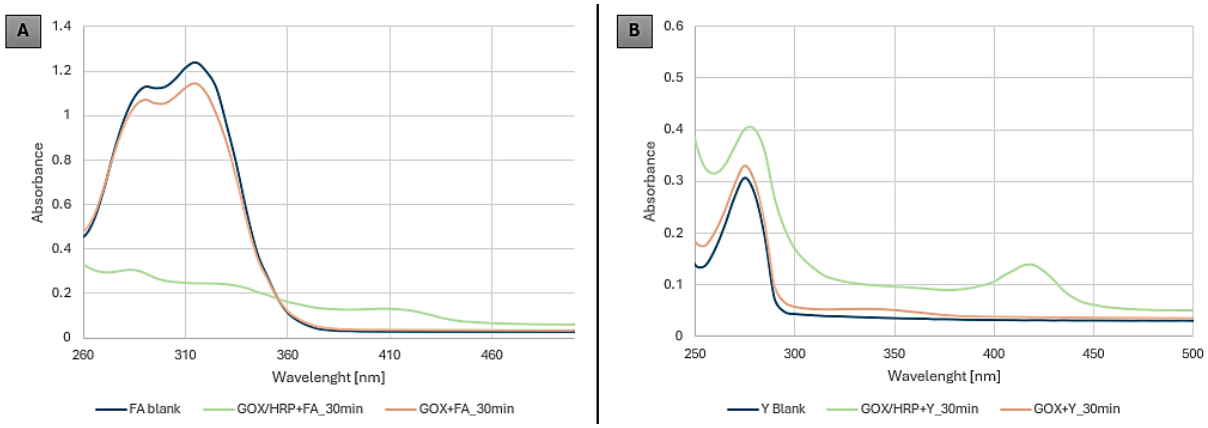

Figure 27: UV spectra of the conversion of FA (A) and Y (B) by GOX (orange) and by the enzyme combination HRP/GOX (green). At pH 4.5 and 30 °C.

The kinetic measurements were analysed only using FA, since no Michaelis-Menten equation could be observed for Y, likely due to the insufficient change in absorbance being measured. The determined Michaelis-Menten and Hanes plots for FA are illustrated in the Appendix in Figure 38. The K_M value for GOX was 0.043 mM, while that for HRP was 0.045 mM. In this enzyme combination, GOX achieved a v_{max} value of 217 U / mL, respectively 190 U / mg, while that for HRP was 1.64 U / mL, respectively 4.94 U / mg. Comparing these results to the kinetic values of FA with HRP alone, the reaction velocity rapidly decreased from 2512 U / mg to 4.94 U / mg. However, the affinity of the enzyme towards the substrate increased approximately six times. Furthermore, in addition to the previous approach, a combination with POX was kinetically investigated (Appendix; Figure 38). The K_M value for FA with this combination was 0.081 mM, while v_{max} achieved a value of 1.89 U / mL, respectively 5.70 U / mg. The results demonstrated a substrate affinity approx. twofold lower, and a slightly higher reaction velocity compared to the enzyme combination with GOX. Therefore, this combination was selected for further analysis.

Before the main cross-linking reaction procedure, it was first necessary to determine the optimal amount of each enzyme required. In order to achieve this, all of the determined kinetic parameters were compared with one another. These are summarised in Table 18 and evaluated via a heat map, thus simplifying the evaluation process.

Table 18 indicates no observable trend regarding the individual substrates. For instance, the highest reaction velocities were achieved with HRP using Htyr-MBTH and FA. However, with the remaining enzymes, the reaction rates were not as high as those observed with HRP. Furthermore, the two substrates were not always the most rapidly converted substrates by the individual enzymes. Therefore, for the subsequent cross-linking experiments, it was decided that the amount of enzyme employed would be equivalent to each distinct substrate. The different determinations of the enzyme activities resulted in an enzyme amount of 0.03 U per 1.5 mL for the conversion of FA, and an enzyme amount of 0.01 U per 1.5 mL for Y.

Table 18: Summary of all kinetic parameters determined using a heatmap[1].

	Enzyme	Substrate	K_M [mM]	v_{max} [U / mL]	v_{max} [U / mg]
Lac	Lac	ABTS[2]	0.036	2.64	587
	Lac	Htyr[2]	0.073	0.055	12.2
	Lac	FA[3]	0.057	0.966	215
	Lac + TYR	FA[3]	0.107	0.976	217
	Lac + TYR	Y[3]	0.238	0.161	35.9
HRP	HRP	ABTS[2]	0.0078	77.5	234
	HRP	Htyr[2]	0.300	1000	3014
	HRP	FA[3]	0.250	833	2512
	HRP + GOX	FA[3]	0.045	1.64	4.94
	HRP + POX	FA[3]	0.081	1.89	5.70
TYR	TYR	Htyr[2]	0.044	1.69	10.7
	TYR	Y[3]	0.504	0.231	1.46
	TYR + Lac	Y[3]	0.238	0.081	0.511
	TYR + Lac	FA[3]	0.107	0.228	1.44
GOX	GOX	ABTS[2]	0.0021	303	265
	GOX + HRP	FA[3]	0.043	217	190
POX	POX	ABTS[2]	0.0020	66.7	5.16
	POX + HRP	FA[3]	0.087	217	190

[1] green represents higher values, while yellow represents lower values; [2] for the substrates ABTS and Htyr 1 U is defined as the change in absorbance of 0.1 / min at 415 nm for ABTS, respectively 500 nm for Htyr-MBTH, at the corresponding pH (4.5 or 6.5) in a McIlvaine buffer (0.3 M), at 25 °C in a reaction volume of 0.34 mL containing 1 mM ABTS, respectively 1 mM Htyr; [3] For FA and Y, 1 U is defined as the change in absorbance of 0.1 / min at 320 nm for FA, respectively 280 nm for Y, at the corresponding pH (4.5 or 6.5) in a McIlvaine buffer (0.3 M), at 25 °C in a reaction volume of 0.34 mL containing 2 mM FA, respectively 0.2 mM Y.

5.3 Cross-linking behaviour of monomers (FA, Y)

5.3.1 Influence of solvents and tensides on enzyme activity

The implementation of sample preparation techniques in this work, such as ultrafiltration and SPE, displayed the potential to negatively influence the cross-linking of monomers to the product formation (*cf.* chapter 4.3.3.1). Especially, no products containing Y could be determined, suggesting that the amino acid was retained by the SPE and not released for the subsequent analysis by LC-MS/MS. Therefore, these procedures were excluded from further analysis. The focus of the following sections was redirected from the evaluation of the enzymes' abilities to catalyse the formation of covalent linkages between FA and Y, analysed via UV-Vis spectroscopy and HPLC-UV, to the peptide conjugation, analysed via LC-MS/MS. This process required a modification to the system configuration and the assurance of adequate peptide solubility. It was hypothesised that these adaptations may influence the enzyme activity. Therefore, a buffer change was required in order to switch to LC-MS/MS friendly conditions. The ammonium acetate (AMAC) buffer was applied for the pH value of 4.5, while the

ammonium bicarbonate (AMBIC) buffer was employed for the pH value of 6.5, both with a concentration of 0.1 M. The primary objective was to investigate the impact of various buffers on the enzyme activities, determining whether there is a significant decrease in enzyme activity or if the effect of another buffer is within an acceptable range. The results are shown in Figure 28 in which the enzyme activities in the McIlvaine buffer were normalised to 100 % (blue bars in Figure 28). It must be acknowledged that, due to the single-time execution of the tests, the error bars are not displayed. In the AMAC buffer, there was no or only a low reduction of the enzyme activity. With the AMBIC buffer, the results were slightly different. While there was no reduction of enzyme activity with TYR, a notable decrease could be observed with HRP. Since HRP was tested at both pH values, only the pH value of 4.5 was used for further LC-MS/MS measurements. However, for the UV-Vis and HPLC-UV measurements, both pH values were examined to gain a more detailed understanding of the effect of the two various pH optima determined in Figure 24 (C – D).

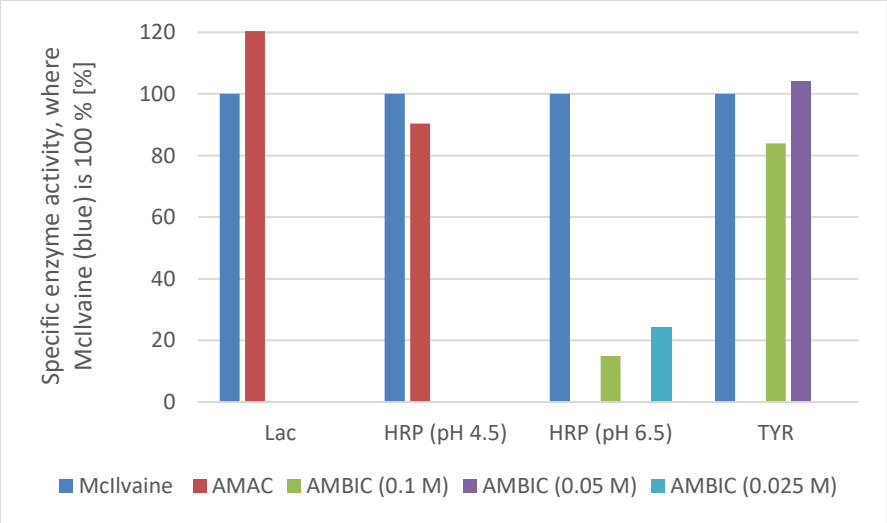

Figure 28: Impact on the enzyme activity after changing the buffer. The enzyme activity in the McIlvaine buffer (blue bars) was standardised to 100% at the y-axis to facilitate comparison with the change in enzyme activity.

The impact of Rapigest and DMF addition on the individual enzyme activities was investigated. As the peptides were not water soluble, these solubility improvers had to be applied. It was hypothesised, that either DMF, which has been previously employed in the Htyr-MBTH assay (cf. chapter 4.3.1.1) to dissolve the Htyr-MBTH complex, or that Rapigest, a detergent that enhances solubility in aqueous solutions without compromising MS, would be a potential candidate. Two concentrations of Rapigest, namely 0.1 % v/v and 0.05 % v/v, were examined. The individual results are presented in Figure 29. The respective enzyme activity was standardised as 100 % in the absence of Rapigest and DMF (blue bars in Figure 29). The addition of 10 % DMF to the reaction solution (purple bars in Figure 29) resulted

in a notable inhibition of the enzyme activity across all three enzymes. This indicated that the proposed method of dissolving peptides using DMF was not a viable option. The addition of 0.1 % Rapigest (red bars in Figure 29) resulted in a relatively low inhibition of HRP activity, while a significant reduction in enzyme activity was observed for Lac and, in particular, TYR. Therefore, a target concentration of 0.05 % for Rapigest was selected to dissolve the peptides (green bars in Figure 29), as it had no or only a minimal impact on the enzyme activity.

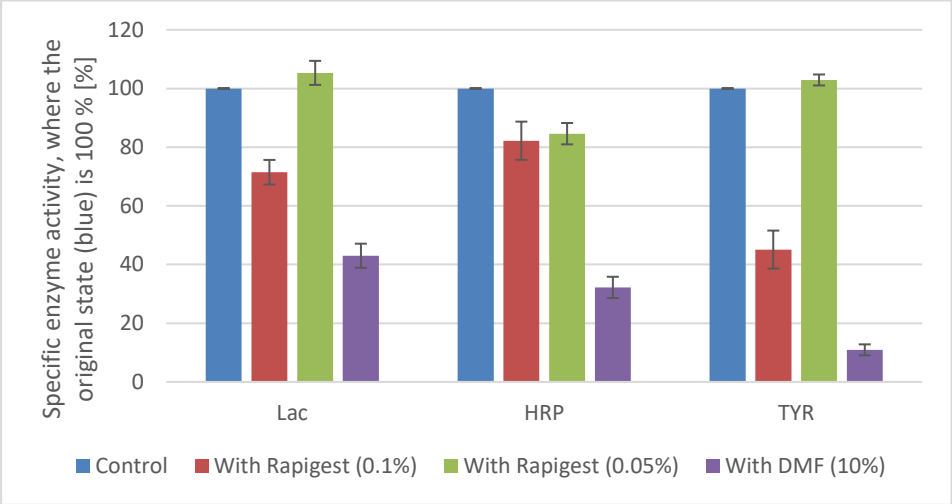

Figure 29: Impact on the enzyme activity after adding Rapigest (0.1 & 0.05 %) and DMF (10 %) to the reaction mixture. The enzyme activity in the McIlvaine buffer (blue bars) was standardised to 100 % at the y-axis to facilitate comparison with the change in enzyme activity. Each measurement was performed in triplicate at 30 °C.

5.3.2 UV-Vis measurements

In the UV-Vis measurements, the absorbances for Y at 280 nm and for FA at 320 nm were determined according to chapter 4.3.3.1. As already known from the literature and from the previous findings in chapter 4.3.2, it was expected that for Y there would be an increase in absorbance at 280 nm. At 320 nm, the opposite was expected, as a decrease in absorbance is characteristic for the FA conversion. Furthermore, the investigation focused on the emergence of additional peaks, particularly in the range of 400 – 500 nm, where quinone products are known to be formed. The reactions were conducted at two FA/Y ratios, specifically 1:1 and 1:5, in an 0.05 M AMAC or AMBIC buffer. The absorption behaviour of the six enzymes or enzyme combinations was evaluated over five time intervals. For this purpose, the intervals after 0, 0.25, 2, 6 and 24 hours were employed. The results at the wavelengths of 280 nm, 320 nm and 405 nm are presented in Figure 30.

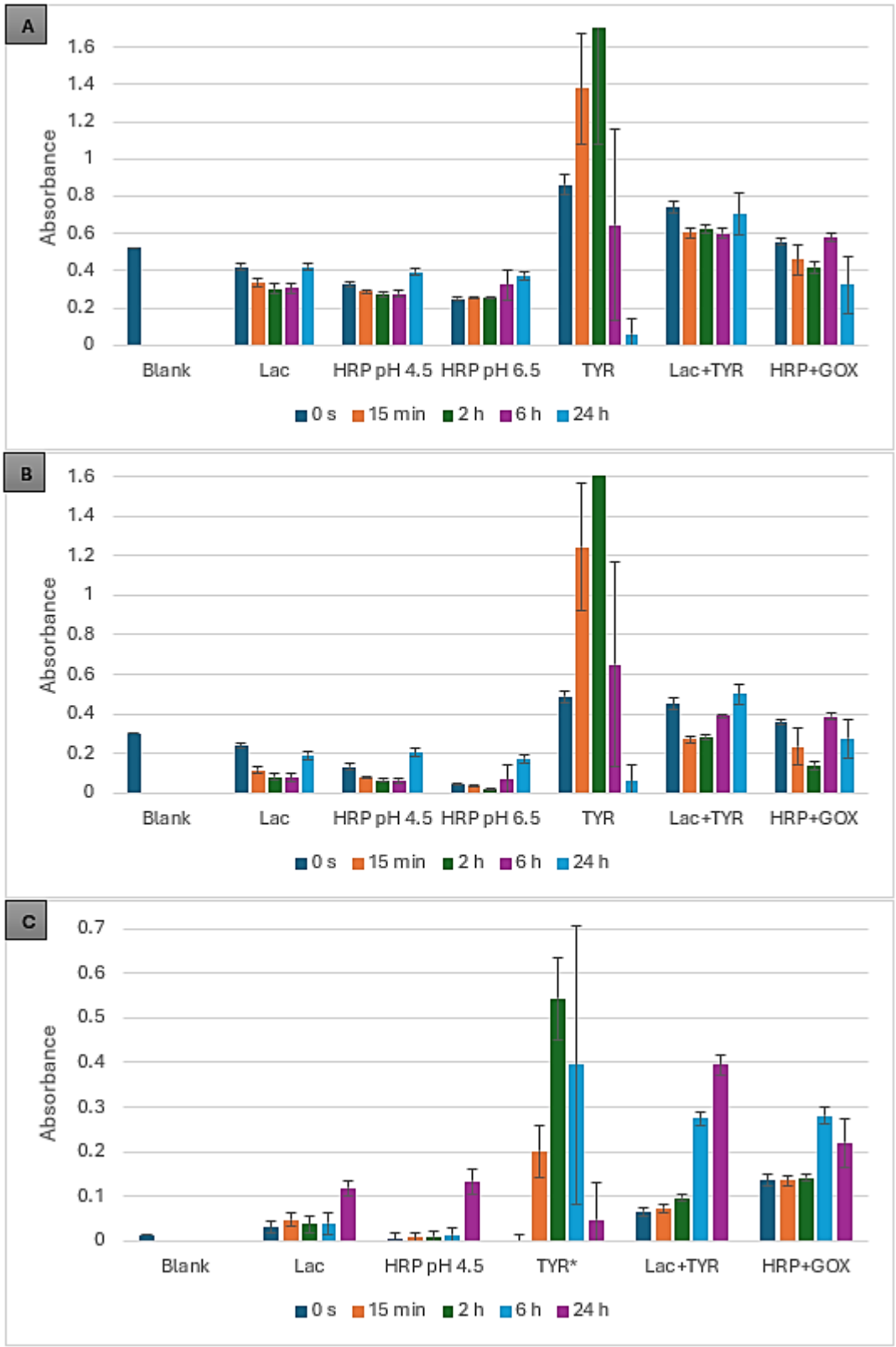

Figure 30: The time-dependent absorbances at 280 nm (A), 320 nm (B) and 405 nm (C) (*in case of TYR at 480 nm) of the individual enzymes with a FA/Y ratio of 1:5. Each measurement was performed in triplicate and the mixtures were incubated at 30 °C. The corresponding enzyme is indicated on the x-axis, while the absorbances are displayed on the y-axis and the various time intervals are marked in different colours.

At a wavelength of 280 nm (*cf*. Figure 30 (A)), the focus was primarily on the increase in absorbance. As expected, the absorbance of TYR began to increase at the start of the reaction, reaching its maximum after 2 h. Subsequently, the absorbance decreased and after 24 h almost all Y was fully converted. The high SD for TYR suggested inconsistency in reaction rates across replicates, but the strong absorbance increase indicated that the enzyme was still active, which was a very important information. The variability likely stemmed from various factors affecting enzyme stability, substrate availability, or reaction kinetics. Furthermore, an additional increase in absorbance was evident with the enzyme combination Lac/TYR, although the maximum was already reached at the start of the reaction. Subsequently, a slight decrease in absorbance was observed, followed by a period of stagnation over time. This outcome could be attributed to the fact that FA exhibited a local maximum at 280 nm and given that Lac was responsible for the conversion of FA in the enzyme combination, a decrease in absorbance was observed at both 320 nm and 280 nm. This effect could also be observed in the case of the other enzymes, where a decrease in absorbance was evident over time. In addition, in the majority of cases an increase in absorbance could be observed after 24 h. However, this result has to be considered with caution, as the rate of increase was consistent across all cases. This phenomenon may be attributed to the evaporation of water during the open incubation at 30 °C, which had the effect of concentrating the reaction mixtures and thereby causing the observed increase in absorbance. The open incubation was necessary to ensure sufficient oxygen availability, which is crucial for the efficient enzymatic cross-linking of these two substrates.

The results at the wavelength of 320 nm are illustrated in Figure 30 (B). As expected, an almost complete conversion of FA was observed with Lac and HRP after only 15 min, which could be confirmed by the clear decrease in absorbance. A decrease in absorbance could also be observed with both enzyme combinations, although there was also an increase in absorbance, which can be explained by the simultaneous conversion of Y. In the case of TYR, a strong increase in absorbance with a maximum after 2 h was again observed, which was mainly influenced by the strong peak increase at 280 nm. Also in this case, a consistent increase in absorbance was observed after 24 h, which could also be caused by the effect mentioned above. In addition, the results of the peak formation between 400 – 500 nm are presented in Figure 30 (C). In the case of Lac, HRP (pH 4.5), Lac+TYR and HRP+GOX, a peak formation at 405 nm was observed, while in the case of TYR, a peak formation at 480 nm was observed. With HRP at pH 6.5, no further peak formation was identified. The single enzyme Lac showed a slight increase in absorbance, reaching a maximum after 24 h. HRP demonstrated no significant increase in absorbance between 0 – 6 h, but after 24 h, it reached a similar maximum as Lac. Also in these cases, the consistent increase in absorbance was seen after 24 h, which was already described above and has to be considered with caution.

In the case of the enzyme combinations, a greater increase in the absorbance was observed. After 6 h, both combinations reached a similar level of absorbance. However, the difference was that the absorbances of the Lac+TYR combination continued to increase, while the absorbances of the HRP+GOX combination decreased after 24 h. However, TYR was the only enzyme that exhibited the products absorption maximum at a different wavelength, namely at 480 nm. The maximum was achieved after only 2 h. With increasing incubation time, the absorbance began to decrease. TYR is well known to produce quinone products that generate an additional peak at around 500 nm and undergo further non-enzymatic coupling reactions [5].

5.3.3 HPLC-UV analysis

As outlined in previous chapters, the focus now shifted to the evaluation of the enzymes' abilities to catalyse the formation of covalent linkages between FA and Y. While UV-Vis spectroscopy provided valuable initial insights into enzyme kinetics and substrate conversion, it lacks the necessary specificity and separation capabilities to definitively identify and quantify cross-linked products. Therefore, HPLC was employed as the primary analytical tool for this part. The ensuing discussion will provide a synopsis of the results and their subsequent analysis, encompassing the examination of cross-linking activity, both individual enzyme-based and enzyme combination-based, and the products resulting therefrom.

The evaluation of the HPLC data (chapter 4.3.3.2) was primarily focused on the wavelength at 280 nm, as the conversion of Y was found to be more limiting compared to the conversion of FA. The available literature, in combination with the current findings, indicates that the conversion of FA by the selected enzymes was considerably more achievable than the conversion of Y. In addition, both substrates demonstrated a maximum at this particular wavelength. To simplify the evaluation, the products identified after 0 h and 24 h were compared with each other at both FA/Y ratios. The retention times of Y and FA were 2.3 min and 8.2 min, respectively. Y is a relatively polar amino acid with a phenolic hydroxyl group and an amino group. Its short retention time indicates a weaker interaction with the non-polar stationary phase, resulting in its rapid elution through the column. In contrast, FA is a phenolic compound with an additional methoxy group and an unsaturated side chain. This structural difference results in FA being less polar than Y, leading to its longer retention time due to its better interaction with the hydrophobic stationary phase. Furthermore, the retention times of the two most prevalent cross-linking products were interpreted, specifically at 9.3 min and 10 min. These products demonstrate a higher retention time compared to the two substrates, indicating an increase in their hydrophobicity as a consequence of intermolecular binding. This could be attributed to a decrease in polarity and/or an increase in molecular weight. The observed increase in hydrophobicity could be

caused by the removal of polar groups, such as those resulting from oxidation or condensation, or by the formation of hydrophobic regions within the molecule.

Calibration curves of the monomers FA and Y were calculated within a concentration range of 0.1 to 18.1 µg / mL and are shown in the Appendix, Figure 39. The time-dependent change in the substrate concentration in the absence of enzymatic addition (further referred to as the "control") is illustrated in Figure 31 (A). It was observed that neither FA nor Y demonstrated a significant change in concentration over time. The Y concentrations were found to be at a FA/Y ratio of 1:1 ~2.1 µg / mL, while at a ratio of 1:5, the concentration was ~14 µg / mL. The concentration of FA remained at both ratios at around 2.8 µg / mL.

The enzymatic development of the reaction mixture with Lac is shown in Figure 31 (B). As expected, Y was not converted and its signal remained constant after 24 h at both substrate ratios. In contrast, the signal for FA decreased by more than twofold at the start of the reaction, and full conversion of FA was achieved after 24 h. Furthermore, two coupling products, one with a retention time of 9.3 min and the other of 10 min, were identified at both substrate ratios at the start of the reaction at 280 nm. A comparison of these results with existing literature data suggests that these two peaks correspond to various dimers. The firstly eluted product could be either a di-Y or a FA-Y cross-link product. The hypothesis that a di-FA product was present was dismissed, as this is known to elute much later due to its high degree of hydrophobicity [4]. Additionally, the product eluting at 10 min could be an isomer of the previous product, given its comparable polarity. However, these products were not detected in the reaction mixtures after 24 h. One potential explanation for this could be the conversion of initially UV-active intermediate products, such as the FA-Y dimer, into less UV-active polymeric end products. Alternatively, these intermediates might have exhibited limited initial solubility, resulting in their precipitation and subsequent loss of detectability due to further enzymatic modifications.

As illustrated in Figure 31 (C), the initial differences between the two substrate ratios were identified in the mixtures following the addition of TYR. The 1:1 FA/Y ratio revealed no significant changes in the Y signal. However, the 1:5 ratio exhibited a slight concentration increase of Y at the start of the reaction, followed by a significant decrease after 24 h, indicating a potential conversion of Y. Furthermore, FA was fully converted at both ratios after 24 h. In this case, none of the two selected products with retention times at 9.3 min and at 10 min were identified.

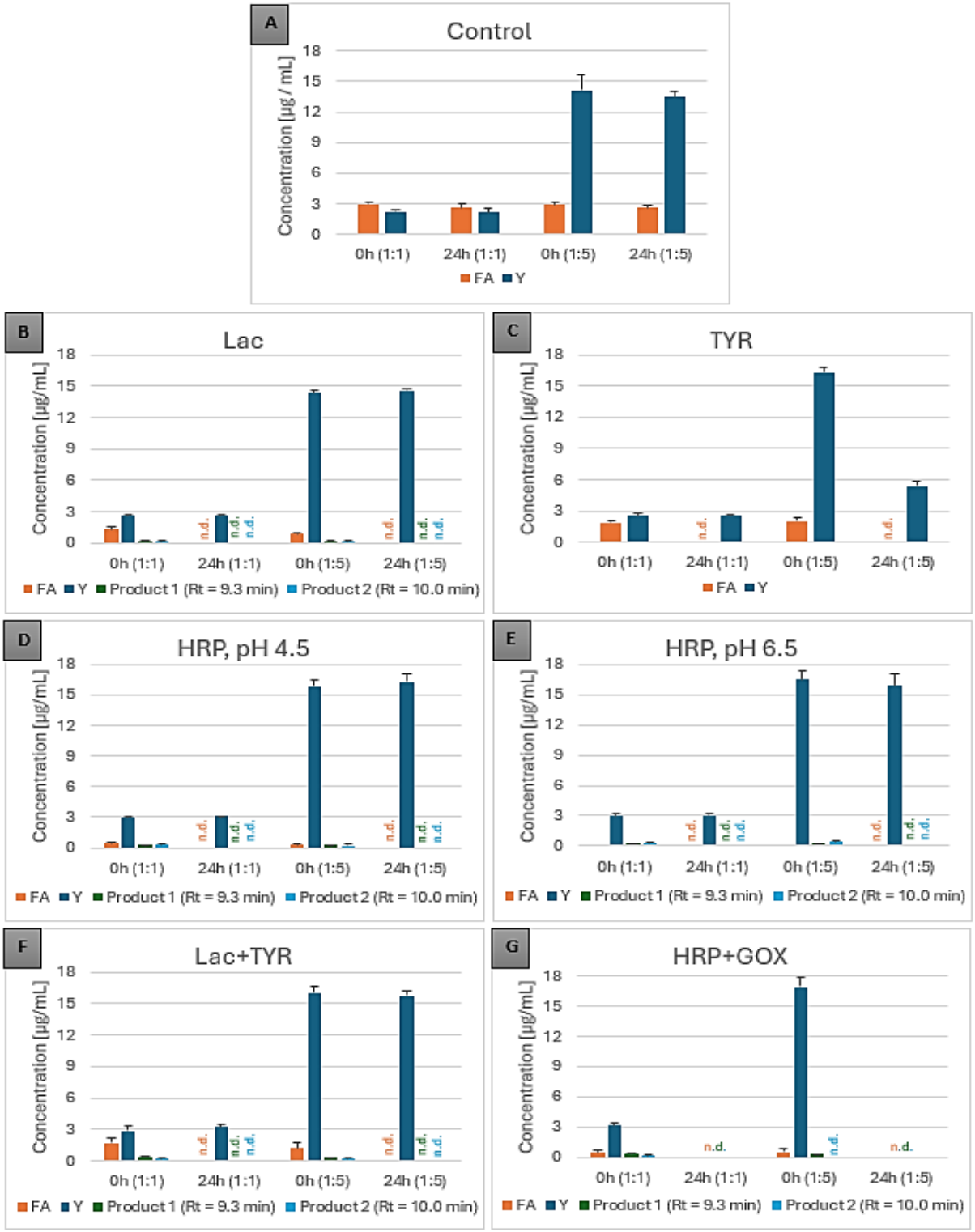

Figure 31: The concentrations of FA, Y and two coupling products (in µg / mL) at 280 nm catalysed by water (**A**), Lac at pH 4.5 (**B**), TYR at pH 6.5 (**C**), HRP at pH 4.5 (**D**) and pH 6.5 (**E**), Lac+TYR at pH 4.5 (**F**) and HRP+GOX at pH 4.5 (**G**). The data is presented for varying reaction times (0 h and 24 h) and substrate ratios (1:1 and 1:5). Each measurement was performed in triplicate and the mixtures were incubated at 30 °C. The shortcut "n.d." stands for "not detected".

The development of the substrates and products catalysed by HRP was analysed at two pH values (4.5 & 6.5) and is illustrated in Figure 31 (D – E). At both pH values, the conversion of Y could not be observed, as the Y amount remained constant after 24 h, respectively slightly increased. In contrast, FA was fully converted at the start of the reaction at pH 6.5. At pH 4.5, a small amount of FA could be observed, but after 24 h it was fully converted. At both pH values, the two chosen products were identified at the start of the reaction. At a 1:1 ratio, the concentrations of the products were found to be similar. However, at the 1:5 ratio, a discrepancy was observed in the signals, with the later eluting product being more predominant at pH 6.5. This shift in product distribution indicates that the excessive Y has a significant impact on the reaction, potentially by directing the reaction towards the formation of the product with the retention time of 10 min. This phenomenon could be attributed to the enzyme's preferential catalysation of the abundant Y at this specific pH, resulting in a novel reaction pathway or a shift in the equilibrium of product formation. The concentration at this pH was more than twofold higher than at pH 4.5, while the signal for the product at 9.3 min remained similar at both pH values. In all cases, these products disappeared after 24 h.

The enzymatic development of the reaction mixtures with the two enzyme combinations is shown in Figure 31 (F – G). The enzyme combination consisting of Lac and TYR (*cf.* Figure 31 (F)) resulted in surprising outcomes. The effect of Lac was accomplished by converting FA, with similar amounts as achieved with the single enzyme (Figure 31 (B)). The surprising finding was that Y was not converted, despite the expectation that TYR in the enzyme combination would catalyse this reaction. As observed with the single enzyme at a substrate ratio of 1:5, a slight increase in concentration was detected at the start of the reaction. However, in contrast to the behaviour of TYR (*cf.* Figure 31 (C)), the signal for Y did not decrease after 24 h. One potential explanation could be the use of pH 4.5, as TYR does not function optimally at this pH (*cf.* Figure 24(E)). Another potential explanation involves the sensitivity of TYR, where its function could be negatively affected by the presence of Lac [105]. Furthermore, both chosen products were identified at the start of the reaction, but disappeared after 24 h, as already seen with the previous enzymes. In this case, the concentrations were slightly higher than those achieved with the Lac alone in the reaction mixture.

The other enzyme combination, consisting of HRP and GOX (see Figure 31 (G)), also resulted in surprising outcomes. The conversion of FA was almost complete at the start of the reaction. After a period of 24 h, no signal for FA was detected. This finding is comparable to the results obtained with HRP alone at pH 4.5 (*cf*. Figure 31 (D)). At a FA/Y ratio of 1:5, a slight decrease in the signal of Y was observed at the start of the reaction, which has not been observed with any enzyme before. In addition, no signal could be observed after 24 h, which would also indicate the complete conversion of Y. However, at both substrate ratios and after 24 h, none of the selected products could be

identified, which leaves the question of which products were formed. One hypothesis to be considered was that the products, which were not identified, were too large and were bound irreversibly by the stationary phase, or alternatively, that the products cannot be qualitatively determined at the selected wavelength.

The integration of UV-Vis and HPLC data provided a more comprehensive understanding of the enzymatic reactions. While UV-Vis offered insights into overall changes in absorbance, indicative of substrate conversion and product formation, HPLC enabled the separation of specific cross-linking products. The findings obtained from this study indicate that FA was efficiently converted by Lac and HRP, while Y conversion was more limited and primarily observed with TYR. On the other hand, the enzyme combinations yielded a range of outcomes. While Lac/TYR failed to convert Y, possibly due to lower pH or inhibitory effects, the combination of HRP/GOX exhibited complex behaviour with Y conversion, raising questions about product identification. The disappearance of cross-linking products in HPLC after 24 h could be attributed to a variety of factors, including further reactions, degradation, or limitations in detection at the chosen wavelengths. The exploration of alternative detection methods, such as mass spectrometry or the analysis of earlier time points could provide insights into these transformations. Having established the enzymes behaviour with monomeric substrates, the subsequent step in the research was to investigate their activity with more complex substrates, such as oligopeptides, with a view to better understanding their potential in food systems.

5.4 Cross-linking behaviour of oligomers

Consequently, the investigation was transitioned from monomeric substrates (FA and Y) to more complex oligopeptides, with the objective of exploring the enzymes' capacity to catalyse cross-linking reactions with larger, more applicable molecules in the context of food applications. The peptides were chosen to be representative of three short, non-unique sequences (P1 – P3) and three longer and unique cereal-specific sequences from rice, oat and maize (P4 – P6). The central question was how the selected enzymes and enzyme combinations perform in cross-linking reactions with these oligopeptides, and how the peptide structure influences the outcome of these reactions. To address this, experiments were conducted using a range of oligopeptides dissolved in a MS compatible surfactant (Rapigest) to ensure solubility. These oligopeptides were then incubated with the previously characterised enzymes and enzyme combinations (Lac, HRP, TYR, Lac/TYR and HRP/GOX) over a time period of 0.5, 2, and 24 h, drawing upon the optimised conditions identified in the earlier experiments with monomeric substrates according to chapter 4.3.4. The primary analytical method employed to analyse the cross-linking reactions was untargeted LC-MS/MS. This technique was used to identify and

characterise the cross-linking products formed between the oligopeptides and a FA-glycoside (FAG), which provided detailed structural information about the cross-linked species. The application of FAG was facilitated by the prevalence of FA in nature, where it is commonly found bound to glycosides (*cf.* Figure 1). In addition, an UV detector was applied, where the wavelengths at 280 nm and 320 nm were monitored, to detect any potential changes in the substrates or products over time. A comprehensive list of all the identified products, accompanied by their respective m/z ratios, is provided in Table 19 for the homogeneous coupling process and in Table 20 for the heterogeneous coupling process. Figure 32 illustrates an example of a chromatogram of FAG with Lac, which was incubated for 0.5 hours, alongside the corresponding MS spectra of the two analysed peaks from Table 19.

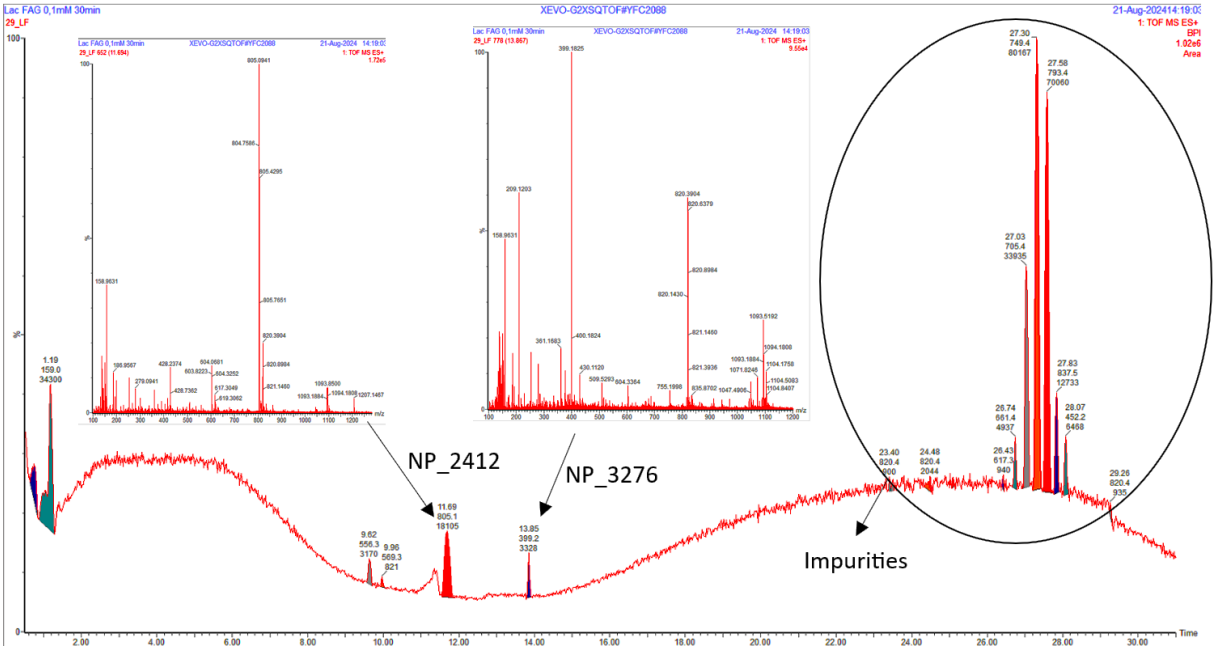

Figure 32: An example of a chromatogram of FAG catalysed by Lac after 0.5 hours. The corresponding retention time (in min) is indicated on the x-axis, while the signal intensity (in %) is displayed on the y-axis. The corresponding MS spectra are also given for the two analysed peaks from Table 19.

Table 19: Results of the homogeneous conversion of FAG or the six peptides (P1 – P6) and the formation of new products using Lac, HRP and TYR over time. The newly identified products were abbreviated using the shortcut NP followed by the identified m/z, the corresponding retention time, charge, and the corresponding time-dependant peak areas.

Substrate	Enzyme	Area	Name	Retention time [min]	Charge	Control	0.5 h	2 h	24 h
FAG	**Lac**	UV	FAG	9.23	-	2,047	-	-	-
		MS	NP_2412	11.69	3	-	18,105	-	-
			NP_3276	13.85	4	-	3,328	-	-
			NP_882	8.78	2	-	-	-	29,364
			NP_1764	12.92	4	-	-	-	398,327
	HRP	UV	FAG	9.23	-	2,047	-	-	-
		MS	NP_3412	10.83	4	-	-	14,019	-
	TYR	UV	FAG	9.23	-	2,047	691	223	-

		MS	NP_176	9.36	1	-	4,264	-	-
P1	**Lac**	MS	P1_820	7.92	1	638,179	751,493	706,816	148,446
			NP_344	6.94	1	-	-	-	28,124
	HRP		P1_820	7.92	1	619,083	577,216	525,978	181,524
	TYR		P1_820	7.92	1	638,179	332,958	167,951	-
			NP_344	7.20	1	-	79,868	249,915	662,006
P2	**Lac**	MS	P2_883	9.00	2	2,629,740	2,466,253	2,422,916	1,160,154
			NP_1046	9.45	2	-	135,831	90,730	-
			NP_582	8.66	1	-	-	-	1,021,640
	HRP		P2_883	9.00	2	2,299,899	2,412,825	2,431,986	2,947,041
	TYR		P2_883	9.00	2	2,629,740	2,351,933	244,595	21,564
			NP_898	8.79	2	-	216,114	283,212	-
			NP_896	8.37	2	-	-	23,708	17,902
			NP_894	11.95	2	-	-	119,933	83,561
			NP_880	12.53	2	-	-	35,000	25,000
			NP_880	12.92	2	-	-	157,213	147,811
			NP_1779	14.58	3	-	-	52,094	-
			NP_1755	21.27	3	-	-	33,574	45,197
P3	**Lac**	MS	P3_792	7.77	2	149,221	-	27,330	49,232
	HRP		P3_792	7.81	2	48,346	38,244	29,363	-
	TYR		P3_792	7.77	2	149,221	72,019	-	-
P4	**Lac**	MS	P4_1839	8.64	2	21,917	5,937	-	-
	HRP		P4_1839	8.64	2	21,917	-	-	-
	TYR		P4_1839	8.64	2	21,917	131,109	184,730	184,730
			NP_1200	7.37	2	-	-	-	122,815
			NP_2013	8.62	3	-	-	-	51,372
P5	**Lac**	MS	P5_1856	14.27	3	2,462	-	-	-
			NP_996	8.86	2	-	21,402	89,837	456,270
			NP_1426	14.12	2	-	49,493	172,460	127,149
			NP_1162	12.19	2	-	-	6,825	874,382
			NP_1590	21.56	3	-	-	115,568	439,397
			NP_569	8.37	1	-	-	-	467,609
			NP_1276	12.29	2	-	-	-	200,000
	HRP		P5_1856	14.27	3	2,462	-	-	-
			NP_996	8.88	2	-	10,574	-	-
			NP_1426	14.21	2	-	32,095	-	-
			NP_1902	14.21	3	-	-	7,122	8,179
	TYR		P5_1856	14.27	3	2,462	-	-	-
			NP_1054	8.88	2	-	1,545	40,932	429,577
			NP_1542	14.29	2	-	38,993	54,332	-
			NP_926	9.38	2	-	-	9,407	176,711
P6	**Lac**	MS	P6_1726	9.1	2	1,263,193	1,058,409	702,657	-
			NP_606	7.84	1	-	90,478	114,546	755,715
			NP_1138	8.06	2	-	88,000	405,782	54,003
			NP_2316	9.86	3	-	24,232	131,312	-

	NP_752	6.81	2	-	-	-	231,120
	NP_1194	9.34	2	-	-	-	35,583
HRP	P6_1726	8.91	2	937,521	794,867	1,077,886	510,982
	NP_606	7.8	1	-	77,775	-	-
	NP_1138	8.09	2	-	98,603	-	-
	NP_2316	9.82	3	-	21,492	-	-
TYR	P6_1726	9.1	2	1,263,193	1,096,746	834,099	-
	NP_974	7.89	2	-	-	89,778	-
	NP_769	8.81	1	-	-	156,719	-
	NP_606	7.99	1	-	-	-	45,409
	NP_589	9.77	1	-	-	-	5,473

Table 20: Results of the heterogeneous conversion between FAG and the six peptides (P1 – P6) and the formation of new products using Lac, HRP, TYR, Lac+TYR and HRP+GOX over time. The newly identified products were abbreviated using the shortcut NP followed by the identified m/z, the corresponding retention time and charge.

Substrate	Enzyme	Area	Name	Retention time [min]	Charge	Control	0.5 h	2 h	24 h
FAG + P1	**Lac**	UV	FAG	9.23	-	2,047	-	-	-
		MS	P1_820	7.78	1	638,179	650,006	774,094	209,645
			NP_344	7.01	1	-	-	-	37,131
	HRP	UV	FAG (320nm)	9.23	-	2,047	745	-	-
			280nm	7.58	-	-	23	-	-
				7.73	-	-	-	-	85
		MS	P1_820	7.92	1	619,083	615,710	160,890	95,337
	TYR	UV	FAG	9.23	-	2,047	720	735	420
		MS	P1_820	7.92	1	638,179	238,841	150,866	-
			NP_344	7.22	1	-	-	289,762	678,445
	Lac+ TYR	UV	FAG	9.23	-	2,047	-	-	-
		MS	P1_820	7.92	2	638,179	101,737	118,809	43,143
			NP_344	7.22	1	-	22,416	72,743	337,812
	HRP+ GOX	UV	FAG	9.23	-	2,047	-	-	-
		MS	P1_820	7.92	1	638,179	202,163	169,658	66,145
FAG + P2	**Lac**	UV	FAG	9.23	-	2,047	-	-	-
		MS	P2_882	9.00	2	2,629,740	2,486,614	2,316,537	2,045,270
	HRP	UV	FAG	9.23	-	2,047	466	-	-
		MS	P2_882	9.00	2	2,299,899	2,499,837	2,365,083	2,927,742
	TYR	UV	FAG	9.23	-	2,047	688	395	168
		MS	P2_882	9.00	2	2,629,740	2,504,553	75,549	43,300
			NP_543	7.82	1	-	123,785	-	-
			NP_896	8.38	2	-	-	20,002	9,499
			NP_898	8.79	2	-	-	46,497	-
			NP_894	11.85	2	-	-	96,835	108,495
			NP_880	12.53	2	-	-	24,563	-
			NP_880	12.92	2	-	-	102,008	4,830
			NP_1755	21.27	3	-	-	30,000	25,682
			NP_848	9.46	2	-	-	-	10,599
	Lac+ TYR	UV	FAG	9.23	-	2,047	-	-	-
		MS	P2_882	9.00	2	2,629,740	2,448,703	2,384,674	1,683,879
			NP_344	7.22	1	-	-	41,241	-
			NP_810	7.95	2	-	-	84,146	-
			NP_582	8.90	2	-	-	-	433,931
			NP_454	9.65	1	-	-	-	557,402

	HRP+ GOX	UV	FAG	9.23	-	2,047	-	-	-
		MS	P2_882	9.00	2	2,629,740	2,330,401	1,248,829	134,429
			NP_720	8.23	2	-	-	-	14,102
FAG + P3	**Lac**	UV	FAG	9.23	-	2,047	-	-	-
		MS	P3_792	7.77	2	149,221	44,390	-	-
	HRP	UV	FAG	9.23	-	2,047	692	-	-
		MS	P3_792	7.77	2	48,346	50,800	35,691	-
			NP_176	9.15	1	-	3,366	-	-
	TYR	UV	FAG	9.23	-	2,047	808	762	-
		MS	P3_792	7.77	2	149,221	113,645	-	-
			NP_176	9.38	1	-	5,658	4,283	-
	Lac+ TYR	UV	FAG	9.23	-	2,047	-	-	-
		MS	P3_792	7.77	2	149,221	23,090	-	-
	HRP+ GOX	UV	FAG	9.23	-	2,047	-	-	-
		MS	P3_792	7.77	2	149,221	93,024	16,844	-
			NP_882	9.09	2	-	22,510	-	-
FAG + P4	**Lac**	UV	FAG	9.23	-	2,047	-	-	-
		MS	P4_1839	8.64	2	21,917	4,035	-	-
	HRP	UV	FAG	9.23	-	2,047	579	-	-
		MS	P4_1839	8.64	2	21,917	-	-	-
			NP_176	9.15	1	-	2,260	-	-
	TYR	UV	FAG	9.23	-	2,047	673	745	585
		MS	P4_1839	8.64	2	21,917	223,702	127,676	-
			NP_1200	7.37	2	-	-	-	61,630
			NP_2346	8.74	3	-	-	-	2,073
	Lac+ TYR	UV	FAG	9.23	-	2,047	-	-	-
		MS	P4_1839	8.64	2	21,917	-	-	-
			NP_457	8.13	1	-	-	4,270	44,106
	HRP+ GOX	UV	FAG	9.23	-	2,047	-	-	-
		MS	P4_1839	8.64	2	21,917	-	-	-
FAG + P5	**Lac**	UV	FAG	9.23	-	2,047	-	-	-
		MS	P5_1856	14.27	3	2,462	-	-	-
			NP_996	8.90	2	-	16,226	49,648	447,518
			NP_1426	12.22	2	-	32,507	79,281	-
			NP_1590	21.87	3	-	-	36,339	91,397
			NP_569	8.38	1	-	-	-	491,026
			NP_440	9.45	1	-	-	-	104,462
			NP_1276	12.15	2	-	-	-	400,878
	HRP	UV	FAG	9.23	-	2,047	597	-	-
		MS	P5_1856	14.27	3	2,462	-	-	-
			NP_176	9.15	1	-	2,364	-	-
			NP_1902	14.17	3	-	16,269	10,177	4,964
	TYR	UV	FAG	9.23	-	2,047	794	922	931
		MS	P5_1856	14.27	3	2,462	-	-	-
			NP_176	9.34	1	-	6,246	9,648	-
			NP_1054	8.91	2	-	-	47,088	446,189
			NP_1542	14.31	2	-	-	24,315	-
			NP_926	9.38	2	-	-	-	138,780
	Lac+ TYR	UV	FAG	9.23	-	2,047	-	-	-
		MS	P5_1856	14.27	3	2,462	-	-	-
			NP_996	9.09	2	-	7,247	49,845	50,000
			NP_1542	14.26	2	-	96,199	147,432	-
			NP_1276	12.68	2	-	-	2,674	118,076

			NP_1378	13.38	2	-	-	2,114	-
			NP_497	8.79	1	-	-	-	212,619
			NP_612	9.43	1	-	-	-	99,205
	HRP+ GOX	UV	FAG	9.23	-	2,047	-	-	-
		MS	P5_1856	14.27	3	2,462	-	-	-
			NP_1920	13.19	3	-	-	23,619	-
			NP_1404	13.01	3	-	-	-	7,169
FAG + P6	**Lac**	UV	FAG	9.23	-	2,047	-	-	-
		MS	P6_1726	9.10	2	1,263,193	932,980	591,259	-
			NP_606	7.85	1	-	120,601	168,456	843,127
			NP_1138	8.07	2	-	177,036	305,275	-
			NP_2316	9.89	3	-	47,932	95,782	-
			NP_1194	9.34	2	-	-	-	15,482
	HRP	UV	FAG	9.23	-	2,047	466	-	-
		MS	P6_1726	9.10	2	937,521	803,315	972,497	394,317
	TYR	UV	FAG	9.23	-	2,047	674	793	517
		MS	P6_1726	9.10	2	1,263,193	925,450	448,429	-
			NP_769	8.74	1	-	38,854	72,216	-
			NP_974	7.85	2	-	-	41,663	-
			NP_606	7.97	1	-	-	49,205	27,589
			NP_1562	8.59	2	-	-	61,389	-
			NP_176	9.38	1	-	-	-	1,352
			NP_589	9.79	1	-	-	-	2,689
	Lac+ TYR	UV	FAG	9.23	-	2,047	-	-	-
		MS	P6_1726	9.10	2	1,263,193	910,958	410,372	-
			NP_606	7.99	1	-	30,819	55,400	15,844
			NP_1136	8.30	2	-	115,897	150,248	-
			NP_2313	10.11	3	-	28,976	56,475	-
			NP_519	8.40	1	-	-	-	494,147
			NP_769	8.79	1	-	-	-	76,800
			NP_1108	10.10	2	-	-	-	36,264
			NP_1358	10.25	2	-	-	-	13,675
	HRP+ GOX	UV	FAG	9.23	-	2,047	-	-	-
		MS	P6_1726	9.1	2	1,263,193	939,476	127,845	3,985

The homogeneous conversion of FAG with Lac, HRP and TYR and the resulting products are listed in Table 19, while the heterogeneous conversion with the additional two enzyme combinations are listed in Table 20. As expected, a rapid conversion of FAG was observed with Lac and HRP using the UV detector, with a full conversion of FAG being achieved after 0.5 h. In the case of TYR, a peak for FAG was still evident after 2 h, although this also disappeared within 24 h. In addition, various products were formed up to a m/z of 3412, which may indicate the presence of FAG oligomers. However, it is notable that each enzyme forms different products at different time intervals, with no clear trend in the formation of specific products. Lac formed four various oligomeric products ranging from a potential trimer (m/z of 882) up to a potential nonamer (m/z of 3276). HRP generated the biggest product (m/z of 3412) with potentially consisting of up to ten monomers. TYR generated only a product with a m/z of 176, which is a typical fragment of FA that has lost a methyl group on the methoxy group (Figure 1) [106].

First, the peptide VNLYQNA (P1; MW = 820.90 g/mol), which occurs in rice, oat and maize, was used for cross-linking experiments. The peptide with Y in the middle (P1) showed an efficient conversion with TYR, reaching complete conversion within 24 h. In contrast, the other two enzymes were less effective, as 20 – 30 % of the peptide remained after the same period. A product with a m/z of 344 was detected in the presence of Lac and TYR, with TYR producing it in much higher amounts. This could be a fragment of the peptide that has been cleaved by the enzyme at the peptide bond adjacent to the Y residue. However, no signs of oligomerised products were identified. In case of the heterogeneous reaction between FAG and P1, FAG was fully converted after 2 h with all enzymes except TYR. With TYR, approximately 20 % of the initial FAG amount was present within 24 h, indicating its much lower convertibility to this substrate, as previously described in various literature sources [6]. In contrast, TYR was the only enzyme that fully converted the peptide within 24 h. The only product identified by cross-linking these two substrates displayed a m/z value of 344, which has previously been found in the homogeneous conversion of P1. This fragment was found in the presence of Lac, TYR and Lac+TYR, with TYR alone producing the highest amounts. The absence of any further products identified suggests that FAG and P1 did not generate any heterogeneous cross-linking products.

Another oligopeptide investigated was LIIPQHY (P2; MW = 883.06 g/mol), which also occurs in all of the three cereals. The homogeneous coupling of the peptide with a terminal Y (P2) showed slightly different results compared to P1. The convertibility with TYR resulted in the production of various products after 2 h. Five products of different polarity, ranging between 880 – 898 m/z, were found after 2 h and were also mainly present within 24 h. These could be various Y modifications, as TYR catalyses Y to a quinone, which leads to the formation of various adducts. In case of the product with a m/z of 898, TYR could be hydroxylating the Y residue, adding an oxygen atom (approximately +16 Da), which could explain the mass increase from 883 to 898. In addition, two probably dimeric products were identified after 2 h, which corresponds to the simultaneous conversion of the peptide. The slight difference in m/z between 1779 and 1755 could be due to different coupling sites or additional modifications. In contrast, Lac converted approximately 55 % of the peptide within 24 h, while HRP has not converted it during this period. In accordance with the results of the homogeneous conversion of P2 from Table 19, the heterogeneous cross-linking reaction between FAG and P2 resulted in a variety of products, especially when oxidised by TYR. The conversion of each substrate showed analogous results to those achieved with FAG and P1, where TYR was the only enzyme that did not fully convert FAG, but displayed the most efficient conversion rate with the peptide. Furthermore, the identified products were in a great accordance with that achieved in the homogeneous reaction listed in Table 19, suggesting a comparable reaction mechanism and homogeneous cross-linking products. Moreover,

the heterogeneous cross-linking reactions produced two additional products with TYR (m/z of 543 and 848), which could be attributed to the presence of FAG in the heterogeneous mixture. The hydrophilic dimeric product with a m/z value of 1755 was also found in the heterogeneous reaction mixture, indicating the homogeneous cross-linking of two P1 monomers. When the two enzyme combinations were employed, different products were formed, with no signs of polymerisation.

The final shorter oligopeptide examined was KAEREGC (P3; MW = 791.88 g/mol), which did not contain Y, but cysteine and lysine, as these two amino acids have the potential to crosslink [1]. Neither of the two amino acids, cysteine and lysine, were present in the previous two peptides. The results demonstrate that all enzymes were capable of converting the peptide, with TYR being the most efficient one. The only difference observed compared to the previous two peptides was the absence of any products. This could be associated to the missing Y in the peptide sequence, which is the primary coupling point in such coupling reactions. The heterogeneous conversion of FAG and P3 resulted as well in the generation of nearly no products. Despite the full conversion of the substrates within 24 h, no products could be identified after this time period. The only products identified were with a m/z of 172 and 882. The smaller product has been already found in the homogeneous reaction mixture of FAG and suggests the occurrence of a typical fragment of FA that lost a methyl group on the methoxy group [106]. The larger product was obtained with HRP+GOX after a duration of two hours. Given that it exhibited a greater mass than the peptide, it can be hypothesised that it is either a heterogeneous coupling product or a modification of the peptide that was specifically achieved by this particular enzyme combination.

The specific rice peptide under investigation was EYFDEKNEQFQCTGT (P4; MW = 1838.92 g/mol), which can be found in the glutelin type-B 4 storage protein. As indicated by the amino acid sequence, the peptide contains a single Y residue within the chain. During the conversion process, a complete conversion was observed with Lac and HRP after 2 h, but no products were identified. However, an increase in the peptide signal was observed with TYR, whereby two further products were formed simultaneously within 24 h. The product with a m/z value of 1200 could be a fragment of the cleaved peptide. Given the large drop in molecular weight, a break in the peptide backbone likely occurred, leading to e.g. YFDEKNEQF as this peptide corresponds to a mass of approximately 1200. The larger product with a m/z of 2013 suggests the dimer formation, where P4 could crosslink with a smaller fragment, or two smaller fragments were dimerised. Similar findings were observed in the heterogeneous cross-linking reactions, where despite the complete conversion of the substrates (with the exception of FAG with TYR), almost no additional products were identified. HRP generated a product with a m/z of 176, a typical demethylated FA fragment [106], and Lac/TYR generated a small fragment with a m/z value of 457 with a slightly smaller hydrophobicity as the starting peptide.

Notably, the reaction catalysed by TYR was the only exception, producing two products (m/z of 1200 and 2346) within 24 h. The smaller product has been already found in the homogeneous cross-linking of the peptide, but the larger product has not been previously detected. This product could be a trimer consisting of one molecule P4, one molecule FAG and one molecule FA, from which the glycoside was cleaved. The presence of trimeric products consisting of one molecule peptide and two molecules FA has already been found in the literature [4]. The presence of the larger molecule is a crucial hint for heterogeneous cross-linking, as this product was not detected in the homogeneous mixture.

Another specific cereal peptide was KQGDVVALPAGIVHWCY (P5; MW = 1856.18 g/mol), which can be found in oat in the 12S seed storage globulin 1 protein. As indicated by the amino acid sequence, the peptide contains a terminal Y residue within the chain. The homogeneous conversion of the oat (P5) produced together with the maize peptide (P6) the highest amounts of various products. The oat peptide was fully converted with each enzyme within just 0.5 h. The lowest number of products was observed in the case of HRP, which formed two various products within 0.5 h (m/z of 996 and 1426) and one product within 2 h, which remained stable within 24 h (m/z of 1902). The smaller products could be peptide fragments due to the significant decrease in mass. The distinguishing factor between the two fragments is the location of the cleavage points. Furthermore, the larger product exhibited a modest increase in mass, suggesting a potential peptide modification, such as oxidation of certain amino acids. Lac produced the two products with a m/z of 996 and 1426, which were also formed by HRP. In contrast to HRP, the product signals increased with time, indicating the production of more stable products. The smaller product showed a shorter retention time, indicating a more hydrophilic character compared to the oat peptide, while the larger product demonstrated a comparable hydrophobicity to the peptide. In both cases, it can be assumed that fragments of the cleaved peptide with different polarity are involved. In addition, the production of four further products with a m/z of 569, 1162, 1276 and 1590 was observed after a period of 2 h, and subsequently within 24 h. It can be hypothesised that these products are constituted of fragments of the peptide, which have been cleaved at specific points within the sequence of the peptide. In conclusion, TYR generated completely different products but with a similar m/z and polarity as achieved with Lac and HRP. The results obtained indicate that each enzyme provides a distinct oxidation of the peptide, yielding to a range of products. Lac and HRP demonstrate a similar reaction mechanism, which results in the formation of the same products. In contrast, TYR displays a divergent mechanism, resulting in a distinct set of peptide fragments.

The heterogeneous coupling of FAG and the oat peptide (P5) resulted, as in the homogeneous coupling of P5, to a bright variety of products. In contrast to the homogeneous coupling, this process revealed

that each individual enzyme generated a unique product profile. In contrast to the homogeneous reactions, where Lac and HRP generated analogous products, such findings were not observed in the heterogeneous reactions. It has been demonstrated that both HRP and TYR generate the typical demethylated FA fragment with a m/z of 176 [106], and products that have been already identified in the homogeneous cross-linking. Lac generated exactly the same products as in the homogeneous mixture, with the exception of an additional product with a m/z of 440, which has been identified. As this product was not found in the homogeneous reactions, it can be assumed that a heterogeneous fragment occurred. One hypothesis for this could be a cross-link between the cleaved dipeptide CY and FA, cleaved from FAG, followed by a further modification. The coupling of such short peptides and a FA has already been mentioned in the literature [4]. In addition, both enzyme combinations resulted in a variety of products and fragment ions. Lac+TYR, for instance, produced some products found with the individual enzymes, but also generated new products with a m/z of 497, 612 and 1378. Since these products were absent in homogeneous cross-linking reactions, it can be hypothesized that they are heterogeneous complexes composed of FA or FAG and various peptide fragments. Furthermore, HRP+GOX formed two products (m/z of 1404 and 1920) that were different from the products formed by HRP alone. Notably, both systems produced a molecule with a slightly larger mass than the initial peptide, thereby indicating a coupling reaction between the substrates or their fragments. The results indicate the occurrence of heterogeneous cross-linking products; however, the exact identification of these products remains hypothetical. Furthermore, the enzyme combinations resulted in the production of entirely new products that have not been identified with the single enzymes.

The last specific cereal peptide was YQLPSYRTNPCGVSAA (P6; MW = 1726.93 g/mol), which can be found in maize in the zein beta storage protein. As indicated by the amino acid sequence, the peptide contains one terminal Y and one Y residue within the chain. In contrast to P5, the maize peptide was only fully converted by Lac and TYR within 24 h. In case of HRP, more than 50 % of the peptide was left within 24 h. Both Lac and HRP generated identical products, with m/z values of 606, 1138 and 2316. Theoretically, the smallest product could be a modified YQLPS (m/z of 588) residue, formed through the cleavage between serine and Y. The second product most likely consisted of the other part of the peptide, namely the YRTNPCGVSAA residue, as this exactly corresponds to the mass of 1138. It can be hypothesised that the cleavage of the peptide was the result of a combination of enzymatic oxidation and MS-induced fragmentation. Lac and HRP most likely modified the peptide by creating weak points, particularly between serine and Y. The MS process then caused the peptide to fragment at these weakened points. The largest product displayed most likely a dimeric structure, consisting hypothetically of the P6 and the smaller fragment (1727 + 606 = 2315 m/z). Among these, the two smaller molecules exhibited a lower degree of hydrophobicity, whereas the larger molecule showed a higher hydrophobicity compared to the original maize peptide. Furthermore, the products catalysed

by HRP appeared only within 0.5 h and then disappeared, in contrast to the effects of Lac, which facilitated a continuous accumulation of these products over time. In addition, Lac generated two additional products with a m/z value of 752 and 1194. These could be as well various peptide fragments that were cleaved at different positions within the chain or were additionally modified, for example, through oxidation. In addition, TYR produced products that were distinctly different from those of the other two enzymes, which supports the hypothesis that they employ different reaction mechanisms.

The heterogeneous mixtures consisting of P6 and FAG exhibited a similar level of efficiency to that achieved with P5. However, no products were detected in the presence of HRP and HRP+GOX and the peptide was not fully converted. Nevertheless, the use of other enzymes resulted in the generation of a bright spectrum of products. The products identified with Lac and TYR are mostly analogous to the homogeneous coupling products listed in Table 19. The only exceptions were the products with a m/z of 176 and 1562, which were achieved with TYR. The smaller product was identified as the characteristic demethylated FA fragment [106], which was frequently encountered in the heterogeneous mixtures. The larger product was hypothesised to be a potential heterogeneous cross-linking fragment, as it had not been previously observed in the homogeneous coupling reaction. One theoretical possibility is the coupling of two peptide fragments with the m/z of 606 and one molecule of FAG (606 + 606 + 356 = 1568 m/z), which would result in a similar m/z value as detected. Furthermore, the enzyme combination Lac+TYR produced products that were found with the single enzymes, but also produced new products, as previously observed in the coupling between FAG and P5. The newly identified products exhibited m/z values of 519, 1108, 1358 and 2313. The three lower m/z values are likely to be various cross-linking fragments, consisting of peptides cleaved at different sites. Furthermore, the product with a m/z value of 2313 could be both heterogeneous and homogeneous, as evidenced by the identification of a similar product in the homogeneous reaction mixture (m/z of 2316) with a comparable retention time. This could be attributed to slight modifications in the resulting product. However, the possibility of a heterogeneous cross-linking product cannot be discounted.

In summary, the results showed that the peptide with a terminal Y (P2) generated significantly more products than the peptide with Y within the chain (P1). The peptide P3 was only found to produce a negligible amount of products, primarily due to the absence of Y. A similar outcome was observed in the case of cereal-specific peptides, where the rice peptide with Y within the chain (P4) produced much lower amounts of products compared to the oat (P5) and maize peptides (P6), which contained a terminal Y. This observation could be explained by the better accessibility of the Y within the chain, a hypothesis already proposed by Mattinen [51]. The presence of Y within the chain could be limited by

the surrounding amino acids through steric hindrance, resulting in a reduced or absent extent of cross-linking. Consequently, this could be a key factor in explaining the observed variation in the amount of products formed with peptides with a terminal Y and those without. Furthermore, the heterogeneous coupling reactions resulted in some cases in the generation of products that were not identified in the homogeneous coupling reaction. This finding validates the hypothesis that these peptides can heterogeneously cross-link with FAG, thereby demonstrating the potential for the generation of heterogeneous networks. In addition, the analysis revealed that certain enzymes produced a more diverse range of products than others. In general, the product pattern for P5 and P6 was found to be very similar. Lac and HRP generated products with a high degree of similarity, with Lac resulting in a greater amount of varied products, and TYR producing products that were partially different, but with a polarity similar to that achieved with Lac and HRP. While the homogeneous coupling reactions (Table 19) exhibited relatively similar product amounts for each enzyme, in the heterogeneous cross-linking (Table 20), the highest product yields were observed for Lac, TYR and their combination, particularly when converting the peptides with a terminal Y.

6 Conclusion and Outlook

Gluten, an essential component in baking due to its gas-holding capacity and elastic properties, poses a significant challenge in the contemporary context where celiac disease (CD) and gluten sensitivity are on the rise, thereby driving a substantial demand for gluten-free (GF) products. Nonetheless, these alternatives often fall short of the quality exhibited by wheat bread. Therefore, current research project aims to address this by creating enzymatically induced biopolymer networks of proteins and arabinoxylans (AXs) in GF cereals, through coupling of tyrosine (Y) and ferulic acid (FA) *via* enzymes to form a gluten-like structure without the need for additives that are required by law to be labelled. This thesis contributed to this ongoing research by characterising cross-linking enzymes and investigating the network development between the monomers and subsequently of glycolised FA and oligomers, such as the model peptides from rice, oat, and maize. The potential of five oxidoreductases, namely laccase (Lac), peroxidase (HRP), tyrosinase (TYR), glucose oxidase (GOX), and pyranose oxidase (POX) for food-relevant cross-linking reactions was investigated, with a focus on enhancing the functional properties through enzymatic modification. A multi-stage approach was employed, whereby enzymes were initially characterised through various enzyme assays. This was followed by assessing cross-linking reactions with monomers and oligomers, using analytical techniques such as reversed phase high performance liquid chromatography with a UV detector (RP-HPLC-UV) and liquid chromatography coupled with a mass spectrometer (LC-MS/MS) for product determination.

The results of the enzyme characterisation indicated that none of the enzymes could efficiently convert both substrates simultaneously, which arose the hypothesis that combining two enzymes might be a promising approach. The HPLC and UV-Vis data showed across time intervals from 0 to 24 hours, that Lac and HRP efficiently converted FA, while TYR primarily converted Y, with enzyme combinations showing varied results. Lac/TYR effectively converted FA, mirroring Lac alone, but failed to convert Y, possibly due to suboptimal pH or TYR inhibition, with cross-linked products disappearing after 24 h. HRP/GOX rapidly converted FA, consistent with HRP, and uniquely showed Y conversion, though no products were detected after 24 h. The disappearance of cross-linked products after 24 h, observed across these time points, suggested potential further reactions or detection limitations such as the solubility of the products, necessitating alternative methods. Building on monomeric substrate results, the study progressed to investigating enzyme activity with oligopeptides to assess their food system potential, maintaining the focus on time-dependent transformations.

The final analytical determination of the oligomers revealed the occurrence of homogeneous and heterogeneous cross-linking between the glycoside of FA and six various peptides, consisting of three

shorter peptides each with a different Y location, and three longer cereal-specific (rice, oat and maize) peptides. The initial identification of various fragments and cross-linking products confirmed that higher oligomers of FA and Y-consisting peptides can also undergo cross-linking. This was accomplished by FAG, which was rarely applied in the literature, as the non-glycolysated FA was mainly applied. In contrast, Y-containing peptides were more frequently reported in the literature, where especially shorter peptides, such as GY and GYG, were commonly used. The central objective was to establish a connection between simplified model systems and complex food matrices by investigating the enzyme behaviour across monomeric and, ultimately, oligomeric levels in order to predict their performance in subsequent dough systems. In contrast to previous studies, this work examined cereal-specific peptides that mimicked the non-gluten containing rice, oat, and maize proteins, and employed a 1:5 FA/Y ratio that reflected realistic conditions. Given that the peptides represent protein segments, it was anticipated that variations in amino acid sequence and enzyme selection would influence cross-linking efficiency and product formation. Subsequent studies in part of the project will use matrix-assisted laser desorption/ionisation (MALDI) for larger product identification, followed by cross-linking of proteins and AXs isolates to develop a stable network, and rheological characterisation of model foams and doughs. The ultimate aim will be to model the network formation in gluten-free doughs and create a system with comparable properties to gluten-containing ones.

List of figures

Figure 1: Chemical structure of arabinoxylan. ..... - 10 -

Figure 2: Tyrosine and the corresponding mesomeres of its radical after oxidation. ..... - 12 -

Figure 3: Michaelis-Menten (left) and Hanes-Woolf (right) equations and plots ..... - 13 -

Figure 4: The two-step oxidation of ABTS. ..... - 14 -

Figure 5**:** Schematic representation of the three copper site types and their coordination, including the distances between the ligands. ..... - 16 -

Figure 6: Catalytic cycle of HRP with ferulate as a reducing substrate. ..... - 18 -

Figure 7: Formation of o-quinone from Tyrosol in presence of TYR and O_2. ..... - 19 -

Figure 8: General reaction of β-D-glucose with glucose oxidase (GO) to form δ-D-gluconolactone and hydrogen peroxide. ..... - 20 -

Figure 9: General reaction of β-D-glucose with pyranose oxidase (P2O) to form 2-keto-glucose and hydrogen peroxide. ..... - 21 -

Figure 10: The catalytic cycle of pyranose oxidase with glucose as a substrate. ..... - 21 -

Figure 11: Ferulic acid and the corresponding mesomeres of its radical after oxidation. ..... - 22 -

Figure 12: The potential cross-linking products of tyrosine by Lac. ..... - 25 -

Figure 13: Proposed formation of tri-Y through a Michael addition reaction. ..... - 26 -

Figure 14: Oxidation of FA by HRP (A) leading to various FA trimers (B). ..... - 28 -

Figure 15: Oxidation of the tripeptide GYG by HRP (A) and the eight possible heterogenous products resulting from two isomeric GYG radicals (A) and four isomeric FA trimer radicals. ..... - 29 -

Figure 16: General instrumentation of a high-performance liquid chromatography (HPLC). ..... - 30 -

Figure 17: Construction of the Xevo G2-XS QTof mass spectrometer by Waters ..... - 32 -

Figure 18: Schematic illustration of an ESI ion source generating ions. ..... - 32 -

Figure 19: The entire experimental procedure divided into three main categories ..... - 40 -

Figure 20: The colouration of the reaction mixtures for ABTS (A) and MBTH (B) ..... - 50 -

Figure 21: Absorption spectra of different concentrations of ABTS (0 – 28 µM) with laccase in excess in McIlvaine buffer at a pH of 4. ..... - 51 -

Figure 22: Absorption spectra of different Htyr concentrations (0-53 µM) with $NaIO_4$ and MBTH in excess in McIlvaine buffer at a pH of 4. ..... - 52 -

Figure 23: Calibration curve for the determination of the protein concentration ..... - 54 -

Figure 24: Results of the determination of pH optima for Lac using ABTS assay (A) and Htyr-MBTH assay (B), HRP using ABTS assay (C) and Htyr-MBTH assay (D), TYR using Htyr-MBTH assay (E), GOX (F) and POX (G) using ABTS-HRP co-assay. ..... - 56 -

Figure 25: Results of the determination of temperature optima for Lac (A) and HRP using ABTS assay (B), TYR using Htyr-MBTH assay (C), and GOX (D) and POX (E) using ABTS-HRP co-assay. ..... - 60 -

Figure 26: UV spectra of the conversion of FA (2 mM) and Y (0.2 mM) by Lac (A, B), HRP (C, D), TYR (E, F), GOX (G, H) and POX (I, J) at 30 °C. ..... - 67 -

Figure 27: UV spectra of the conversion of FA (A) and Y (B) by GOX (orange) and by the enzyme combination HRP/GOX (green). ..... - 70 -

Figure 28: Impact on the enzyme activity after changing the buffer. ..... - 73 -

Figure 29: Impact on the enzyme activity after adding Rapigest (0.1 & 0.05 %) and DMF (10 %) to the reaction mixture. ..... - 74 -

Figure 30: The time-dependent absorbances at 280 nm (A), 320 nm (B) and 405 nm (C) (*in case of TYR at 480 nm) of the individual enzymes with a FA/Y ratio of 1:5. ..... - 75 -

Figure 31: The concentrations of FA, Y and two coupling products (in µg / mL) at 280 nm catalysed by water (**A**), Lac at pH 4.5 (**B**), TYR at pH 6.5 (**C**), HRP at pH 4.5 (**D**) and pH 6.5 (**E**), Lac+TYR at pH 4.5 (**F**) and HRP+GOX at pH 4.5 (**G**) ..... - 79 -

Figure 32: An example of a chromatogram of FAG catalysed by Lac after 0.5 hours. ..... - 82 -

Figure 33: Results for the determination of the molar extinction coefficient of ABTS at six different pH values ..... - 108 -

Figure 34: Results for the determination of the molar extinction coefficient of Htyr at six different pH values ..... - 109 -

Figure 35: The corresponding Michaelis-Menten curve (left) and Hanes-Woolf plot (right) of Lac with ABTS (A; pH 4; 35 °C) and Htyr (B; pH 4.5; 35 °C), of HRP with ABTS (C; pH 4; 30 °C) and Htyr (D; pH 6.5; 30 °C) and of TYR with Htyr (E; pH 6.5; 25 °C). ..... - 110 -

Figure 36: The corresponding Michaelis-Menten curve (left) and Hanes-Woolf plot (right) of GOX with ABTS (F; pH 4.5; 40 °C) and of POX with ABTS (G; pH 5.5; 35 °C). ..... - 111 -

Figure 37: The corresponding Michaelis-Menten curve (left) and Hanes-Woolf plot (right) of Lac with FA (A; pH 4.5; 30 °C), of HRP with FA (B; pH 4.5; 30 °C), of TYR with Y (C; pH 6.5; 30 °C), the enzyme combination of Lac (D) and TYR (E) with FA (pH 4.5; 30 °C). ..... - 112 -

Figure 38 The corresponding Michaelis-Menten curve (left) and Hanes-Woolf plot (right) of the enzyme combination consisting of Lac (A) and TYR (B) with Y (pH 4.5; 30 °C), of HRP (C) and GOX (D) with FA (pH 4.5; 30 °C), and of HRP (E) and POX (F) with FA (pH 6.5; 30 °C). ..... - 113 -

Figure 39: External calibration curves for Y and FA at 280 nm for the HPLC analysis. ..... - 114 -

List of tables

Table 1: Applied chemicals and the corresponding manufacturer and CAS or Lot number. ..... - 35 -

Table 2: Prepared solutions divided according to the two main experimental parts. ..... - 36 -

Table 3: Used equipment with the corresponding name and manufacturer ..... - 38 -

Table 4: Applied gradient of eluent A (20 mM KH_2PO_4, pH 2.0), eluent B (25 % ACN (w/w) in KH_2PO_4 buffer, pH 2.0) and eluent C (50 % ACN (w/w) in water) for the HPLC measurements. ..... - 45 -

Table 5: Settings for the RP-HPLC-UV analysis. ..... - 45 -

Table 6: Applied LC flow gradient of eluent A and B. ..... - 46 -

Table 7: Settings for the measurements with LC-MS/MS. ..... - 47 -

Table 8: Applied solutions and the volumina for the determination of the path length. ..... - 49 -

Table 9: The measured absorbances of three different ABTS concentrations in cuvettes (d = 1 cm) and plate, and the calculated layer thickness of the plate. ..... - 50 -

Table 10: Molar extinction coefficients of ABTS at six different pH values compared to literature. - 51 -

Table 11: Extinction coefficients of Htyr with MBTH as a coupling reagent at six different pH values compared to the literature. ..... - 53 -

Table 12: The protein concentrations calculated in triplicate for Lac, HRP, TYR, GOX and POX ..... - 54 -

Table 13: The determined kinetic values, K_M and v_{max}, for Lac with both substrates in triplicate and the corresponding literature values. ..... - 63 -

Table 14: The determined kinetic values, K_M and v_{max}, for HRP with both substrates and the corresponding literature values. ..... - 63 -

Table 15: The determined kinetic values, K_M and v_{max}, for TYR with Htyr and the literature data. .. - 64 -

Table 16: The determined kinetic values, K_M and v_{max}, for GOX and POX with ABTS and the literature data. ..... - 65 -

Table 17: A summary of the determined optimal pH and temperature conditions for all five enzymes with ABTS and Htyr as a substrate. ..... - 65 -

Table 18: Summary of all kinetic parameters determined using a heatmap[1]. ..... - 72 -

Table 19: Results of the homogeneous conversion of FAG or the six peptides (P1 – P6) and the formation of new products using Lac, HRP and TYR over time. ..... - 82 -

Table 20: Results of the heterogeneous conversion between FAG and the six peptides (P1 – P6) and the formation of new products using Lac, HRP, TYR, Lac+TYR and HRP+GOX over time. ..... - 84 -

Table 21: Pipetting scheme for the determination of the molar extinction coefficient of ABTS and the corresponding ABTS concentration in each well..... - 108 -

Table 22: Determined absorbances of the blank measurements for the Bradford assay. ..... - 109 -

Table 23: Determined absorbance values of the standard solutions for the Bradford assay..... - 109 -

References

I have made every effort to locate all owners of the image rights and have obtained their permission to use the images in this work. Should a copyright infringement nevertheless become known, I request that you notify me.

Uncategorized References

1. Manhivi, V.E., E.O. Amonsou and T. Kudanga, *Laccase-mediated crosslinking of gluten-free amadumbe flour improves rheological properties.* Food Chemistry, **2018**. 264: p. 157-163.
2. Mordor Intelligence, *Europe Gluten-Free Food Market Size & Share Analysis - Growth Trends & Forecasts (2025 - 2030)*. **2024**, Mordor Intelligence: India.
3. Caio, G., L. Lungaro, N. Segata, et al., *Effect of Gluten-Free Diet on Gut Microbiota Composition in Patients with Celiac Disease and Non-Celiac Gluten/Wheat Sensitivity.* Nutrients, **2020**. 12(6): p. 1832.
4. Oudgenoeg, G., R. Hilhorst, S.R. Piersma, et al., *Peroxidase-Mediated Cross-Linking of a Tyrosine-Containing Peptide with Ferulic Acid.* Journal of Agricultural and Food Chemistry, **2001**. 49(5): p. 2503-2510.
5. Nordlund, E., *Tyrosinase and Laccase as Novel Crosslinking Tools for Food Biopolymers.* 978-951-38-7117-8, **2008**.
6. Dai, Y. and C. Tyl, *A review on mechanistic aspects of individual versus combined uses of enzymes as clean label-friendly dough conditioners in breads.* Journal of Food Science, **2021**. 86(5): p. 1583-1598.
7. Wu, T., C. Liu and X. Hu, *Enzymatic synthesis, characterization and properties of the protein-polysaccharide conjugate: A review.* Food Chemistry, **2022**. 372: p. 131332.
8. Izydorczyk, M.S. and C.G. Biliaderis, *Cereal arabinoxylans: advances in structure and physicochemical properties.* Carbohydrate Polymers, **1995**. 28(1): p. 33-48.
9. Fincher, G.B. and B. Stone. *Cell walls and their components in cereal grain technology*. 1986.
10. Berlanga-Reyes, C.M., E. Carvajal-Millan, J. Lizardi-Mendoza, et al., *Enzymatic Cross-Linking of Alkali Extracted Arabinoxylans: Gel Rheological and Structural Characteristics.* International Journal of Molecular Sciences, **2011**. 12(9): p. 5853-5861.
11. Correia, M.A.S., K. Mazumder, J.L.A. Brás, et al., *Structure and Function of an Arabinoxylan-specific Xylanase.* Journal of Biological Chemistry, **2011**. 286(25): p. 22510-22520.
12. Mendis, M. and S. Simsek, *Arabinoxylans and human health.* Food Hydrocolloids, **2014**. 42: p. 239-243.
13. Bento-Silva, A., M.C. Vaz Patto and M. do Rosário Bronze, *Relevance, structure and analysis of ferulic acid in maize cell walls.* Food Chemistry, **2018**. 246: p. 360-378.
14. Marinangeli, C.P.F., M.G. Nosworthy and A.-K. Shoveller, *Cereal proteins in the human diet: Reflecting on their contributions to daily protein intake.* Journal of Cereal Science, **2024**. 117: p. 103908.
15. Sagu, S.T., L.T. Wiedemann, K. Nichani, et al., *The Optimization of the Osborne Extraction Method for the Fractionation and Characterization of Oat Proteins.* Separations, **2024**. 11(9): p. 271.
16. Hans-Dieter Belitz, W.G., Peter Schieberle, in *Lehrbuch der Lebensmittelchemie*. **2007**, Springer Berlin, Heidelberg: Berlin. p. 691-768.

17. Bassingthwaighte, J.B. and T.M. Chinn, *Reexamining Michaelis-Menten enzyme kinetics for xanthine oxidase.* Advances in Physiology Education, **2013**. 37(1): p. 37-48.

18. Zhang, B., S. Dhital and M.J. Gidley, *Densely packed matrices as rate determining features in starch hydrolysis.* Trends in Food Science & Technology, **2015**. 43(1): p. 18-31.

19. Soukup, K. *Unterlagen zum Übungsbeispiel ENZYMKINETIK*. Biochemische Übungen I **2012** [Last accesed: 18.01.2025]; Available from: https://boku.ac.at/fileadmin/data/H03000/H77000/LVA/772112_FA/EK_Skriptum.pdf.

20. Prince, W.S., E. Pungor, V. Sluzky, et al., *3.33 - Therapeutic Enzymes and Biomimetic Substrates: A Case Study of Recombinant Human Arylsulfatase B (Naglazyme®) Substrate Selection and Application*, in *Comprehensive Biotechnology (Second Edition)*, M. Moo-Young, Editor. **2011**, Academic Press: Burlington. p. 377-389.

21. Branchi, B., C. Galli and P. Gentili, *Kinetics of oxidation of benzyl alcohols by the dication and radical cation of ABTS. Comparison with laccase–ABTS oxidations: an apparent paradox.* Organic & Biomolecular Chemistry, **2005**. 3(14): p. 2604-2614.

22. Ren, J., K. Danchana, K. Sasaki, et al., *Fluorometric assay of laccase in mushroom extracts and comparisons with absorption spectrophotometry.* Journal of food composition and analysis, **2023**. 123.

23. Merck. *Enzymatic Assay: Glucose Oxidase*. **2024** [Last accesed: 18.01.2025]; Available from: https://www.sigmaaldrich.com/AT/de/technical-documents/protocol/protein-biology/enzyme-activity-assays/enzymatic-assay-of-glucose-oxidase.

24. Leitner, C., J. Volc and D. Haltrich, *Purification and Characterization of Pyranose Oxidase from the White Rot Fungus Trametes multicolor.* Applied and Environmental Microbiology, **2001**. 67(8): p. 3636-3644.

25. Espín, J.C., M. Morales, P.A. García-Ruiz, et al., *Improvement of a Continuous Spectrophotometric Method for Determining the Monophenolase and Diphenolase Activities of Mushroom Polyphenol Oxidase.* J. Agric. Food Chem, **1997**. 45: p. 1090.

26. Espín, J.C., C. Soler-Rivas, E. Cantos, et al., *Synthesis of the antioxidant hydroxytyrosol using tyrosinase as biocatalyst.* J Agric Food Chem, **2001**. 49(3): p. 1187-93.

27. Baldrian, P., *Fungal laccases – occurrence and properties.* FEMS Microbiology Reviews, **2006**. 30(2): p. 215-242.

28. Piontek, K., M. Antorini and T. Choinowski, *Crystal Structure of a Laccase from the FungusTrametes versicolor at 1.90-Å Resolution Containing a Full Complement of Coppers.* Journal of Biological Chemistry, **2002**. 277(40): p. 37663-37669.

29. Dwivedi, U.N., P. Singh, V.P. Pandey, et al., *Structure–function relationship among bacterial, fungal and plant laccases.* Journal of Molecular Catalysis B: Enzymatic, **2011**. 68(2): p. 117-128.

30. Giardina, P., V. Faraco, C. Pezzella, et al., *Laccases: a never-ending story.* Cellular and Molecular Life Sciences, **2010**. 67(3): p. 369-385.

31. Bugg, T.D.H., M. Ahmad, E.M. Hardiman, et al., *Pathways for degradation of lignin in bacteria and fungi.* Natural Product Reports, **2011**. 28(12): p. 1883-1896.

32. Wang, X., S. Chen, D. Wu, et al., *Oxidoreductase-Initiated Radical Polymerizations to Design Hydrogels and Micro/Nanogels: Mechanism, Molding, and Applications.* Advanced Materials, **2018**. 30(17): p. 1705668.

33. Jeon, J.-R. and Y.-S. Chang, *Laccase-mediated oxidation of small organics: bifunctional roles for versatile applications.* Trends in Biotechnology, **2013**. 31(6): p. 335-341.

34. Li, X., S. Li, X. Liang, et al., *Applications of oxidases in modification of food molecules and colloidal systems: Laccase, peroxidase and tyrosinase.* Trends in Food Science & Technology, **2020**. 103: p. 78-93.

35. Hoopes, J.T. and J.F.D. Dean, *Ferroxidase activity in a laccase-like multicopper oxidase from Liriodendron tulipifera.* Plant Physiology and Biochemistry, **2004**. 42(1): p. 27-33.

36. Thurston, C.F., *The structure and function of fungal laccases.* Microbiology, **1994**. 140(1): p. 19-26.

37. Blaich, R. and K. Esser, *Function of enzymes in wood destroying fungi.* Archives of Microbiology, **1975**. 103(1): p. 271-277.

38. Hofrichter, M., R. Ullrich, M.J. Pecyna, et al., *New and classic families of secreted fungal heme peroxidases.* Applied Microbiology and Biotechnology, **2010**. 87(3): p. 871-897.

39. Hamid, M. and R. Khalil ur, *Potential applications of peroxidases.* Food Chemistry, **2009**. 115(4): p. 1177-1186.

40. Veitch, N.C., *Horseradish peroxidase: a modern view of a classic enzyme.* Phytochemistry, **2004**. 65(3): p. 249-259.

41. National Center for Biotechnology Information, *Enzyme Summary for Enzyme 1.14.18.1, Tyrosinase (EC 1.14.18.1)*, in *PubChem*. **2024**, National Library of Medicine: Bethesda, USA.

42. Selinheimo, E., K. Autio, K. Kruus, et al., *Elucidating the Mechanism of Laccase and Tyrosinase in Wheat Bread Making.* Journal of Agricultural and Food Chemistry, **2007**. 55(15): p. 6357-6365.

43. Lontie, R., *Tyrosinase*, in *Copper Proteins and Copper Enzymes*. **2018**, CRC Press. p. 207-240.

44. Min, K., D.-H. Park and Y.J. Yoo, *Electroenzymatic synthesis of l-DOPA.* Journal of Biotechnology, **2010**. 146(1): p. 40-44.

45. Hanft, F. and P. Koehler, *Studies on the effect of glucose oxidase in bread making.* Journal of the Science of Food and Agriculture, **2006**. 86(11): p. 1699-1704.

46. Bauer, J.A., M. Zámocká, J. Majtán, et al., *Glucose Oxidase, an Enzyme "Ferrari": Its Structure, Function, Production and Properties in the Light of Various Industrial and Biotechnological Applications.* Biomolecules, **2022**. 12(3): p. 472.

47. Wongnate, T. and P. Chaiyen, *The substrate oxidation mechanism of pyranose 2-oxidase and other related enzymes in the glucose–methanol–choline superfamily.* The FEBS Journal, **2013**. 280(13): p. 3009-3027.

48. Kostelac, A., L. Sützl, J. Puc, et al., *Biochemical Characterization of Pyranose Oxidase from Streptomyces canus—Towards a Better Understanding of Pyranose Oxidase Homologues in Bacteria*. International Journal of Molecular Sciences, **2022**. 23(21): p. 13595.

49. Daniel, G., J. Volc, E. Kubatova, et al., *Ultrastructural and Immunocytochemical Studies on the H2O2-Producing Enzyme Pyranose Oxidase in Phanerochaete chrysosporium Grown under Liquid Culture*. Applied and Environmental Microbiology, **1992**. 58(11): p. 3667-3676.

50. Giffhorn, F., *Fungal pyranose oxidases: occurrence, properties and biotechnical applications in carbohydrate chemistry.* Applied Microbiology and Biotechnology, **2000**. 54(6): p. 727-740.

51. Mattinen, M.L., K. Kruus, J. Buchert, et al., *Laccase-catalyzed polymerization of tyrosine-containing peptides.* The FEBS Journal, **2005**. 272(14): p. 3640-3650.

52. Carvajal-Millan, E., S. Guilbert, J.-L. Doublier, et al., *Arabinoxylan/protein gels: Structural, rheological and controlled release properties.* Food Hydrocolloids, **2006**. 20(1): p. 53-61.

53. Bunzel, M., J. Ralph, P. Brüning, et al., *Structural Identification of Dehydrotriferulic and Dehydrotetraferulic Acids Isolated from Insoluble Maize Bran Fiber*. Journal of Agricultural and Food Chemistry, **2006**. 54(17): p. 6409-6418.

54. Bunzel, M., J. Ralph, C. Funk, et al., *Structural elucidation of new ferulic acid-containing phenolic dimers and trimers isolated from maize bran.* Tetrahedron Letters, **2005**. 46(35): p. 5845-5850.

55. Steffensen, C.L., A. Stensballe, U. Kidmose, et al., *Modifications of amino acids during ferulic acid-mediated, laccase-catalysed cross-linking of peptides*. Free Radical Research, **2009**. 43(12): p. 1167-1178.

56. Jia, W., X. Zhang, H. Wang, et al., *Study on the Polymerization and Mechanism of Amino Acid Catalyzed by Laccase.* Journal of Natural Fibers, **2023**. 20(2): p. 2198277.

57. Steffensen, C.L., M.L. Andersen, P.E. Degn, et al., *Cross-Linking Proteins by Laccase-Catalyzed Oxidation: Importance Relative to Other Modifications.* Journal of Agricultural and Food Chemistry, **2008**. 56(24): p. 12002-12010.

58. Oudgenoeg, G., *Peroxidase Catalyzed Conjugation of Peptides, Proteins and Polysaccharides via Endogenous and Exogenous Phenols*. **2004**, Wageningen University and Research: Netherlands. p. 198.

59. Oudgenoeg, G., E. Dirksen, S. Ingemann, et al., *Horseradish Peroxidase-catalyzed Oligomerization of Ferulic Acid on a Template of a Tyrosine-containing Tripeptide.* Journal of Biological Chemistry, **2002**. 277(24): p. 21332-21340.

60. Matissek, R., M. Fischer, *Lebensmittelanalytik*. **2021**, Springer Spektrum Berlin. p. 44-88; 103-165.

61. Moldoveanu, S.C. and V. David, *Chapter 4 - Basic Information Regarding the HPLC Techniques*, in *Selection of the HPLC Method in Chemical Analysis*, S.C. Moldoveanu and V. David, Editors. **2017**, Elsevier: Boston. p. 87-187.

62. Wellings, D.A., *A Practical Handbook of Preparative HPLC*. 1 ed. **2006**, Chantilly. 193.

63. Waters. *Xevo G2-XS QTof mass spectrometer*. **2014** [Last accesed: 18.01.2025]; Available from: https://www.waters.com/waters/library.htm?lid=134800563#:~:text=The%20XS%20Collision%20Cell%20is,instruments%20without%20compromising%20mass%20resolution.

64. Banerjee, S. and S. Mazumdar, *Electrospray Ionization Mass Spectrometry: A Technique to Access the Information beyond the Molecular Weight of the Analyte*. International journal of analytical chemistry, **2012**: p. 282574.

65. Toyama, A. *On the Accurate Understanding of Mass Measurement Accuracy in Q-TOF MS*. **2019** [Last accesed: 12.11.2024]; Available from: https://www.shimadzu.com/an/lcms/9030/index.html

66. McIlvaine, T., *A BUFFER SOLUTION FOR COLORIMETRIC COMPARISON*. Journal of Biological Chemistry, **1921**. 49: p. 183-186.

67. Manzano-Nicolas, J., A. Taboada-Rodriguez, J.A. Teruel-Puche, et al., *Enzymatic oxidation of oleuropein and 3-hydroxytyrosol by laccase, peroxidase, and tyrosinase.* Journal of Food Biochemistry, **2021**. 45(8).

68. Bradford, M.M., *A rapid and sensitive method for the quantitation of microgram quantities of protein utilizing the principle of protein-dye binding.* Analytical Biochemistry, **1976**. 72(1): p. 248-254.

69. Reid, L.O., M. Vignoni, N. Martins-Froment, et al., *Photochemistry of tyrosine dimer: when an oxidative lesion of proteins is able to photoinduce further damage.* Photochemical & Photobiological Sciences, **2019**. 18(7): p. 1732-1741.

70. Kuipers, B.J.H. and H. Gruppen, *Prediction of Molar Extinction Coefficients of Proteins and Peptides Using UV Absorption of the Constituent Amino Acids at 214 nm To Enable Quantitative Reverse Phase High-Performance Liquid Chromatography−Mass Spectrometry Analysis*. Journal of Agricultural and Food Chemistry, **2007**. 55(14): p. 5445-5451.

71. Kaeswurm, J.A.H., A. Scharinger, J. Teipel, et al., *Absorption Coefficients of Phenolic Structures in Different Solvents Routinely Used for Experiments.* Molecules, **2021**. 26(15): p. 4656.

72. Zou, J., Y. Huang, L. Zhu, et al., *Multi-wavelength spectrophotometric measurement of persulfates using 2,2'-azino-bis(3-ethylbenzothiazoline-6-sulfonate) (ABTS) as indicator.* Spectrochimica Acta Part A: Molecular and Biomolecular Spectroscopy, **2019**. 216: p. 214-220.

73. Garcia-Leis, A., D. Jancura, M. Antalik, et al., *Catalytic effects of silver plasmonic nanoparticles on the redox reaction leading to ABTS˙ + formation studied using UV-visible and Raman spectroscopy.* Phys Chem Chem Phys, **2016**. 18: p. 26571.

74. Morinaka, T. and T.P. Silverstein, *Literature discrepancy: What is the moLar absorptivity of abts?* Journal of Undergraduate Chemistry Research, **2022**. 21(4): p. 100.

75. Fürst, S., *Characterization and modification of a laccase from Aspergillus flavus for application as antioxidant biosensor* in *Department for Agrobiotechnology, IFA-Tulln*. **2019**, University of Natural Resources and Life Sciences Tulln an der Donau. p. 71.

76. Childs, R.E. and W.G. Bardsley, *The steady-state kinetics of peroxidase with 2,2'-azino-di-(3-ethyl-benzthiazoline-6-sulphonic acid) as chromogen.* Biochemical Journal, **1975**. 145(1): p. 93-103.

77. Osman, A.M., K.K.Y. Wong and A. Fernyhough, *ABTS radical-driven oxidation of polyphenols: Isolation and structural elucidation of covalent adducts.* Biochemical and Biophysical Research Communications, **2006**. 346(1): p. 321-329.

78. Ike, P.T.L., A.C. Moreira, F.G. De Almeida, et al., *Functional characterization of a yellow laccase from Leucoagaricus gongylophorus.* SpringerPlus, **2015**. 4(1).

79. Ilyasov, I.R., V.L. Beloborodov, I.A. Selivanova, et al., *ABTS/PP Decolorization Assay of Antioxidant Capacity Reaction Pathways.* International Journal of Molecular Sciences, **2020**. 21(3): p. 1131.

80. Wong, K.-S., M.-K. Cheung, C.-H. Au, et al., *A Novel Lentinula edodes Laccase and Its Comparative Enzymology Suggest Guaiacol-Based Laccase Engineering for Bioremediation.* PLOS ONE, **2013**. 8(6): p. e66426.

81. Nnamchi, C.I., B.N. Okolo, A.N. Moneke, et al., *Comparative analysis of the kinetic properties of peroxidases from two improved sorghum varieties.* Tropical Journal of Natural Product Research, **2021**. 5(7): p. 1286-1294.

82. Espín, J.C., J. Tudela and F. García-Cánovas, *4-Hydroxyanisole: The Most Suitable Monophenolic Substrate for Determining Spectrophotometrically the Monophenolase Activity of Polyphenol Oxidase from Fruits and Vegetables.* Analytical Biochemistry, **1998**. 259(1): p. 118-126.

83. Halaouli, S., M. Asther, K. Kruus, et al., *Characterization of a new tyrosinase from Pycnoporus species with high potential for food technological applications.* J Appl Microbiol, **2005**. 98(2): p. 332-43.

84. Espín, J.C., M. Morales, R. Varón, et al., *A continuous spectrophotometric method for determining the monophenolase and diphenolase activities of apple polyphenol oxidase.* Analytical biochemistry, **1995**. 231(1): p. 237-246.

85. Rodriguezlopez, J.N., J. Escribano and F. Garciacanovas, *A Continuous Spectrophotometric Method for the Determination of Monophenolase Activity of Tyrosinase Using 3-Methyl-2-benzothiazolinone Hydrazone.* Analytical Biochemistry, **1994**. 216(1): p. 205-212.

86. Godbey, W.T., *Chapter 5 - Cell growth*, in *Biotechnology and its Applications (Second Edition)*, W.T. Godbey, Editor. **2022**, Academic Press. p. 117-150.

87. Kunkel, J. and P. Asuri, *Function, Structure, and Stability of Enzymes Confined in Agarose Gels.* PLoS ONE, **2014**. 9(1): p. e86785.

88. Isabel Pastor, L.P., *Influence of Macromolecular Crowding on the Oxidation of ABTS by Hydrogen Peroxide Catalyzed by HRP.* Journal of Biocatalysis & Biotransformation, **2013**. 02(01).

89. Flander, L., U. Holopainen, K. Kruus, et al., *Effects of tyrosinase and laccase on oat proteins and quality parameters of gluten-free oat breads.* J Agric Food Chem, **2011**. 59(15): p. 8385-90.

90. Selinheimo, E., M. Saloheimo, E. Ahola, et al., *Production and characterization of a secreted, C-terminally processed tyrosinase from the filamentous fungus Trichoderma reesei.* The FEBS Journal, **2006**. 273(18): p. 4322-4335.

91. Anjum Zia, M., R. Khalil Ur, K.S. M, et al., *Thermal Characterization of Purified Glucose Oxidase from A Newly Isolated Aspergillus Niger UAF-1.* J Clin Biochem Nutr, **2007**. 41(2): p. 132-8.

92. Mirón, J., M.P. González, J.A. Vázquez, et al., *A mathematical model for glucose oxidase kinetics, including inhibitory, deactivant and diffusional effects, and their interactions.* Enzyme and Microbial Technology, **2004**. 34(5): p. 513-522.

93. Zhu, Z., C. Momeu, M. Zakhartsev, et al., *Making glucose oxidase fit for biofuel cell applications by directed protein evolution.* Biosensors and Bioelectronics, **2006**. 21(11): p. 2046-2051.

94. Pisanelli, I., M. Kujawa, O. Spadiut, et al., *Pyranose 2-oxidase from Phanerochaete chrysosporium—Expression in E. coli and biochemical characterization.* Journal of Biotechnology, **2009**. 142(2): p. 97-106.

95. Li, M., H. Deng, R. Ma, et al., *Biochemical and mutational analyses of a Trametes pyranose oxidase and comparison of its mutants in breadmaking.* AMB Express, **2018**. 8(1).

96. Rando, D., G.W. Kohring and F. Giffhorn, *Production, purification and characterization of glucose oxidase from a newly isolated strain of Penicillium pinophilum.* Applied Microbiology and Biotechnology, **1997**. 48(1): p. 34-40.

97. Höfer, C. and D. Schlosser, *Novel enzymatic oxidation of Mn2+ to Mn3+ catalyzed by a fungal laccase.* FEBS Letters, **1999**. 451(2): p. 186-190.

98. Rekuć, A., J. Bryjak, K. Szymańska, et al., *Very Stable Silica-gel-bound Laccase Biocatalysts for the Selective Oxidation in Continuous Systems.* Bioresource technology, **2010**. 101: p. 2076-83.

99. Lu, Q., Y. Kim, N. Bassim, et al., *Catalytic activity and thermal stability of horseradish peroxidase encapsulated in self-assembled organic nanotubes.* Analyst, **2016**. 141(7): p. 2191-2198.

100. Xie, P., L. Fan, L. Huang, et al., *Oxidative polymerization process of hydroxytyrosol catalysed by polyphenol oxidases or peroxidase: Characterization, kinetics and thermodynamics.* Food Chemistry, **2021**. 337: p. 127996.

101. Yu, Y., Y. Wang and M. Li, *Reliable method for the detection of horseradish peroxidase activity and enzyme kinetics.* Analyst, **2019**. 144(4): p. 1442-1447.

102. Witt, S., M. Singh and H.M. Kalisz, *Structural and Kinetic Properties of Nonglycosylated Recombinant Penicillium amagasakiense Glucose Oxidase Expressed in Escherichia coli.* Applied and Environmental Microbiology, **1998**. 64(4): p. 1405-1411.

103. Nishimura, I., K. Okada and Y. Koyama, *Cloning and expression of pyranose oxidase cDNA from Coriolus versicolor in Escherichia coli.* Journal of Biotechnology, **1996**. 52(1): p. 11-20.

104. Perna, V., J.W. Agger, J. Holck, et al., *Multiple Reaction Monitoring for quantitative laccase kinetics by LC-MS.* Scientific Reports, **2018**. 8(1).

105. Chaudhary, D., F. Chong, T. Neupane, et al., *New Inhibitors of Laccase and Tyrosinase by Examination of Cross-Inhibition between Copper-Containing Enzymes*. International Journal of Molecular Sciences, **2021**. 22: p. 13661.

106. M. Sinosaki, N., A. P. Tonin, M. Ribeiro, et al., *Structural Study of Phenolic Acids by Triple Quadrupole Mass Spectrometry with Electrospray Ionization in Negative Mode and H/D Isotopic Exchange*. Journal of the Brazilian Chemical Society, **2019**. 31.

Appendix

I. Zusammenfassung

Gluten, ein wichtiger Bestandteil vieler Backwaren, ist für die gewünschten Backeigenschaften essentiell. Allerdings stellt der Konsum von Gluten für Menschen mit Zöliakie oder nicht-Zöliakie-assoziierter Glutensensitivität eine große Herausforderung dar, da aktuell die einzige wirksame Therapie eine strenge glutenfreie Diät ist. Diese Studie ist ein Teil des PROTAX-Projekts und untersucht die enzymatische Quervernetzung von Proteinen und Arabinoxylanen (AXs) zur Bildung Gluten-ähnlicher Netzwerke. Der Fokus dieser Arbeit ist die Charakterisierung von fünf verschiedenen Enzymen, nämlich Laccase (Lac), Tyrosinase (TYR), Peroxidase (HRP), Glucose- (GOX) und Pyranose-Oxidase (POX). Zunächst wurden die pH- und Temperatur-Optima bestimmt, gefolgt von der Ermittlung der wichtigsten kinetischen Parameter. Im Anschluss daran wurden die Enzyme auf ihre Vernetzung unter optimalen Bedingungen untersucht. Die Analyse der Produkte erfolgte unter Verwendung fortgeschrittener analytischer Techniken wie HPLC-UV und LC-MS/MS. Dabei wird auf die Substrate Ferulasäure (FA) und Tyrosin (Y) fokussiert, wobei danach getreidespezifische Peptidmodelle angewendet werden, um die Lücke zwischen einfachen Monomeren und komplexen Peptiden zu schließen. Die Ergebnisse zeigten eine erfolgreiche Vernetzung von FA- und Y-Monomeren sowie von getreidespezifischen Peptiden und dem FA-Glykosid (FAG). Die Analyse zeigte homogene als auch heterogene Kopplungsreaktionen zwischen FAG und den Peptiden auf, die zur Bildung von Produkten mit unterschiedlichen Molekulargewichten und Polaritäten führten. Vor allem Peptide mit endständigen Y-Resten wiesen eine höhere Vernetzungseffizienz auf als solche mit Y innerhalb der Kette. Darüber hinaus zeigte die Analyse, dass bestimmte Enzyme eine vielfältigere Produktausbeute lieferten als andere. So wurden durch Lac und HRP sehr ähnliche Produkte erzeugt, während TYR teilweise unterschiedliche Produkte produzierte. Diese Ergebnisse bilden die Grundlage für weitere Untersuchungen an glutenfreien Teigstrukturen innerhalb des Projektes mit dem Ziel vergleichbare Eigenschaften wie bei glutenhaltigen Produkten zu erreichen.

II. Other data

Table 21: Pipetting scheme for the determination of the molar extinction coefficient of ABTS and the corresponding ABTS concentration in each well.

Laccase solution [µL]	ABTS solution [µL]	Total volume [µL]	Resulting ABTS concentration in well [mM]
340	0	340	0
320	20	340	0.0063
313	27	340	0.0085
305	35	340	0.0110
298	42	340	0.0132
290	50	340	0.0158
282	58	340	0.0183
275	65	340	0.0205
265	75	340	0.0236

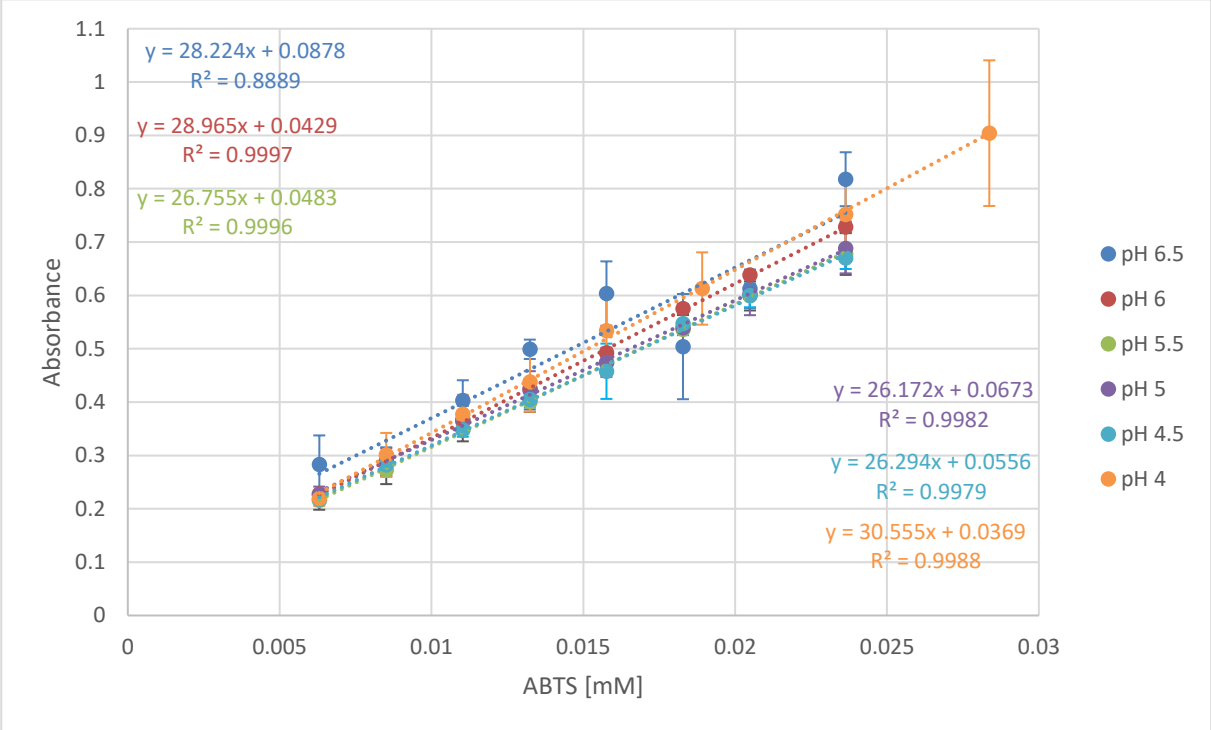

Figure 33: Results for the determination of the molar extinction coefficient of ABTS at six different pH values. Each measurement was performed in triplicate and the mixtures were incubated at 25 °C.

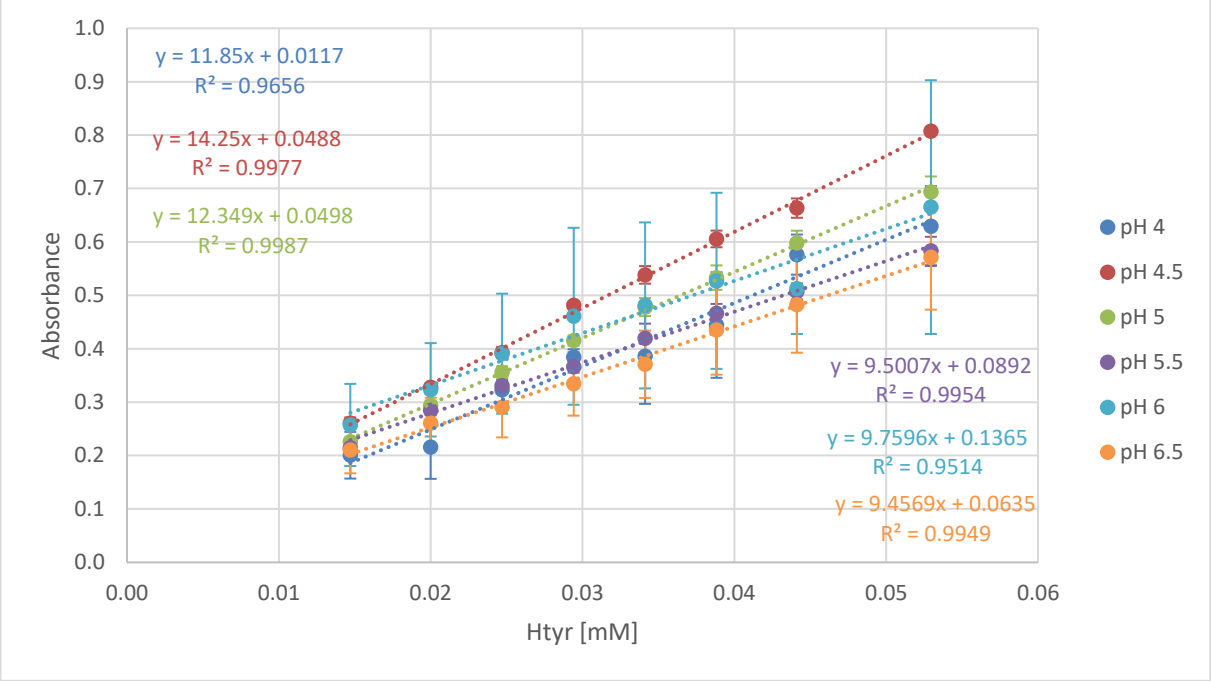

Figure 34: Results for the determination of the molar extinction coefficient of Htyr at six different pH values. Each measurement was performed in triplicate and incubated at 25 °C.

Table 22: Determined absorbances of the blank measurements for the Bradford assay.

Solvent/buffer	Water	Acetate	McIlvaine pH 4	McIlvaine pH 6.5
Mean absorbance	0.639	0.644	0.676	0.722
SD	0.007	0.013	0.018	0.006

Table 23: Determined absorbance values of the standard solutions (0.001-0.5 mg protein/mL) for the Bradford assay.

Protein [mg/mL]	0.001	0.002	0.005	0.01	0.02	0.05	0.1	0.2	0.5
Mean absorbance	0.63667	0.63367	0.648	0.67567	0.78233	1.0153	1.2623	1.608	1.9247
SD	0.01041	0.00321	0.00625	0.00586	0.00808	0.0081	0.0196	0.0375	0.01617
Blank corrected absorbance	-0.00267	-0.00567	0.00867	0.03633	0.143	0.376	0.623	0.9687	1.2853

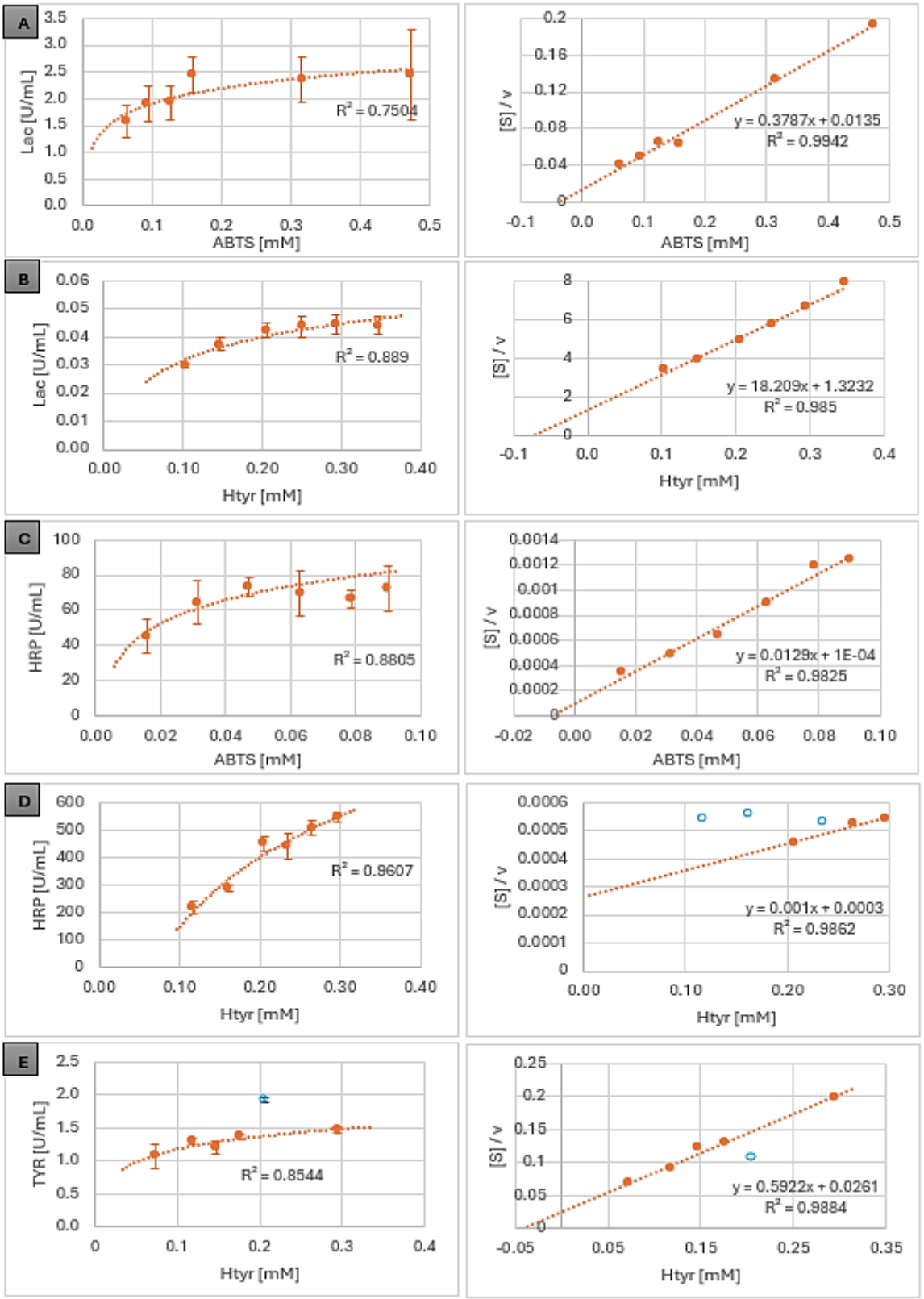

Figure 35: The corresponding Michaelis-Menten curve (left) and Hanes-Woolf plot (right) of Lac with ABTS (A; pH 4; 35 °C) and Htyr (B; pH 4.5; 35 °C), of HRP with ABTS (C; pH 4; 30 °C) and Htyr (D; pH 6.5; 30 °C) and of TYR with Htyr (E; pH 6.5; 25 °C). The blue-marked white spots were excluded from the determination. Each measurement was performed in triplicate.

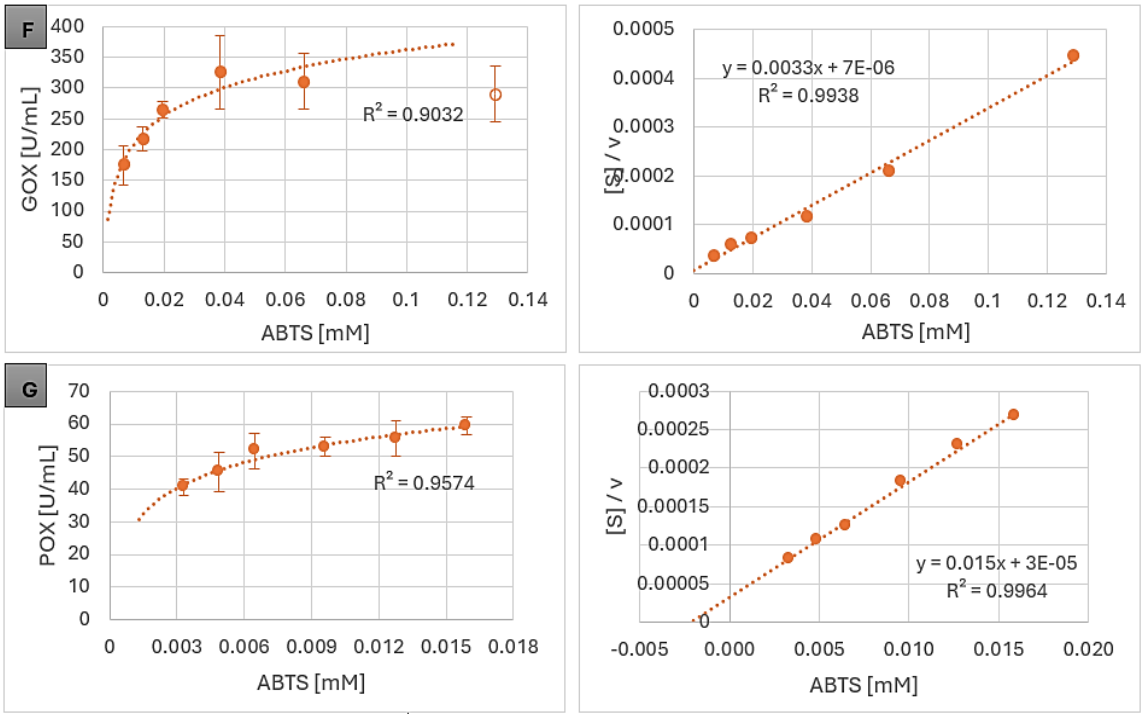

Figure 36: The corresponding Michaelis-Menten curve (left) and Hanes-Woolf plot (right) of GOX with ABTS (F; pH 4.5; 40 °C) and of POX with ABTS (G; pH 5.5; 35 °C). Each measurement was performed in triplicate.

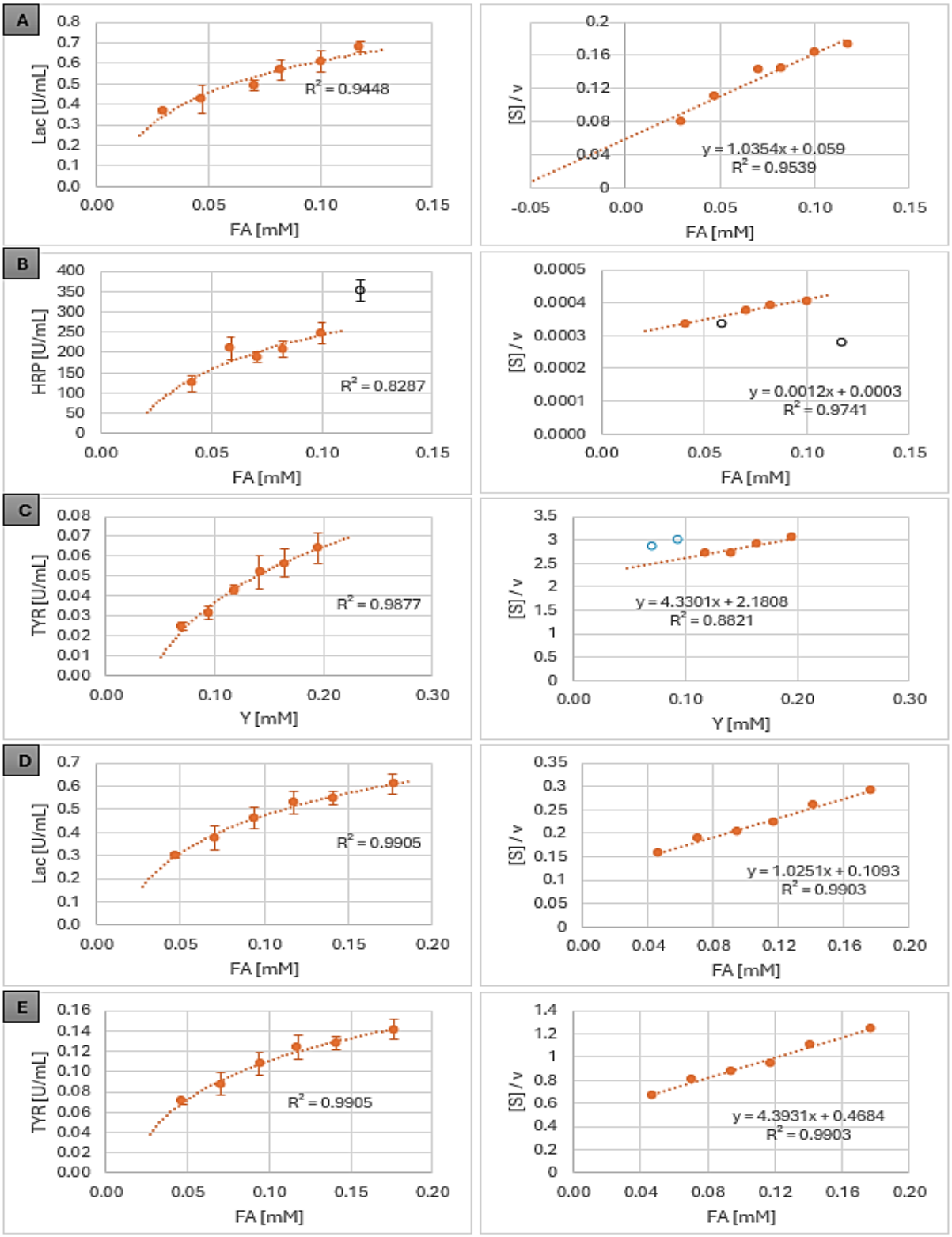

Figure 37: The corresponding Michaelis-Menten curve (left) and Hanes-Woolf plot (right) of Lac with FA (A; pH 4.5; 30 °C), of HRP with FA (B; pH 4.5; 30 °C), of TYR with Y (C; pH 6.5; 30 °C), the enzyme combination of Lac (D) and TYR (E) with FA (pH 4.5; 30 °C). The white spots were excluded from the determination. Each measurement was performed in triplicate.

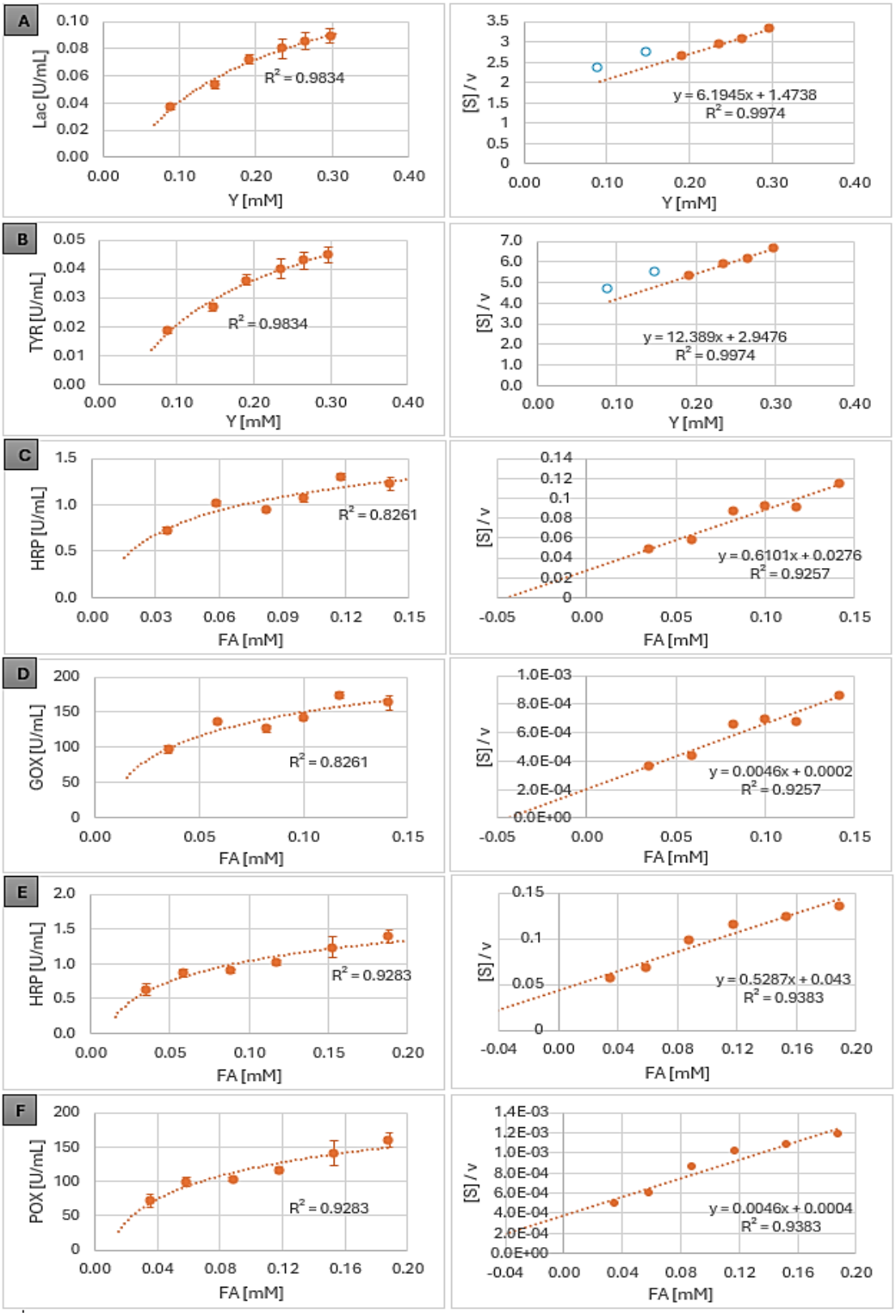

Figure 38 The corresponding Michaelis-Menten curve (left) and Hanes-Woolf plot (right) of the enzyme combination consisting of Lac (A) and TYR (B) with Y (pH 4.5; 30 °C), of HRP (C) and GOX (D) with FA (pH 4.5; 30 °C), and of HRP (E) and POX (F) with FA (pH 6.5; 30 °C). The blue-marked white spots were excluded from the determination. Each measurement was performed in triplicate.

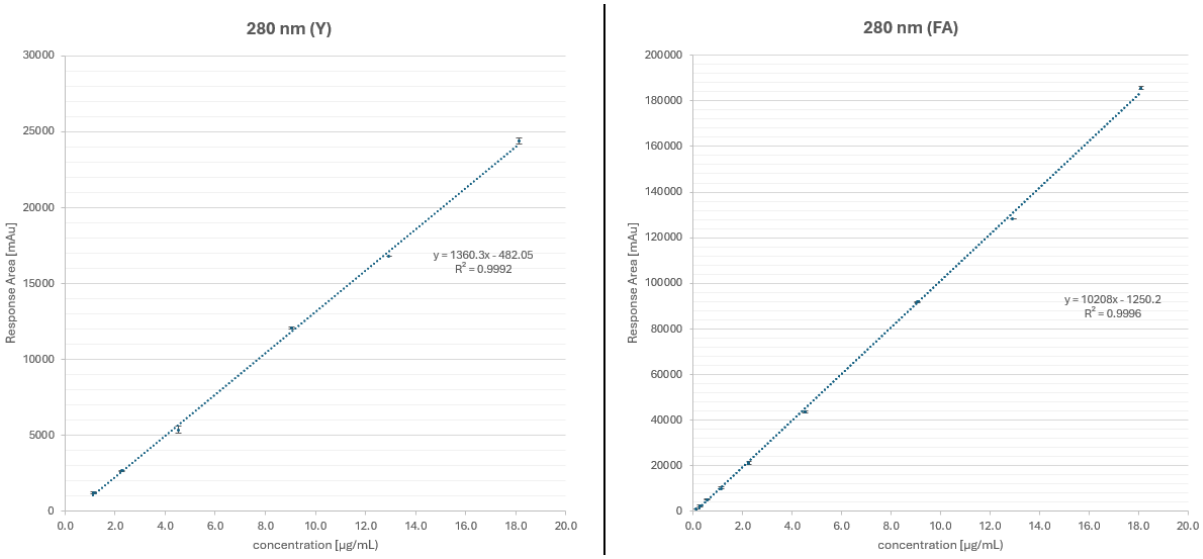

Figure 39: External calibration curves for Y (left) and FA (right) at 280 nm for the HPLC analysis.